

---

# Complete Characterization of Light Waves using Attosecond Pulses

Eleftherios Goulielmakis

---



München 2005



---

# Complete Characterization of Light Waves using Attosecond Pulses

Eleftherios Goulielmakis

---

Dissertation  
an der Fakultät für Physik  
der Ludwig–Maximilians–Universität  
München

vorgelegt von  
Eleftherios Goulielmakis  
aus Heraklion, Kreta, Griechenland

München, den 05.07.05

Erstgutachter: Prof. Dr. Ferenc Krausz

Zweitgutachter: Prof. Dr. Eberhard Riedle

Tag der mündlichen Prüfung: 01.08.05

# Abstract

The most direct way to probe the strength of an electric field, is to measure the force that exerts to a charged particle. For a time varying field, charge placement within an interval substantially shorter than the characteristic period of variation of the field is essential for sampling its temporal evolution. Employing such a scheme to track the field variation of light waves that changes its direction  $\sim 10^{15}$  times per second, charge release shall be confined within a fraction of a femtosecond.

In this thesis, the complete characterization of a light pulse is demonstrated experimentally for the first time by probing its field variation using a 250 attosecond electron burst. Such an ultrafast charge probe, can be generated by the impulsive ionization of atoms, using an XUV attosecond pulse precisely synchronized with the light waveform to be characterized. The technique allows access to the instantaneous value of the electric field of IR, visible, or UV light and thereby opens the door for the synthesis of controlled, extremely broadband and arbitrarily shaped light waveforms.

The above experiments, are presented along with critical pertinent developments on the generation of few-cycle phase-controlled light waveforms and their subsequent exploitation, for the generation of isolated XUV attosecond pulses.

Precisely characterized and controlled light fields and XUV attosecond pulses employed in combination, hold the promise for probe and control of elementary processes evolving on an attosecond time scale.

---

# Zusammenfassung

Der direkteste Weg, die elektrische Feldstärke zu ermitteln, ist, die Kraft an einem geladenen Teilchen zu messen. Für ein zeitlich veränderliches Feld ist es vonnöten, dass diese Ladung nur in einem Zeitintervall vorhanden ist, das deutlich kürzer ist als die charakteristische Zeitdauer der Feldänderung. Um diese Methode für die Aufzeichnung des Verlaufes einer Lichtwelle anzuwenden, bei der das elektrische Feld seine Richtung  $10^{15}$  mal pro Sekunde wechselt, muss das Auftreten der Ladung auf einen Bruchteil einer Femtosekunde ( $1 \text{ fs} = 10^{-15} \text{ s}$ ) beschränkt sein.

In dieser Dissertation wird die erstmals experimentell demonstrierte, vollständige Charakterisierung eines Lichtpulses vorgestellt, bei welcher die Feldänderung mit einem 250 as ( $1 \text{ as} = 10^{-18} \text{ s}$ ) langen Elektronen-Puls abgetastet wird. Eine ultraschnelle Ladungsprobe dieser Art kann durch impulsive Ionisation von Atomen mittels eines Attosekunden-Pulses im XUV Bereich (Extreme Ultraviolet), der präzise mit der zu charakterisierenden Lichtwelle synchronisiert ist, erzeugt werden. Diese Technik ermöglicht den Zugang zum instantanen Wert der elektrischen Feldstärke von infrarotem, sichtbarem oder ultraviolettem Licht und öffnet daher die Tore für die Synthese von geregelten, extrem breitbandigen und beliebig geformten Lichtwellen.

Die oben genannten Experimente werden gemeinsam mit den entsprechenden Entwicklungen auf dem Gebiet von phasengesteuerten Lichtwellen mit wenigen optischen Zyklen und deren Anwendung im Bereich der Erzeugung von isolierten XUV Attosekunden-Pulsen präsentiert. Präzise gesteuerte und charakterisierte Lichtwellen sowie XUV Attosekunden-Pulse, die in einem kombinierten Schema eingesetzt werden, versprechen die künftige Messung und Steuerung von elementaren Prozessen auf einer Attosekunden-Zeitskala.

*We can scarcely avoid the inference that light consists in the traverse undulations of the same medium which is the cause of electric and magnetic phenomena.*

---

James Clerk Maxwell

# Contents

<b>Abstract</b>	<b>v</b>
<b>Contents</b>	<b>ix</b>
<b>Introduction</b>	<b>1</b>
<b>1 Interaction of atoms with intense laser pulses</b>	<b>9</b>
1.1 Atoms in strong fields . . . . .	9
1.1.1 Mechanisms of atomic ionization . . . . .	9
1.1.2 Extreme ultraviolet light generation . . . . .	11
1.1.3 Light Polarization effects . . . . .	16
1.2 Macroscopic response . . . . .	16
1.3 A train of attosecond pulses . . . . .	17
1.4 Isolated attosecond pulses . . . . .	18
1.5 Above threshold ionization . . . . .	23
<b>2 Atomic streak camera</b>	<b>25</b>
2.1 Principles of a streak camera . . . . .	25
2.2 Streak camera on an attosecond time scale . . . . .	27
<b>3 A laser source of few-cycle phase stabilized pulses</b>	<b>35</b>
3.1 The laser system . . . . .	35
3.1.1 The laser oscillator . . . . .	35
3.1.2 The laser amplifier . . . . .	35
3.1.3 Hollow fiber-Chirped mirror pulse compressor . . . . .	37
3.2 Carrier-envelope phase of a laser . . . . .	40
3.2.1 CE phase of a mode locked pulse train . . . . .	40
3.2.2 Observing phase drifts of laser oscillators . . . . .	42
3.3 Observing phase drifts of amplified pulses . . . . .	44
3.4 Phase stabilization of amplified pulses . . . . .	45
3.5 Phase noise of white light continuum generation . . . . .	48
3.5.1 Sources of phase noise . . . . .	48
3.5.2 Linear spectral interferometry . . . . .	49

3.5.3	White light generation in a gas filled hollow fiber . . . . .	50
3.5.4	White light generation in a sapphire plate . . . . .	52
<b>4</b>	<b>Attosecond pump-probe apparatus</b>	<b>53</b>
4.1	XUV light Generation . . . . .	53
4.2	XUV detector based on ionization of residual gas . . . . .	56
4.3	Spatial Separation XUV-laser light . . . . .	56
4.4	XUV light detection . . . . .	56
4.5	The Mo/Si multilayer mirror . . . . .	58
4.6	Alignment procedures . . . . .	60
4.7	A sample of atoms-the gas orifice . . . . .	60
4.8	Electron spectrometer . . . . .	62
<b>5</b>	<b>Metrology of attosecond pulses</b>	<b>65</b>
5.1	Attosecond pulses: Spectral signatures . . . . .	65
5.2	Attosecond pulses: The synthesis . . . . .	68
5.2.1	Scheme I (Pulses with random phase) . . . . .	70
5.2.2	Scheme II (Phase controlled laser pulses) . . . . .	72
5.3	Discussion on the results . . . . .	74
<b>6</b>	<b>Complete characterization of light waves</b>	<b>77</b>
6.1	Attosecond oscilloscope-sampling of light waves . . . . .	78
6.2	Experimental . . . . .	80
6.3	Analysis and discussion . . . . .	82
6.4	Applications of attosecond light sampling . . . . .	84
<b>7</b>	<b>Conclusions and future prospects</b>	<b>87</b>
<b>A</b>	<b>XUV transmission of thin filters</b>	<b>89</b>
	<b>Bibliography</b>	<b>91</b>
	<b>Acknowledgments</b>	<b>101</b>
	<b>Echo</b>	<b>105</b>

# Introduction

The desire to gain insight into fundamental processes in matter, has been the principal impetus behind the exploration of new routes, as well as experimental techniques that allow measurements with ever higher spatiotemporal resolution. Over the centuries, light has been a key tool for the observation of natural phenomena while its employment in physical research and metrology has led to major scientific revolutions in our century, with quantum theory at the first place.

The extent of insight into microscopic physical phenomena attained using light, undoubtedly depends on the degree of control to its features so as to provide adequate resolution. Moreover, steering elementary processes in the microcosm by exerting forces to atoms or electrons exploiting the fields of light, namely: the electric and the magnetic field, is possible if these fields are controlled. Unveiling the properties of atoms and molecules by observing photon, electron, ion, spectra emerging along the absorb of radiation or other interactions in microscopic level is what is referred to as spectroscopy. Light is probably the most important tool of spectroscopy. However conventional spectral measurements do not allow resolving the dynamics of fundamental phenomena on an atomic and molecular scale which is possible only by time resolved observations of the rapidly evolving systems.

A concept to study microscopic processes directly in time, is what usually is referred to as time-resolved spectroscopy. A light burst (pump) drives a system to an excited state (or generally far from its equilibrium) while a second one (probe) is subsequently probing its temporal evolution. The information of the dynamics of the system is imprinted either on the probe light pulse, or on other resultants of the interaction including secondary photons, electrons and ions.

It is possible to discern different eras of time-resolved light spectroscopy determined by the degree of access and control to the fundamental properties of the light-probe waveforms and therefore by the attained resolution. Though time-resolved experiments had been possible much earlier, the first era of systematic studies directly in time was established by the employment of flashed light sources to pump and to probe dynamically photolysis of molecules on a microsecond time scale [1]. There the emission of the pump and probe bursts was driven by electronics that initiated and abruptly terminated a discharge in a flash lamp. The invention of the laser in the early sixties inaugurated the second era, where the control over the properties of light waves became more direct and very soon as a consequence of that, it was followed by the first pulsed sources on the nanosecond time scale and about a decade later on the picosecond time scale. At the same time, laser sources

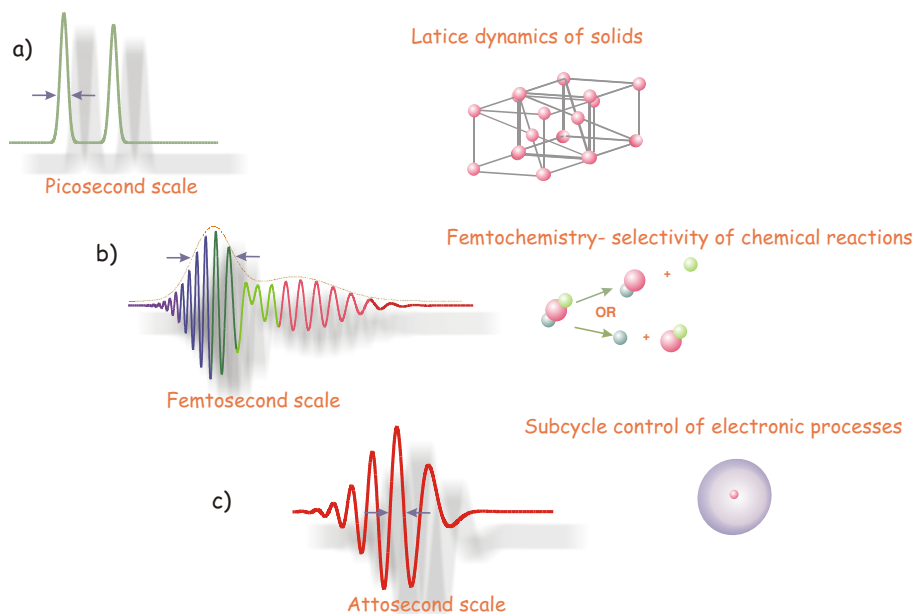


Figure 1: Access and control of the fundamental features of a light waveform in different eras of time-resolved spectroscopy and typical applications on the corresponding time scale. The attained degree of control of the waveform is indicated by the blue arrows. a) Generation of coherent pulsed light sources was the first step of control. b) On a femtosecond time scale shaping of the pulse envelope of a multi-cycle pulse has been possible and has allowed steering chemical reactions. c) Control on an attosecond time scale implies sub-cycle shaping and measurement of light waves.

with fine tuned wavelength allowed advances in conventional spectroscopy to Doppler-free observations and accurate determination of physical constants. Time resolved studies of molecular dynamics that were initiated this period - as the rotation of molecules typically last picoseconds - were further advanced by the invention and employment of femtosecond laser light sources ( $1 \text{ fs} = 10^{-15} \text{ s}$ ) that have provided bursts of light on the time scale of the motion of atoms inside molecules (typically ranging from several hundreds to tens of femtoseconds). This resolution has opened the door to the exploration of phenomena that had never been studied in real time, like formation and rupture of the chemical bond, determination of intermediate transients in chemical reactions, energy transfer between vibrational and rotational modes in a molecule, molecular collisions [2]. The Nobel prize in chemistry was awarded in 1999 to Prof. Ahmed Zewail, for his contributions to this field, namely femtochemistry. Attempts to extend the degree of control to the shape of a light burst by controlling the phase and the amplitude of individual spectral components [3], have played significant role on studying and affecting dynamically the probed systems as well as steering elementary chemical reactions. This is what is usually referred to as quantum control of chemical reactions [4]. The pertinent techniques have been extensively

proliferated to various fields and support research in solids, in semiconductors: carrier relaxation dynamics, in biology: energy transfer in macromolecules. Control of the light waveform at different eras is shown in figure 1 along with relevant applications.

Spectroscopic measurements by employing the broad spectrum of the pump and the probe inherently related with the pulse length in femtosecond time resolved measurements, sounds contradictory to conventional spectroscopy; where high resolution is determined by the monochromaticity of the source employed to resolve energy states and transitions. The difference here (and also the premise of femtochemistry) is that the information about the energy states, and their coherence is encoded in a wavepacket formed by their simultaneous excitation by the pump pulse and can be extracted by tracking how it evolves in time using the probe pulse! This is a critical point and in the case of shorter pulses it becomes of even higher importance.

The limit in the temporal resolution of these techniques is determined by the duration of the pulses employed to study a system. Modern laser systems based on Ti:Sapphire [5], [6] combined with post pulse compression techniques [7], deliver ultra-intense pulses that consist of merely a couple of field oscillations ( $T_0 \sim 2.5$  fs). However, for gaining access to the temporal evolution of phenomena inside atoms, chronoscopic techniques being able to sample at an even shorter time scale are indispensable. On that time scale the decisive processes are dominated by the intra-atomic motion of electrons, as well as, by the ultrafast electron localization inside molecules. The characteristic time scales for these phenomena are expected to range from a few femtoseconds down to the attosecond time scale (1 as =  $10^{-18}$  s).

Attoscience is aiming the dynamic study of processes evolving on an attosecond time scale determined by the motion of electronic wavepackets in which similarly to what alluded all the information is encoded. Starting from the most fundamental phenomena, the periodic "breathing" of the atomic wavepacket formed by the superposition of the 1S and the 2S of the atomic Hydrogen takes 400 as; the most fundamental quantum beat in nature. Auger decay in atoms on the other hand that follows the impulsive or collisional excitation of inner atomic shells, also can be enlisted to these phenomena that could evolve on an attosecond time scale; as the spectral widths measured in spectroscopic observations and modern calculations dictate [8]. Furthermore the sudden removal of an inner electron from an atom has been calculated to result in a characteristic electron density rearrangement with a  $\sim 50$  as time scale and with universal character [9]. On top of that, electron-electron correlations can be dynamically explored once studied with attosecond resolution [10]. Dynamics encoded in the motion of the electron wavepackets in molecules is another topic associated with attosecond resolution. It is probably the resolution needed to study molecules beyond the Born-Oppenheimer approximation [11], [12]. Last, the photoeffect. This essential phenomenon might not further be considered instantaneous, when atoms are studied on an attosecond time scale. So far there is not direct evidence of its "non instantaneous nature". However, as the temporal resolution of the measuring techniques increases, facing the finite duration of the photoeffect is possible. Attaining resolution to observe atomic ionization, on its physical time scale, would probably be a landmark of attoscience.

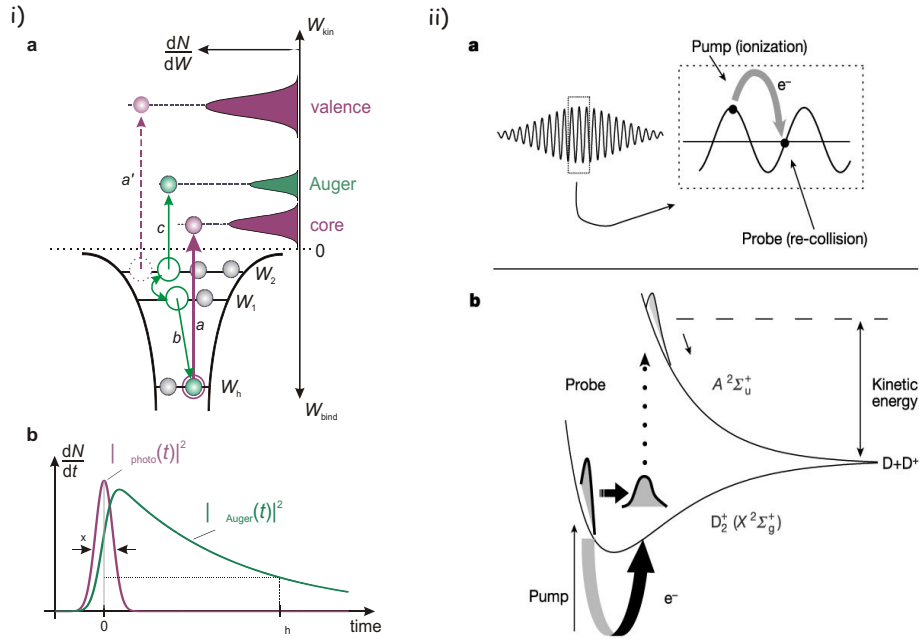


Figure 2: Schemes that have employed attosecond resolution to observe atomic or molecular dynamics. i) Time-resolved Auger decay (from [16]) and molecular dynamics (from [17]).

To reach the resolution necessary to track these phenomena, two main approaches are dominant in this new field. The first is associated with the generation of attosecond bursts of radiation capable to initiate and subsequently to probe the motion of the electron wavepackets either with a similar burst or by a precisely synchronized ultraintense laser field playing the role of a fast streak camera operational on an attosecond time scale. Attosecond pulses in this approach have been generated up today in the XUV part of the spectrum by the nonlinear interaction of a strong laser field with atoms [13], [14], [15]. The strong electric field of the laser drives an electron to the continuum which in turn - driven by the same field - returns in the vicinity of the core and releases its energy into XUV photons upon recombination. This sensitive to the driving field process to generate the XUV attosecond pulse can be restricted to occur only once per laser pulse, if the waveform of the latter is precisely controlled. The first proof of principle experiment to employ an XUV attosecond pulse was to measure Auger decay in Krypton atoms where the evolution of a multi-electron wavepacket which followed the generation of an inner shell vacancy by the attosecond pulse (see figure 2.(i)) is subsequently probed by a synchronized laser field [16]. In the second approach the electron generated by the laser field as in the first case is used to probe directly the dynamics of the same system upon its re-scattering with the parent ion or molecule. For the case of a molecule this is illustrated in figure 2.(ii). The laser field drives the electron to the continuum and at the same time excites the molecule and defines the clock against which the temporal dynamics are tracked.

All approaches are summarized schematically in figure 3 where different colors define

a different scheme to attain attosecond resolution. To attain their maximum resolution all the schemes briefly discussed here draw on a precisely controlled ultraintense laser field. This is because the generation of attosecond bursts or bunches is driven by the light field. On the other hand such field is ideal for steering an ultrafast process by exerting forces to elementary particles like electrons, in combination or not with XUV attosecond pulses. Control in this case is understood not only by making possible reproducible generation of waveforms with controlled field evolution; though that is probably the most elementary step; but even further, to imprint a predefined electric field shape to a light waveform, and if necessary, completely different from a sinusoidal oscillation. Arbitrarily shaped fields on a few femtosecond time scale down to sub-cycles of the order of few hundreds of attosecond, have been pursued by the optical community for years [18], [19], [20]. To attain this extent of control, undoubtedly besides the techniques to generate these waveforms, mostly drawn on multicolor synthesis of distinct light modes or multi-octave super continua, competent techniques to allow their accurate characterization are indispensable.

The principal objective of the research presented here, is to advance the temporal resolution, with which elementary processes of atoms and molecules, can be explored on their natural time scale; faster than a single swing of an optical wave. To reach this objective three key developments are of fundamental importance as dictated by the previous discussion. First, to establish control on the phase of the waveform of amplified few cycle laser pulses. Second, to employ these pulses to generate attosecond XUV bursts lasting a few hundreds of attoseconds by controlling the generation and employing competent techniques for their characterization. Third, by establishing a new direct metrology for light taking the advantage of the previous two developments. There tracking the instantaneous value of the field, by means of an attosecond pulse acting as an ultrafast sampler and thus the potential for extracting the complete information about the light waveforms, becomes possible. It is the waveform of light that as alluded, drives fascinating phenomena in nonlinear optics and thus access to its main features and subsequent control, defines our resolution not only to observe but also to steer physical processes. The title of this thesis emerges from this endeavor for precise characterization of light waves by a universal technique, overcoming the bottlenecks that metrology of broadband light waveforms confronts.

In this attempt the author has contributed in the first period of his doctorate work with developments on the few-cycle phase controlled source and its characterization (Results from this period appear in P10 and P11). With this source available, he worked on the upgrade of the XUV-beamline and contributed with experiments on the first realization of a streak camera operational on an attosecond time scale. These developments were published in P7. Finally based on these developments he focused his efforts in bringing off the first direct light characterization using attosecond pulses as an ultrafast field sampler. The results were published in P4. In parallel, and independent of this thesis work, he has joined external collaborators of the group in experimental projects employing the few-cycle phase stabilized laser source. Results from the conducted experiments can be found in P1, P5, P6, P8, P9.

The structure of this thesis is as follows:

*Chapter 1* is an introduction to the physics of the interaction of intense laser pulses with

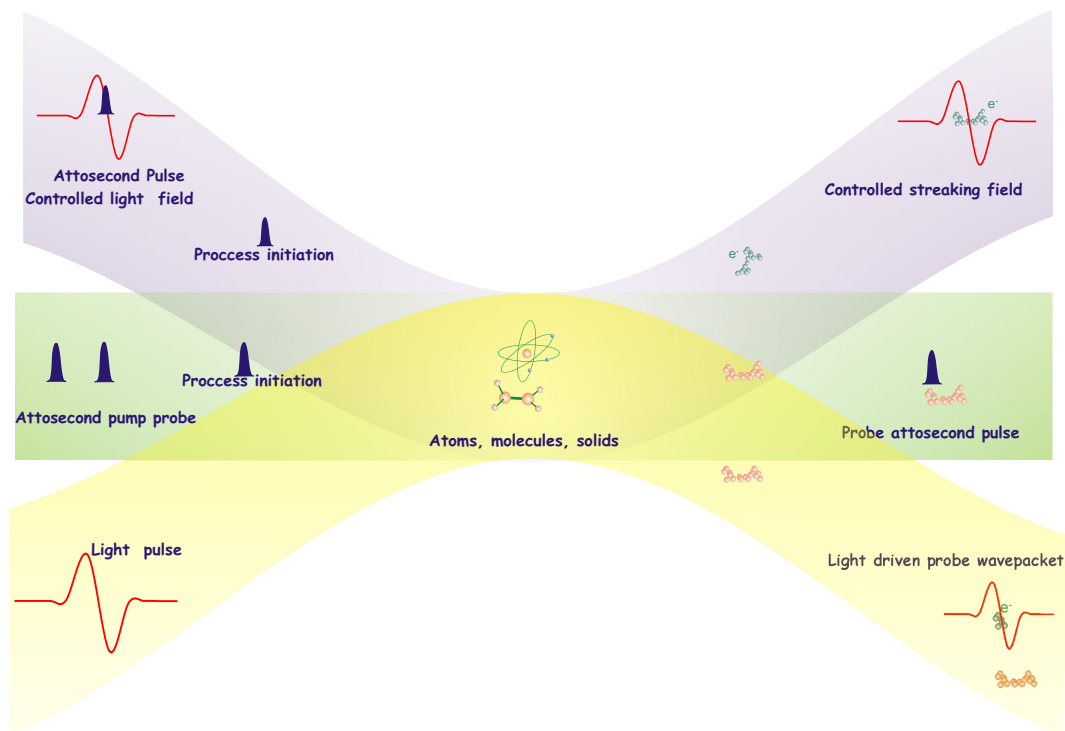


Figure 3: The landscape of modern concepts aiming to track microscopic processes on an attosecond time scale. Each stripe shows the pertinent tools. (Blue stripe) The atomic streak camera. An atomic process is initiated by a fast attosecond impulsive excitation in the presence of a precisely controlled light field, to probe the dynamics imprinted on the emerging electron bunches [21], [22]. (Green stripe) The conventional pump probe technique employing attosecond pulses. (Yellow stripe) An Attosecond electron bunch generated by optical field ionization of atoms or molecules, probes the dynamics of its parent ion upon its re-scattering driven by the laser field [23], [17].

atoms, the generation of XUV light, as well as XUV attosecond pulses. The ideas initially discussed for multi-cycle waveforms, are extended to few-cycle pulses and the relevant advantages are discussed. Ideas to be employed along the thesis for the observation, and controlled generation of attosecond pulses are also introduced here.

*Chapter 2* The concept of the atomic streak camera is presented.

*Chapter 3* concerns the laser source, the post compression techniques that provide ultraintense few cycle pulses and the developments on the phase control of these pulses. Additionally, experiments aiming to characterize the phase noise introduced by the nonlinear process employed in the generation of intense, phase stabilized, few cycle, laser pulses, are presented. Results have been published in (P10) and (P11).

The experimental setup for the generation, characterization, and utilization of attosecond pulses, is presented in *Chapter 4*. The methods for the realization of the theoretical

schemes are discussed.

In *Chapter 5* Observation of spectral signatures of attosecond pulses are discussed and the atomic streak camera concept is put into practice. Second generation of results that followed<sup>1</sup> radical improvement to the experimental setup resulted in higher temporal resolution (almost a factor of 2), is also discussed in accordance with the demands of recently proposed experiments [8], ready to be put into practice employing this concept.

In *Chapter 6* the complete characterization of light waves utilizing an isolated attosecond pulse as a probe is presented. This chapter deals with the third aforementioned objective. These results have been published in Science in August 2004 (P4).

The conclusions and future prospects are discussed in *Chapter 7*. Schemes for the implementation of this new light characterization technique (already under development) for multi-color light pulse synthesis, are also discussed.

## List of publications

Publications in the framework of this thesis are marked with a \*. Publication P4 is reprinted.

### *Peer reviewed*

- P1 F. Lindner, M.G. Schatzel, H. Walther, A. Baltuska, E. Goulielmakis, F. Krausz, G.G. Paulus *Attosecond double-slit experiment* Phys. Rev. Lett. 95, 040401 (2005)
- P2 Kienberger R, Uiberacker M, Goulielmakis E, Baltuska A, Drescher M, Krausz F *Single Sub-fs Soft-X-ray Pulses: Generation and Measurement with the Atomic Transient* J. Mod. Opt., 52, 261 (2005)
- P3 Uiberacker M, Goulielmakis E, Kienberger R, Baltuska A, Westerwalbesloh T, Kleineberg U, Heinzmann U, Drescher M, Krausz F *Attosecond metrology with controlled light waveforms* Laser Physics, 15, 195 (2005)
- P4 \* Goulielmakis E., Uiberacker, M., Kienberger, R., Baltuska, A., Yakovlev, V., Scrinzi, A., Westerwalbesloh, Th., Kleineberg, U., Heinzmann, U., Drescher, M., Krausz, F. *Direct Measurement of Light Waves* Science 305, 1267 (2004).
- P5 Liu X, Rottke H, Eremina E, Sandner W, Goulielmakis E, Keeffe KO, Lezius M, Krausz F, Lindner F, Schatzel MG, Paulus GG, Walther H *Nonsequential double ionization at the single-optical-cycle limit* Phys. Rev. Lett. 93 (26) 2004.
- P6 Schatzel MG, Lindner F, Paulus GG, Walther H, Goulielmakis E, Baltuska A, Lezius M, Krausz F *Long-term stabilization of the carrier-envelope phase of few-cycle laser pulses*, Appl. Phys. B, 79, 1021 (2004).
- P7 \* Kienberger R, Goulielmakis E, Uiberacker M, Baltuska A, Yakovlev V, Bammer F, Scrinzi A, Westerwalbesloh T, Kleineberg U, Heinzmann U, Drescher M, Krausz F *Atomic Transient Recorder*, Nature, 427, 817 (2004).

---

<sup>1</sup>First results published in Nature (P7) early 2004.

- P8 F. Lindner, G. Paulus, H. Walther, A. Baltuska, E. Goulielmakis, M. Lezius, F. Krausz, *The Gouy effect for few-cycle laser pulses* Phys. Rev. Lett., 92, 11 (2004).
- P9 Paulus GG, Lindner F, Walther H, Baltuska A, Goulielmakis E, Lezius M, Krausz F, *Measurement of the phase of few-cycle laser pulses* Phys. Rev. Lett., 91, 25 (2003).
- P10 \* Baltuska A, Uiberacker M, Goulielmakis E, Kienberger R, Yakovlev VS, Udem T, Hänsch TW, Krausz F *Phase-controlled amplification of few-cycle laser pulses* IEEE J. Quantum Electron, 9, 972 (2003).
- P11 \* Baltuska A, Udem T, Uiberacker M, Hentschel M, Goulielmakis E, Gohle C, Holzwarth R, Yakovlev VS, Scrinzi A, Hänsch TW, Krausz F *Attosecond control of electronic processes by intense light fields* Nature, 422, 189 (2003)

*More public writing*

1. Eleftherios Goulielmakis and Ferenc Krausz, *Ein Oszilloskop für Lichtwellen*, Spectrum der Wissenschaft, (to appear).

*Conference proceedings*

- C1 \* Kienberger R, Goulielmakis E, Baltuska A, Uiberacker M, Westerwalbesloh T, Kleineberg U, Heinzmann U, Drescher M, Krausz F *Reproducible generation and measurement of isolated sub-fs XUV pulses with phase-controlled few-cycle light* 4th International Conference on Ultrafast Optics, JUN, 2003 ULTRAFAST OPITCS IV : 241-246, 2004
- C2 \* Baltuska A, Uiberacker M, Goulielmakis E, Udem T, Hentschel M, Kienberger R, Holzwarth R, Hänsch TW, Krausz F *Stabilization and characterization of the carrier-envelope phase in intense few-cycle pulses* 4th International Conference on Ultrafast Optics, JUN, 2003 ULTRAFAST OPITCS IV : 203-208, 2004
- C3 Lindner F, Paulus GG, Walther H, Baltuska A, Goulielmakis E, Lezius M, Krausz F *Measurement of the absolute phase of few-cycle laser pulses* 4th International Conference on Ultrafast Optics, JUN, 2003 ULTRAFAST OPITCS IV : 209-213, 2004
- C4 Lindner F, Schatzel M, Paulus G, Walther H, Baltuska A, Goulielmakis E, Lezius M, Krausz F *Spatiotemporal determination of the absolute phase of few-cycle laser pulses* 14th International Conference on Ultrafast Phenomena, JUL 25-30, 2004 ULTRAFAST PHENOMENA XIV : 94-96, 2005

# Chapter 1

## Interaction of atoms with intense laser pulses

### 1.1 Atoms in strong fields

One of the most exciting regimes of modern physics is reached when atoms are exposed to electric fields comparable in strength with those keeping electrons in motion around the nucleus (for Hydrogen this is  $E_H = 5.1 \times 10^9$  V/cm). These extraordinary strong electric fields, can be today attained by means of ultrashort laser pulses releasing their energy within a few hundreds femtoseconds [24] down to a few femtoseconds in the visible-IR regime [5], [6]. Depending on the particular laser design and aimed application, intensities of the order of  $10^{20}$  W/cm<sup>2</sup> are within reach and already far beyond the limit over which any atom could resist ionization. The effect of those fields to an atomic system, cannot be considered as a small perturbation to its field free states and therefore, different treatment becomes necessary for the interpretation of the interaction. This oddity, however, is the source of a plethora of interesting phenomena of modern nonlinear optics among which, XUV light generation, synthesis of XUV attosecond pulses, above threshold ionization, as well as their modern applications for metrology. The key process behind these phenomena is ionization of atoms driven by the strong laser field.

#### 1.1.1 Mechanisms of atomic ionization

Atoms are ionized when a photon of energy  $\hbar\omega$ , greater than the ionization potential  $I_p$ , is absorbed according to the photoelectric equation:

$$E_k = \hbar\omega - I_p \quad (1.1)$$

with  $E_k$  the final kinetic energy of the ejected electron.

However, if an atom is exposed to a strong electric field, ionization can take place in spite of the above consideration. The dominant mechanism behind ionization process in this case is effectively depending on the field strength. A way to define systematically

different regimes of atomic ionization was given by Keldysh [25], introducing the parameter  $\gamma$  defined as:

$$\gamma = \left( \frac{I_p}{2U_p} \right)^{1/2} \quad (1.2)$$

essentially comparing the time it would take an atom to ionize, with the oscillating period of the field.  $U_p$ <sup>1</sup> is the quiver energy of the electron inside the field defined as:

$$U_p = \frac{e^2 E^2}{4m\omega^2} \quad (1.3)$$

where  $E$  the electric field of light,  $\omega$  its frequency,  $e$  and  $m$  the charge and the mass of the electron. When  $\gamma > 1$ , that is, ionization lasts longer as compared to the field period, multiphoton ionization is dominating and to a certain extent perturbative treatment of the relevant dynamics is possible. Under this scheme, an atomic or molecular system absorbs a certain number of photons before ionization is reached as illustrated in figure 1.1(a).

On the other hand, if  $\gamma < 1$ , or equivalently  $I_p < 2U_p$ , atomic ionization is governed by the tunneling of the electron through the strongly suppressed by the laser electric field atomic potential, as shown in figure 1.1(b). This regime is what is referred to as optical field ionization. Reaching it, is not only possible by extremely strong laser fields, but also by keeping the frequency of the field low, as dictated by the equation 1.3. An electric field interacting with atoms can be considered of low frequency, if its period is safely longer as compared to a typical period of the orbit of a bound electron of the atom in a classical consideration [26]. For the hydrogen atom where  $T_0 \sim 150$  as for the first Bohr radius, a modern infrared-optical laser field with  $T \sim 2.5$  fs or more, can be safely classified as low frequency one. For such a frequency reaching the  $\gamma < 1$  condition for tunnel ionization, lets say for Argon (Ar,  $I_p=15.76$  eV), it would be needed an intensity of  $3 \times 10^{14}$  W/cm<sup>2</sup> for  $\gamma = 0.66$ . These conditions, are now typically attainable by a modern femtosecond laser. In the excessive case illustrated in figure 1.1(c), the atomic potential is completely suppressed and the electron escapes without tunneling. When the Keldysh parameter is close to unity  $\gamma \sim 1$  a safe approximation would call for a treatment where tunneling and multiphoton dynamics are both taken into account.

Ionization rates, as expected, are inextricably connected to the aforementioned mechanisms. Within the regime where our interest is focused in this work,  $\gamma < 1$ , ionization is treated successfully by mainly two analytical approximations. The first one is the Keldysh [25] approximation, whilst the second is the Ammosov-Delone-Krainov approximation or shortly ADK [27]. Both rely on the adiabatic approximation, that is, ionization occurs fast enough so that the light field can be considered practically static all along the ionization process. This basic consideration emerging from the fact that  $\gamma < 1$ , limits their validity and applicability for different regimes of ionization. The Keldysh approximation completely neglects the atomic potential for calculating the ionization rates. The ADK ionization rate on the other hand, includes the particular atomic parameters, resulting in

---

<sup>1</sup>Or directly in eV is possible by:  $U_p(\text{eV}) = 9.33 \times 10^{-14} I(\text{W/cm}^2) \lambda^2(\mu\text{m})$ .

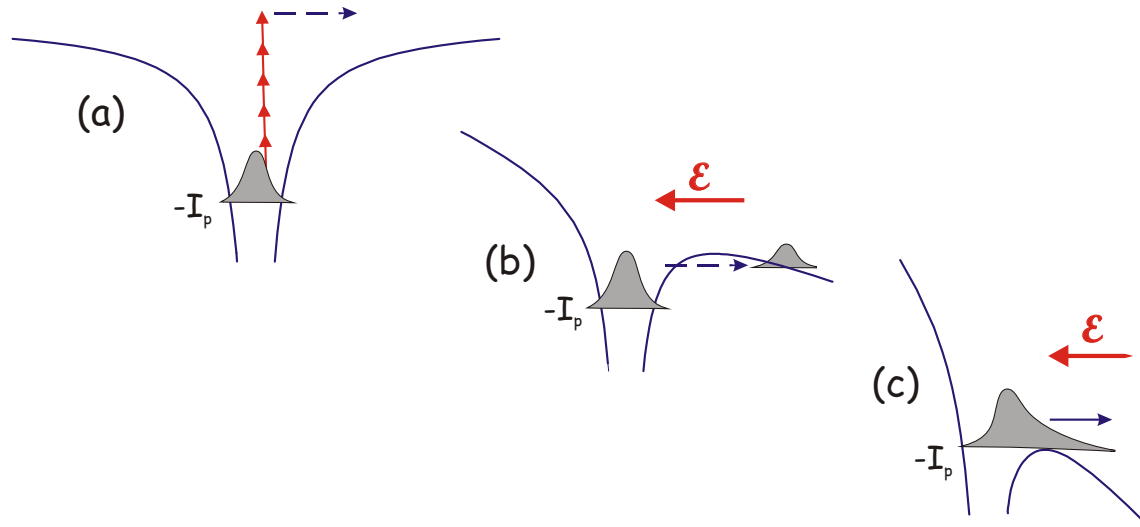


Figure 1.1: Mechanisms of atomic ionization. Blue line atomic potential. At low or moderate intensities where  $\gamma > 1$ , ionization is reached by the absorption of sufficient number of photons ( multiphoton ionization) (a). For higher laser intensities ( $\gamma < 1$ ) tunneling ionization dominates (b). At even higher intensities the barrier is suppressed and the electron escapes without tunneling(c).

remarkable accuracy in comparison with ab-initio calculations [28]. A more complete approximation for  $\gamma$  independent regimes has been recently proposed in [29], where the abrupt variation of the laser field from cycle to cycle rather than a cycle average is considered.

A general and common feature of both approximations is the exponential dependence of the ionization, as a function of the electric field. For the Hydrogen atom for example the ADK rate can be expressed as:

$$W_H \propto I_p \exp(-4I_p/3h\omega_t) \quad (1.4)$$

where  $\omega_t = eE/(2mI_p)^{1/2}$ . The probability of ionization at an instance  $t$  of the field can be written as:

$$P(t) = 1 - e^{-\int_{-\infty}^t W(t')dt'} \quad (1.5)$$

This equation allows the calculation of the total ionization yield across the temporal profile of a pulse.

### 1.1.2 Extreme ultraviolet light generation by optical field ionization and recombination

XUV light in form of odd harmonics of a fundamental frequency is generated when atoms are exposed to high intensity laser light pulses. After the revolution that Ti:Sapphire lasers [30], [31] and chirped pulse amplification [32] introduced to the field of ultrafast optics,

high harmonics spectrally spanning from UV to soft X-Rays [33], [34], [35], [36], are easily generated by focusing laser pulses into atomic gas targets. The phenomenon was initially observed by [37]. A high harmonic spectrum over a broad range is shown in figure 4.3 of chapter 4 and a calculated one in figure 1.3. XUV spectra generated from ultrashort pulses, are presented at several sections of this thesis as well. The constant efficiency over several harmonic orders and an abrupt cut-off, are the key characteristics and imply that a perturbation based treatment of the interaction, will fail to explain the behavior of this spectrum [38]<sup>2</sup>. A three step quasi-classical model, proposed by [39], has allowed the qualitative description of harmonic light emission, supporting at a same time a simple and intuitive picture of the underlying processes. According to this model the electron tunnels to the continuum through the suppressed by the field barrier (a), is accelerated driven by the laser light field (b) and re-scatters or recombines on/with the parent ion (c). This is shown schematically in figure 1.2.

- **Optical field ionization**

in principle ionization is possible at every instance of the interaction between a strong field and an atom, due to the quantum nature of the processes. Equation 1.4 however, along with the discussion in the previous section, suggests that, when the atomic barrier is suppressed, that is, when the field reaches a local maximum, this probability grows exponentially. It is therefore reasonable to consider, that tunneling ionization generates instantaneously an electron into the continuum, with the highest probability around the field peak.

- **Electron motion inside the field**

Steered by the electric field of the laser, the electron can in principle return to vicinity of the atom, provided that it is born at a field phase that supports such a returning trajectory. The maximum kinetic energy an electron accumulates before reencountering the core, is also depending on the tunneling instance  $t$ . By means of simple treatment of the electron motion, that is, integrating the total energy that an electron accumulates when born at different instances of the field, it turns out that the maximum kinetic energy is  $3.17 U_p$  for electrons generated around the field maximum and precisely  $17^\circ$  after the field peak. If to this energy one adds the  $I_p$  to be accumulated upon recombination, then a compact formula for the maximum energy can be written as:

$$E_{max} = I_p + 3.17U_p \tag{1.6}$$

---

<sup>2</sup>A perturbative treatment of the interaction would predict an exponential drop of the efficiency, as a function of the harmonic order.

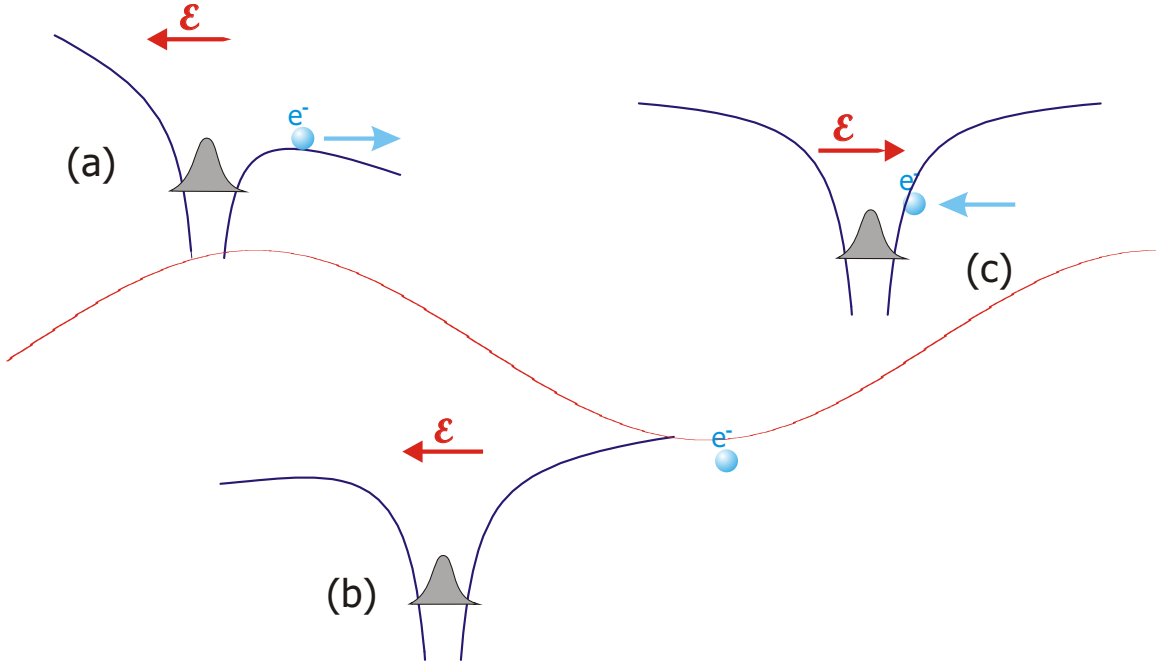


Figure 1.2: Illustration of the three step model. a) tunneling b) excursion through the continuum and accumulation of kinetic energy from the field. c) recombination with the parent ion and generation of photons. The positioning under the field oscillation (red line) is roughly defined in the figure, in order to include also generation of lower energies as discussed in the text. The maximum energy of a recombining electron corresponds to tunneling at approximately  $17^\circ$  after the field maximum.

- **Recombination with the parent ion**

To release its energy in form of photons, an electron has to recombine with the parent ion upon returning to its vicinity. This can be regarded as a manifestation of the momentum conservation principle, where the presence of a third body is necessary for the emission or absorption of radiation<sup>3</sup>. The recombination takes place with a certain quantum mechanical probability and along with ionization, they are the key parameters to determine the single atom response in terms of high harmonic light conversion. It becomes apparent by equation 1.6 and 1.3, that both laser frequency and field strength determine the cut-off and therefore, generation of harmonics of longer wavelength fundamental could result at the same maximum energy at moderate intensities [38], [41]. The accumulation of kinetic energy several tens of times that of the fundamental photon energy of the field by an electron, during its excursion through the continuum, is not coming free of expense. Dispersion of the electron wavepacket, direct consequence of its quantum nature, results in a decrease of the probability to encounter the core upon its return decreasing the recombination probability accordingly. A free electron wavepacket for example spatially confined

<sup>3</sup>In the relativistic regime where different treatment is necessary [40] irradiation is possible.

in  $\delta x(0) = 1$  a.u., will expand according to the equation 1.7 to 20 a.u. in about 1.3 fs [42], [43].

$$\delta x(t) = \sqrt{(\delta x(0))^2 + (t/2\delta x(0))^2} \quad (1.7)$$

Two particular features need to be further discussed for completing the picture of the emission. First the constant efficiency of the XUV light generation responsible for the formation of an energetic plateau extending over several tens of eV. Second, the harmonic peaks of the plateau.

In high contrast with what perturbation theory would predict, that is, an exponential drop of the conversion efficiency as a function of the harmonic order, the plateau harmonics are generated with constant efficiency at least within an order of magnitude and over several tens of eV in the energy range [33]. The kinetic energy that an electron accumulates inside the field before returning to the core, depends precisely on the instance of its birth. Therefore, electrons generated at consecutive instances inside the field would result in the emission of different photon energies, upon their recombination. Actually, recombination is not favored by all instances of tunneling, as several trajectories of the electron never encounter the core and lead to ionization. The probability that a certain photon is generated is therefore inextricably linked with that of tunneling of an electron, at the right phase of the field. The tunneling probability on the other hand by evaluating equation 1.4, turns out to be rather similar over an extended range of phases close to the field maximum. Therefore electrons generated at different phases around the peak, accumulate different amount of kinetic energy, but recombine with similar probability and that gives rise to a constant conversion efficiency to XUV photons over an extended spectral range.

So far, we have discussed only the single re-collision case corresponding to radiation emerging from a single half-cycle of a laser field. A laser pulse however, consists of several cycles in general, and merely a few in what is to be discussed in the next paragraphs and along this thesis. As a result, over the profile of a pulse consisting of about 10-20 cycles, the generation is taking place each time an electron reencounters the core, that is, when the laser field is approximately around the zero transition. The overall emitted radiation will be the result of the interference of photons generated over consecutive cycles under the pulse envelope. A single recombination with the core is not expected to result in a spectrum with particular features as it resembles the Bremsstrahlung radiation emitted by an accelerated particle; inelastically scattered by a heavy nucleus. Accordingly, a spectral continuum up to the initial kinetic energy of the particle is emitted. However, if such a spectrum emerges every half cycle by the field vector pointing at opposite directions from peak to peak, only odd multiples of the fundamental stay in phase forming a typical harmonic spectrum with peaks appearing every  $2\hbar\omega$  with  $\omega$  the central frequency of the laser. The multi-cycle origination of the harmonic spectrum implies that the confinement of the generation within a single cycle, could result in useful coherent continua of radiation in the XUV for the synthesis of pulses with the corresponding temporal localization, depending on the bandwidth of the emitted radiation.

Apart from this quantitative picture for the generation of XUV light from laser fields interacting with atoms, the most straightforward way - though at the expense of an intu-

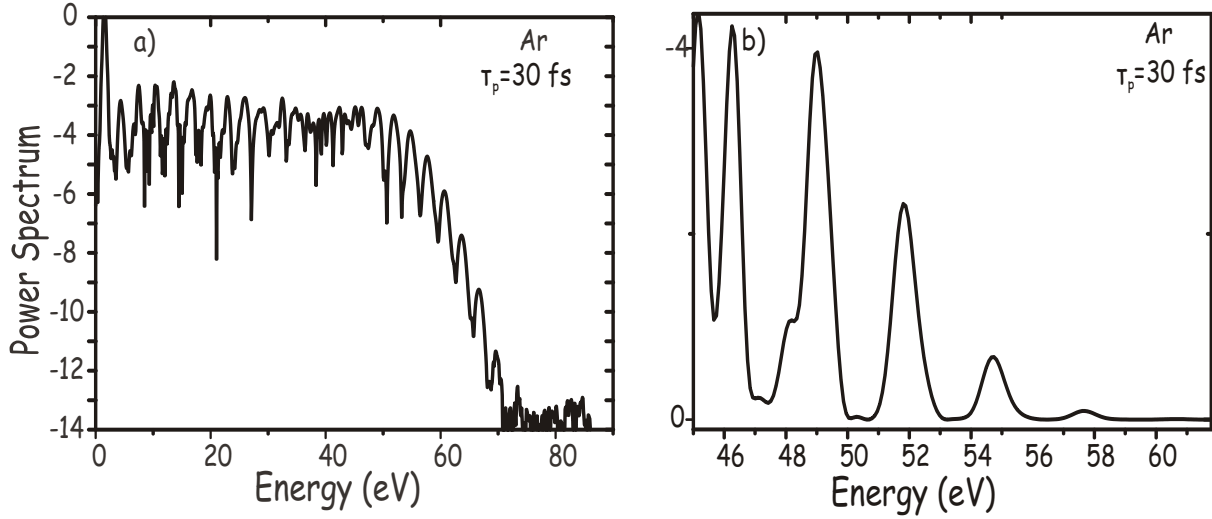


Figure 1.3: a) Calculated XUV spectrum generated by a 30 fs, 800 nm pulse, intensity  $7 \times 10^{14} \text{ W/cm}^2$  by the numerical integration of the Schrödinger equation. The plateau and the abrupt cut-off sufficiently resemble behavior of the experimental spectra. b) Cut-off regime plotted in linear scale.

itive picture sometimes - to reach accurate results, is to directly solve the time depended Schrödinger equation (TDSE) with the hamiltonian modified to include the electric field term. The integration is of course possible only numerically as this differential equation is not an analytically soluble one. In the case of a single electron approximation the Schrödinger equation can be written as:

$$i\hbar\dot{\psi} = \left( \frac{\hat{p}^2}{2m} + V(r) + \hat{H}' \right) \psi \quad (1.8)$$

with

$$\hat{H}' = -\frac{e}{mc} A(t)\hat{p} + e^2 A^2(t)/2mc^2 \quad (1.9)$$

where  $V(r)$  is the atomic potential,  $A(t)$  the vector potential,  $\hat{p}$  the momentum operator,  $m$  the mass of the electron and  $c$  is the speed of light. This kind of approximation treats even multi-electron atoms as single electron ones, where, by means of a model-potential, the features of particular atomic species are taken into consideration. A typical harmonic spectrum resulting from the direct integration of the Schrödinger equation is shown in figure 1.3 and has been calculated by a code developed by the author [44] where the interaction is treated in one dimension. Even with this relatively simplified consideration, the main spectral features of laser driven XUV light generation are sufficiently resembled with a broad plateau and an abrupt cut-off.

An approximation developed by Lewenstein [45] - in principle an extension of the three step model discussed previously - approaches the accuracy of a numerical TDSE calculation and on the other hand supports an intuitive picture. The premise behind this approach is the assumption that a) all atomic bound states are neglected except the ground state and b) only the part of the Hamiltonian describing the electron motion inside the field is considered. These two assumptions make Schrödinger equation exactly soluble. Modification of this model to accurately include the influence of the atomic potential to the continuum states, can provide results [28] comparable with the numerical solution beyond the qualitative approximation. Though this approach will not be described in detail here, it is important to discuss its most outstanding contribution to the understanding of the mechanism of XUV light generation, which is, the intensity dependence of the atomic dipole emission. According to this approximation, two main classical-like trajectories of the electron could lead to emission of photons in the plateau, with the same final energies but with different phases. These orbits, usually are referred to as the short and the long trajectory and are distinguished by the time it would take to the electron to return to the core vicinity. For the efficient generation of high harmonics and their application for the synthesis of attosecond pulse trains to be discussed in section 1.3, separation of light photons resulting from these different trajectories has turned out to be essential [46], [47] as they affect critically the pulse duration of the XUV bursts of the train.

### 1.1.3 Light Polarization effects

If the polarization of light is not linear, the interpretation of emission process using the quasi-classical picture is as well possible [48]. When atoms are exposed to elliptically polarized fields the electron escapes in the direction of the strongest polarization component of the light field into the continuum with the highest probability. Driven by the electric field of light, the electron has a finite probability to re-encounter the core, owing to its quantum character as there is no crossing of the core with any possible classical trajectory. As a result, a quick drop of the efficiency of XUV light generated by elliptically polarized fields, is expected. The effects have been studied comprehensively [49], [50], [48] while the involvement of pulses with non uniform polarization across their temporal profile for the synthesis of isolated attosecond pulses, has resulted substantial progress and recently, encouraging experimental evidence has been provided [51], [52].

## 1.2 Macroscopic response

Experimentally, XUV photons are not irradiated only by a single atom, but rather from a sample of atoms emanating from a nozzle inside the focus of an intense laser beam. Therefore, the efficiency, and the spatiotemporal characteristics of the generated XUV, are influenced by propagation effects [33]. The generation of XUV light in gases is mainly affected by the interplay of four phenomena.

- The intensity dependence of the atomic dipole phase and consequently of the generated XUV light. This term is inextricably related to the trajectory (short or long path), that the electron follows before coming across the core [46]. A phase for the dipole as  $\varphi \sim -U_p$  is expected.
- Dispersion introduced by the ionized medium to the fundamental. Though the formed plasma does not affect the XUV light, and neutral atoms contribute only slightly to dispersion, phase shifts introduced gradually by free electrons to the fundamental wave lead to phase mismatch. The coherent length in this case is given by:

$$L_{fe} = \frac{2\pi c\omega_L}{\omega_p(\tau)^2 N} \quad (1.10)$$

with  $\omega_L$  the frequency of the fundamental,  $N$  the harmonic order and  $\omega_p$  the plasma frequency, resulting from the generated electrons.

- The Gouy phase. This is a geometric source of de-phasing between the fundamental field and the harmonics. The coherence length in this case inside the focus is:

$$L_c = \frac{\pi^2 w_0^2}{N\lambda_0} \quad (1.11)$$

with  $w_0$  the  $1/e^2$  of the beam radius at the focus and  $\lambda_0$  the central wavelength.

- Reabsorption of photons inside the focus resulting in inner shell excitation of the gas atoms.

The above reasons prevent efficient phase matching in the laser focus and along with the limited single atom response, restrict the efficiency for the generated XUV light; typically of the order of  $10^{-7}$  for plateau radiation. Experimental attempts to confront the above constraints and to attain phase matching include: guiding of the fundamental through filled straight and modulated waveguides [36], [53], long focal length gently focusing [54], non-adiabatic phase matching based on few cycle laser pulses [35], [55], [56] and self guiding of the fundamental in the generation medium [57].

### 1.3 A train of attosecond pulses

Proposed already in the year 1990 by Hänsch [58], and Farkas [59], a series of spectral modes could serve - if properly timed - to the synthesis of attosecond pulse trains, in a similar manner that a comb of longitudinal modes in a laser cavity properly locked, generate a train of laser pulses. Furthermore,  $N$  harmonic peaks of a fundamental frequency spaced by  $2\omega_L$ , could result in a train of attosecond pulses with a pulse duration scaling as  $\sim 1/N^2$  and separated in time by  $T \sim 1/2\omega_L$ . These bursts could originate from High Harmonic Generation in a gas spectrally located in the XUV, or, over several octaves and very

efficient, by Raman scattering in molecules. In this particular case, the employment of two lasers that differ in frequency as much as the Raman shift of a medium [60], [61], [18] is necessary. Appropriate phase relationship between spectral modes is essential in all mentioned techniques. Though harmonic spectra could be measured with high accuracy almost from the very beginning after their first observation, access to the corresponding temporal domain was impeded by the lack of techniques, competent to retrieve the phase along with the amplitude of the spectral components. Further steps towards retrieval of the relative phase of a series of high harmonics had been possible by [14]. There, the XUV light generated was used to ionize atoms at a second gas jet, while the generation was dressed by the laser field. The laser field produced side bands to the harmonic peaks, linking the phase of consecutive harmonics, and allowed the determination of the phasing of a series of plateau harmonics, as well as the determination of the pulse duration of the bursts inside the train. It shall be mentioned that the internal chirp of individual harmonics, that is, the chirp within the  $\sim 1$  eV or so, broad harmonic peak, is not accessed by such a technique. A recent improved version of the technique has been employed for the determination of timing of a broad range of harmonic modes, with which information on the potential to synthesize attosecond pulse trains has been inferred [62]. Autocorrelation for a pulse train has been also possible, by employing the two photon ionization of He atoms [63]. Though their measurement - and therefore the prove of their existence - had been a challenge for years, the ultra high repetition rate (almost 1.3 fs apart) associated with attosecond pulse trains introduce difficulties for their implementation in a pump-probe scheme with a descent dynamic range. Therefore special treatment would be probably necessary. Polarization gating techniques, that take the advantage of the high sensitivity of HHG to the degree of ellipticity of the fundamental, can restrict under certain conditions the generation in a single cycle of the field and might be the way against these constraints [64]. However, isolating the generation within a single cycle of the laser field, is more effective if a few-cycle pulse is employed. In that case, the energy content of the single cycle to be gated, is still significant as compared to the energy of the entire pulse in high contrast with the case of a multi-cycle pulse. Taking advantage of the rapid intensity evolution of a few-cycle pulse, a temporal gate can be established with appropriate control of the phase and adequate spectral filtering of the XUV generated light, as presented in the following section.

## 1.4 Soft x-ray generation within a few cycles and synthesis of attosecond pulses

The generation of laser pulses consisting of a few light field oscillations ( $T_L = 2.5$  fs) has opened the way for several applications in optics and probably a new era for ultrafast Science. For the technology of extreme ultraviolet light there are numerous advances that few cycles pulses have introduced. A glimpse to equations 1.4 and 1.5 reveals that the ionization probability scales not only with the intensity of the field but also on the interaction time. Indeed, when ionization is studied from a purely quantum perspective,

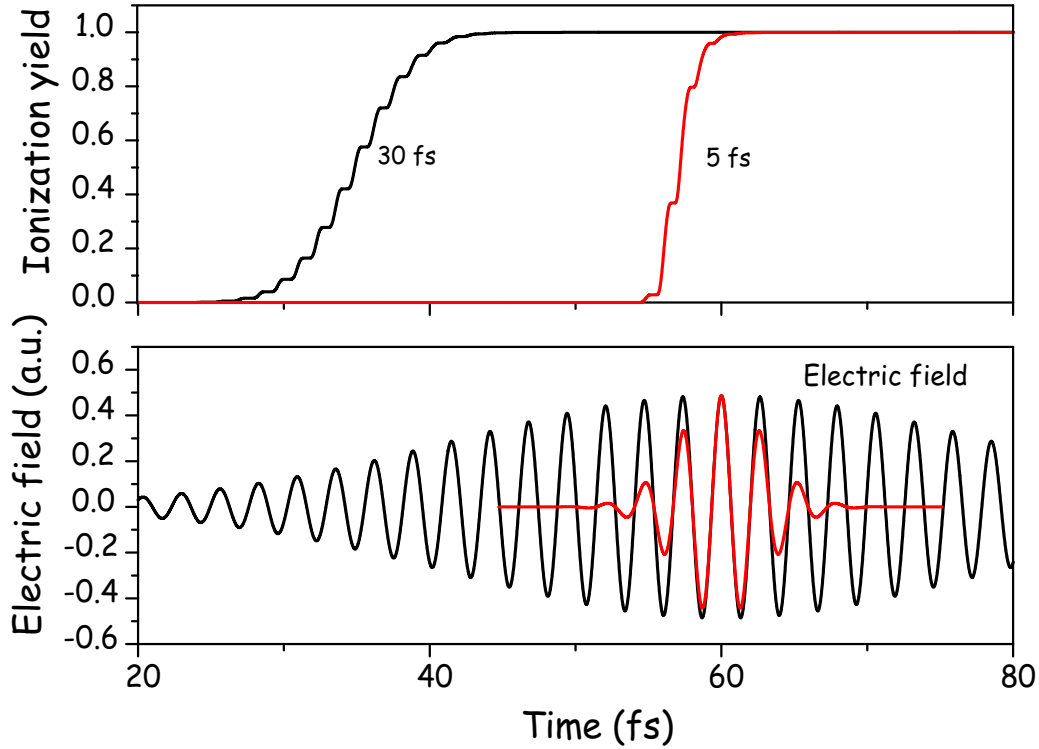


Figure 1.4: Ionization of H as predicted by the ADK approximation (upper panel) at high  $3\text{-}5 \times 10^{15} \text{ W/cm}^2$  for a 30 fs (black) and a 5 fs (red) laser pulse (lower panel). Ionization reaches saturation well in advance before the field maximum for multi-cycle pulses. For a few cycle pulse ionization evolved until the field reaches its maximum allowing full exploitation of the attainable ponderomotive forces.

it can be considered as the consequence of multiple scattering of the electron wavepacket by the core potential, resulting in a dramatic increase of the plain waves, rather than pure atomic eigenstates employed for its reconstruction. Owing to this essential fact, when multiple-cycle pulses with high intensity are used, ionization of atoms could reach saturation long before the peak of the pulse resulting in inefficient frequency conversion to XUV photons [43]. On the other hand, when few cycle pulses are employed, the ionization threshold is reached only by field oscillations close to the peak enabling in principle, the exposure of atoms at higher fields and complete exploitation of the attainable intensities. This is illustrated in figure 1.4 where ionization of an H atom in the presence of a 30 fs pulse and a 5 fs pulse at 800 nm, is plotted as a function of time. For the calculation of the ionization yield the ADK scheme introduced in section 1.1.1 has been employed.

The influence of the alluded issues, on the efficiency of generation of XUV light has been demonstrated theoretically and experimentally by [43], and recently [56] with the generation of photons with energies exceeding the 1 keV that has opened the door to the exploitation of coherent X-rays for Science and applications.

## 1.4 Isolated attosecond pulses

---

$\tau_L/T_0$	$\Delta/(E_L^2(t))_{\max}$	$\Delta(\hbar\omega)_{cont}@125eV$
2	0.16	20 eV
3	0.07	8.8 eV
4	0.04	5.0 eV
5	0.03	3.8 eV

Table 1.1: Expected spectral width of the cutoff continuum as a function of the pulse duration.

Synthesis of single attosecond XUV pulses, based on the aforementioned phenomena, as has been pointed out already, demands isolation of light generated within a single recombination of an electron driven by a laser pulse.

Whereas a multicycle pulse steers electrons to a sequence of re-combinations; translating to a train of XUV bursts in time domain, a single re-collision, calls for a light field that drives the electron only once to the vicinity of the parent ion. Definitely, even a few-cycle pulse does not directly comply with this request, because, even in that case, electrons driven by the field will reencounter the core a couple of times before the end of the pulse.

According to equation 1.6, the XUV spectrum produced by a single re-collision, strongly depends on the accumulated energy by the electron, before reencountering the core. For a pulse consisting of several oscillations of the field, the maximum accumulated energy by an electron is approximately constant for several cycles around the peak and the corresponding XUV spectral intensity accordingly comparable. For a few-cycle laser pulse, due to the steep build up of the field from cycle to cycle, each re-collision would intuitively be expected to end up with a different final energy, with the highest one to be attained by the most intense cycle of the few-cycle waveform. Therefore, XUV light emitted in the regime of the cut-off by a few-cycle pulse, shall possess the signature of a single recombination of the electron with the core and in principle, the unique potential to synthesize an isolated attosecond pulse. In this context, the accurate selection of photons generated by a single recombination, could allow the synthesis of a pulse as short as the fourier limit of the generated spectrum suggests. Looking the same event from the spectral domain perspective, a single laser driven recombination would lead to a continuum spectrum. Using equation 1.6 and the linear dependence of the cut-off energy as a function of the intensity, one could estimate the width of this continuum  $\Delta(\hbar\omega)_{cont}$ , by taking into account the intensity difference between the strongest half cycle and its neighboring one. Under these assumptions the continuum bandwidth can be expressed as:

$$\Delta(\hbar\omega) = (\hbar\omega_{cutoff} - I_p) \frac{\Delta}{(E_L(t)^2)_{\max}} \quad (1.12)$$

The ration ( $\Delta$ ) is the intensity difference for consequence sub-cycles and  $(E(t)^2)_{\max}$  is the intensity of the stronger one. Results for a central energy (of 125 eV) are shown in table 1.1 for different pulse duration settings ( $\tau_L/T_0$ ), where  $T_0$  is the field period. Similarly for the range of 90-100 eV, which is extensively employed in experiments discussed in the next

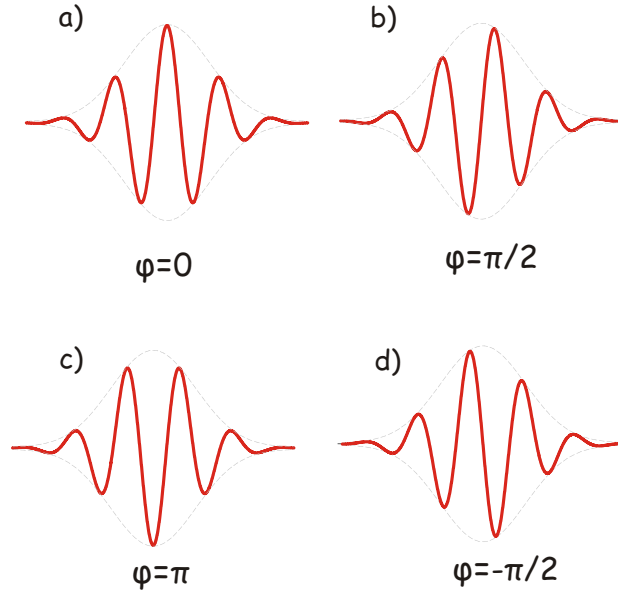


Figure 1.5: Resulting few-cycle waveform under various phase settings for the carrier with respect to the envelope peak (CE phase).

chapters a  $\tau_L/T_0 \leq 2.5$  suffices for the formation of a continuum of  $\sim 10$  eV.

The previous discussion assumes pulse with a field waveform as shown in figure 1.5.a where the field maximum is located in the middle of the few-cycle pulse, coinciding with the peak of the surrounding envelope. However, for few-cycle light waveforms the carrier frequency is not necessarily locked with the envelope of the pulse and various waveforms can result under the pulse duration, as shown in figure 1.5. Actually, the difference in group and phase velocity, inside a laser cavity - result of the dispersion of the active medium - leads to the contrary, namely: different phase for consecutive pulses. This important point will be discussed in detail in chapter 3. Taking the envelope of a short pulse as shown in figure 1.5 as a reference, the pulse in (a) is referred to as a cosine pulse because it resembles a cosine wave if the axes zero is defined by the envelope peak. Accordingly, a shift of the phase by  $\pi/2$  results in a sine pulse. (c) and (d) are the field symmetric of a cosine and a sine. A reference to them as anti-cosine and anti-sine is possible. If the pulse envelope becomes comparable with the field oscillation, the phase of the latter can result in dramatic consequences on the shape of light waveform as it was pointed out. In the case of a long pulse, clearly, switching the phase does not result in any observable intensity redistribution among successive cycles. The lower Panel of figure 1.4 where the field of a few cycle and a multi-cycle pulse are drawn in comparison illustrates this perspective. In order to invoke this principle for the generation of isolated attosecond pulses, that is, every laser pulse to spawn a single attosecond burst, it becomes clear at this point, that the control over the phase is essential. Figure 1.6 illustrates the effect of the phase on the generation of XUV light. For a certain bandwidth close to the cut-off, only a single half cycle can reach

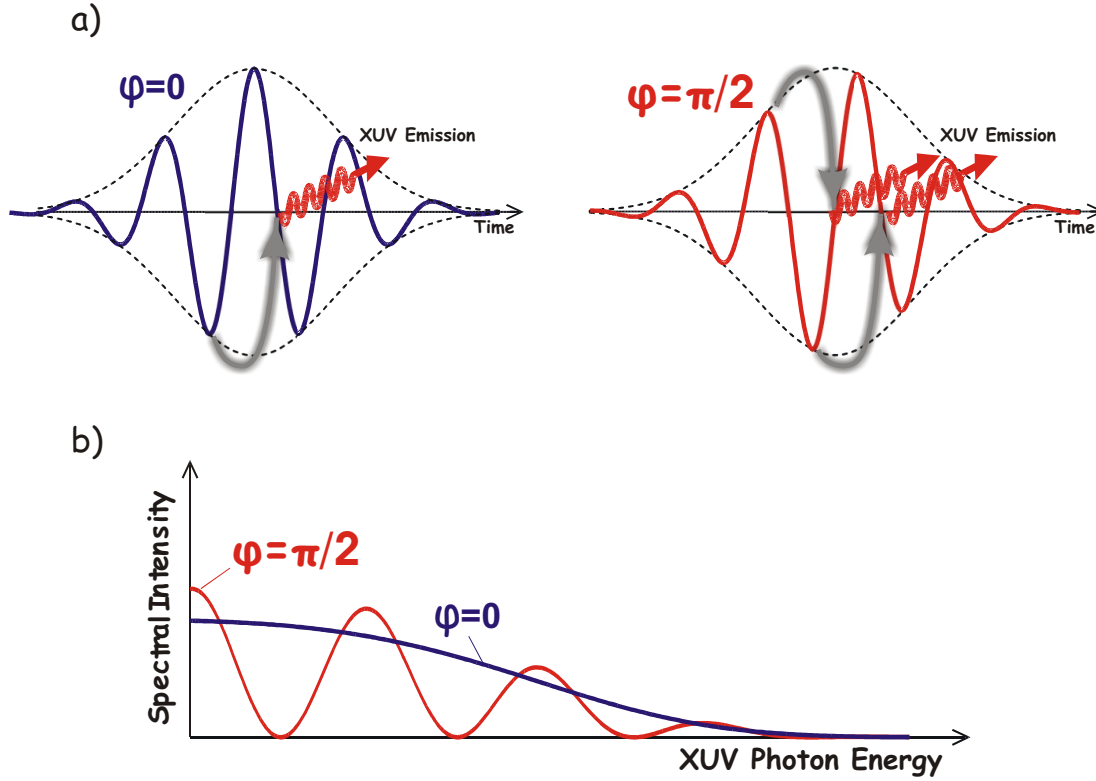


Figure 1.6: Temporal and spectral manifestation of the generation of XUV pulses at different phase settings of a few-cycle laser pulse. (a) With  $\phi = 0$  (cosine waveform) the generated photons are confined to one single burst, whilst for  $\phi = \pi/2$  the threshold for emission of XUV photons around the cut-off is exceeded twice within the laser pulse. As a result the corresponding spectrum is continuous or quasi-periodically modulated (b).

the appropriate intensity threshold to emit photons for the case of a cosine like waveform, whilst for a pulse with the phase shifted by  $\pi/2$ , two half cycles can exceed the intensity threshold and result in XUV emission. In the lower panel the spectral manifestation of the above description is illustrated. A single re-collision translates to an XUV continuum, while a highly structured spectrum - result of spectral interference of consecutive XUV bursts - manifests generation at least twice within the pulse envelope. Therefore, estimations of a potential duration for the isolated XUV burst, based on the spectra emitted by a single recombination, shall always include the phase factor that defines not only the contrast but also the ability to restrict the generation only once under the pulse envelope. The ability to extract this important information about the localization of XUV generation from the spectral domain is related with the fact that a few-cycle pulse reduces dramatically the complexity of the process behind a harmonic spectrum, produced by a multi-cycle laser pulse. On the other hand the necessity of control of the phase of a few-cycle ultraintense pulse, is a challenge that emerges simultaneously with the aforementioned advantage.

## 1.5 Above threshold ionization (ATI)

Not all electrons driven back to the atomic core by a strong laser field recombine to release XUV photons. Actually the cross section of the recombination process is rather small as dictated by the conversion of the fundamental to XUV photons. Those electrons that do not re-combine, are re-scattered by the core, leave the atom vicinity with kinetic energy corresponding to a photon number much higher than necessary to reach the ionization threshold. The process is manifested in the spectral domain by a series of photoelectron peaks separated by the energy of the fundamental photon. The plateau behavior discussed for harmonics so far is also present for ATI electrons, implying the existence of the same mechanism behind the two phenomena. Today the effect is understood within the framework of the three step model as well [39]. The fact that the same mechanism governs XUV light generation and ATI, implies that at the few-cycle limit a series of interesting phenomena are to appear when the interaction of atoms with short pulses is taking place. Recent experiments with the involvement of phase stabilized pulses, have unveiled a plethora of interesting features with a huge range of applications for the determination of the absolute phase of short pulses [65], [66], or even the demonstration of the double slit experiment for electrons in the time domain [67].

## *1.5 Above threshold ionization*

---

# Chapter 2

## Schemes for temporal measurements on an attosecond time scale

The theoretical approaches concerning the generation of attosecond pulses in the XUV and X-ray regime, as well as for steering the generation process by means of waveform control of few-cycle light pulses, have been introduced in the preceding chapter. However, generation of attosecond pulses shall be always combined with a competent measuring technique for their qualitative and quantitative characterization. Characterization of attosecond pulse trains, has been achieved up today by means of the techniques mentioned in chapter 1. For the experiments discussed in chapter 5, aiming the characterization of isolated attosecond pulses and in chapter 6 for direct tracking of the evolution of light waveforms, the technique of the atomic streak camera is employed. This chapter is devoted to the introduction of this concept, and how its employment could allow gaining temporal access to phenomena evolving on an attosecond time scale.

### 2.1 Principles of a streak camera

Before presenting the concept of a streak camera operating on an attosecond time scale, a short introduction to the conventional streak camera is essential. The streak camera was invented by [68], [69] and in principle, incorporates ideas overtaken from an oscilloscope as well as from a conventional film camera. While the conceptual impact of the former to the design of a streak camera is more apparent, it shares several common features with the latter as well. Here instead of using a sequence of film frames to record the time evolution of an event, the image is streaked and projected in a single slide. The streak camera principle is illustrated in figure 2.1. An optical pulse or waveform to be characterized, impinges on a photocathode and generates a backside photoemission of an electron bunch, that in principle imitates the temporal structure of the laser pulse. In the illustrated case for example, a pulse consisting of a double feature generates two electron bunches of similar temporal shape. The generated electrons enter a capacitor, where a fast temporally rising voltage applied to its plates forms a fast ramping electric field between them. If the

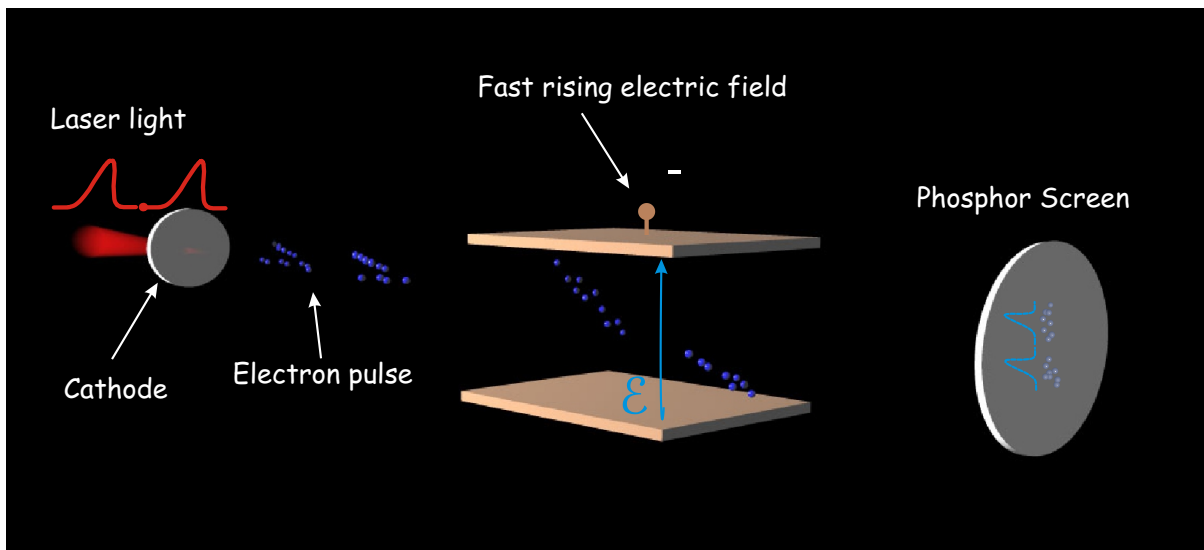


Figure 2.1: Schematic of a conventional streak camera. A laser pulse with arbitrary shape (a double optical burst here for illustrating the concept) impinges on a thin cathode and results in a back side photoemission. A fast ramping voltage, well timed with the laser pulse is applied to the plates of a capacitor. Electrons localized at the leading or at the trailing edge of the bunch are deflected asymmetrically while passing through the plates. A detector with spatial sensitivity allows resolving this asymmetry which is directly associated with the pulse duration.

field ramp is temporally faster or at least comparable with the electron bunch duration, the overall lateral displacement of an electron at the leading edge of the bunch will be significantly different than that of one at the trailing edge. By projecting the resulting bunch to a phosphor screen, a transversally elongated spot resulting from the effect of the field to the bunch will be formed. Under identical voltage conditions, a short pulse will result in a less elongated trace, as compared to that of a long one.

The deduction of the temporal information about the bunch from this trace, requires the precise knowledge of the temporal evolution of the field between the plates, as well as the degree of synchronization between the electron bunch and this field. Alternatively, a temporally characterized bunch could allow the retrieval of the fast electric field ramp.

At a very first glance, the concept does not seem to face any severe limitation as related to the shorter pulse that could be characterized. The experimental implementation of these ideas however, confronts multiple bottlenecks that so far have resulted to a maximum achieved temporal resolution for streak cameras, of the order of a few hundreds of femtoseconds. A key limitation arises from the lack of perfect synchronization between the ramping electric streaking field and the generated electron replica of the optical pulse, as well as in-

trinsic energy dispersion of the generated photoelectrons on the cathode and space charge, translating to temporal dispersion of the bunch that does not any more mimic the optical pulse. Additionally, manipulation and acceleration of the generated electron replica, results in further deterioration of the temporal characteristics of the original electron bunch, reducing even further the resolution of the device.

Nevertheless, a streak camera is a device that dominates in sub nanosecond regime down to a few hundreds of femtoseconds, for time resolved applications.

## 2.2 Streak camera on an attosecond time scale

A streak camera operational on the attosecond time scale, calls for dramatic improvements or revolutionary modifications, as the temporal resolution has to be increased by almost 3 to 4 orders of magnitude as compared to a conventional one. In order to reach such a resolution, the deflecting field has to increase by several orders of magnitude, as well as the synchronization between that field and the electron bunch - an attosecond electron bunch this time - shall be better than hundreds of attoseconds. The concept of an attosecond streak camera has been put forward by Corkum and colleagues [21] and it is based on the idea that, the rapid electric field ramp of the conventional concept, can be substituted by the sub-cycle hyperfast variation of the light field of a modern ultrafast laser and under certain conditions to streak electrons with attosecond localization. The concept was proposed initially to characterize XUV attosecond pulses that imprint their temporal structure to a bunch of photoelectrons, by ionizing atoms in a gas target.

The exact imitation of the attosecond pulses by the bunch of photoelectrons can be guaranteed if two requirements are fulfilled:

- Photoionization of atoms, occurs with the same cross section across the entire spectral bandwidth of the attosecond pulse.
- The photoelectric effect is considered an instantaneous process<sup>1</sup>.

The first condition is fulfilled, provided that non resonant processes are involved including auto-ionization and Auger decay. A dependence of  $\sim \lambda^2$  for the cross section for very broadband XUV pulses might be important.

The field of light applied simultaneously, shall not induce any substantial modification at the ionization yield of the atoms to be ionized.

Provided that the attosecond pulse is mimicked by a bunch of electrons, the electric field to probe those electrons - the streaking field in accordance with the conventional streak camera - has to fulfill a series of requirements.

- It has to be precisely synchronized to the attosecond electron bunch.

---

<sup>1</sup>Though, as any atomic process the photoeffect is not expected to be instantaneous but a rather short lasting effect instead.

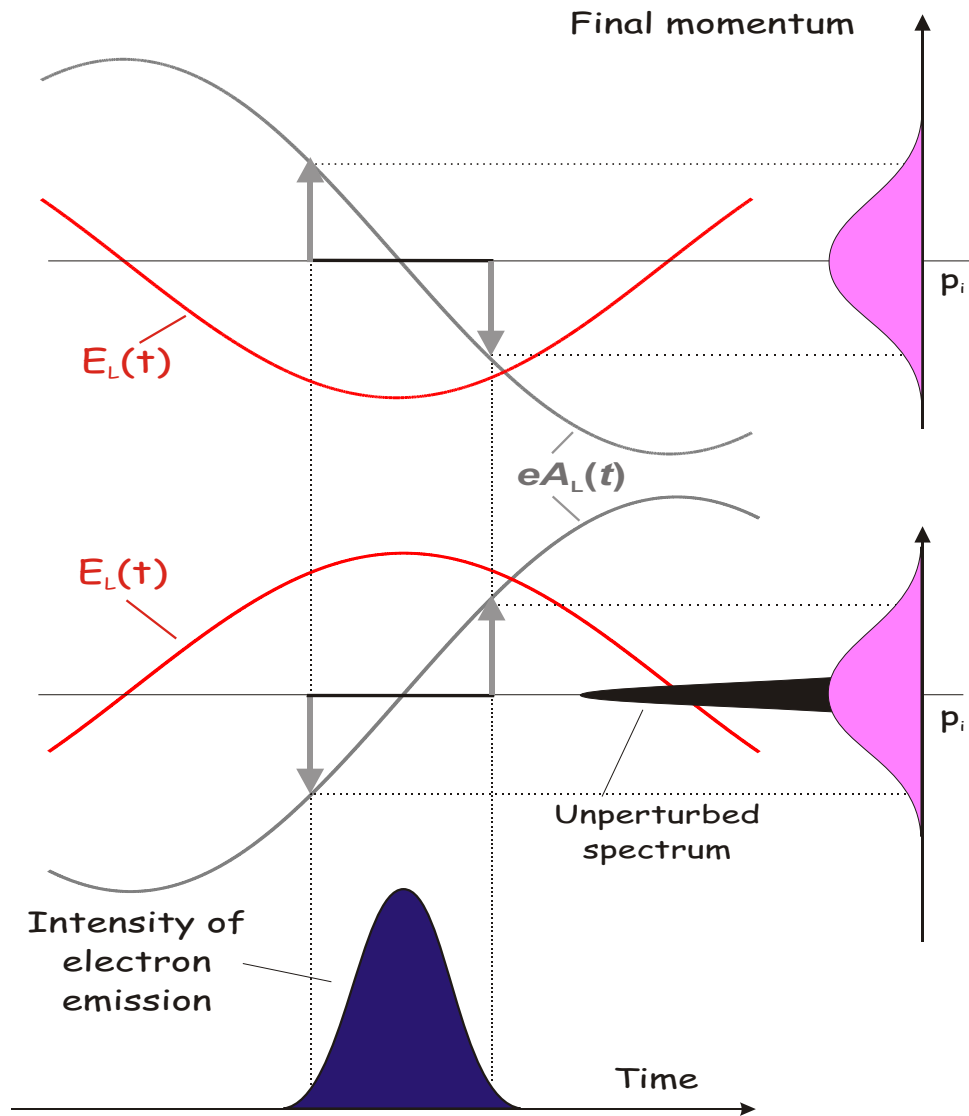


Figure 2.2: Streak camera on an attosecond time scale. An electron bunch with an initial momentum distribution (blue profile) is probed around the maximum of the electric field of a laser pulse (red line). The momentum transfer to the photoelectrons (given by the vector potential, grey line) results in symmetrically broadened final momentum distributions (pink profile), when probed at adjacent, zero transitions of the vector potential.

- It has to be precisely reproducible, since a single acquisition is not enough to retrieve the information about the attosecond pulse (This will be discussed in detail shortly).

This idea can be realized experimentally, by the synchronized focusing of the XUV pulse - of which the temporal characteristics should be retrieved - along with a laser pulse, into an atomic gas target. Such a scheme has some very interesting features. If the laser pulse is the one that generates the XUV light at an earlier stage of an experimental setup, their synchronization is ensured by the generation process, as discussed in the previous chapter. Under this scheme, the synchronization of the two fields can be affected only by a possible interferometric setup, employed to bring together the two pulses.

In case that the two fields have parallel polarizations - the case to be discussed here - the laser field is not deflecting the photoelectrons (by affecting their trajectory), but modifies their final kinetic energy instead. Given that modern electron spectrometers can attain descent accuracy and resolution, measuring the energy of the electrons rather than a spatial deflection is probably advantageous.

Before discussing the effects of the light field to an electron bunch and how this could allow retrieving its temporal structure, it is instrumental to introduce some useful formulas associated with the motion of a single electron inside an oscillating field. This is essential, since a generalization of those equations applies also for a distribution of particles. The premise behind such a consideration, is that the effects of photoionization by the XUV pulse and the motion of the electron inside the electric field can be considered independent. In this context the motion of an electron, released inside the field of the laser is described by the classical equation of motion as:

$$m\ddot{x} = qE = -qE_l = -qE_l(t) \cos \omega_l t \quad (2.1)$$

$$\dot{x} = -\frac{e}{m} \int_{t_d}^{\infty} E_l(t) \cos \omega_l t \quad (2.2)$$

where  $x$  is the displacement,  $m$  the mass of the electron,  $e$  the electron charge, and  $E$  the electric field oscillating at a frequency  $\omega_l$ . After the end of the pulse and with the adiabatic approximation for the field variation  $dE/dt \ll E_l \omega_l$  the velocity component that is added to the final velocity of the electron parallel to the electric field is:

$$u_l = \frac{e}{m} \frac{E_l(t) \sin \omega_l t_d}{\omega_l} = \sqrt{\frac{4U_p(t_d)}{m}} \sin \omega_l t_d \quad (2.3)$$

The final energy is:

$$W_f = W_0 - U_p(t_d) + U_p(t_d) \cos 2\omega_l t_d + \sqrt{8W_0 U_p(t_d)} \sin \omega_l t_d \quad (2.4)$$

where  $W_0$  the initial kinetic energy of the electrons entering the field. Under the assumption that  $W_0 > U_p(t_d)$  the equation can be written as:

$$\Delta W = W_f - W_0 \approx \sqrt{8W_0 U_p(t_d)} \sin \omega_l t_d \quad (2.5)$$

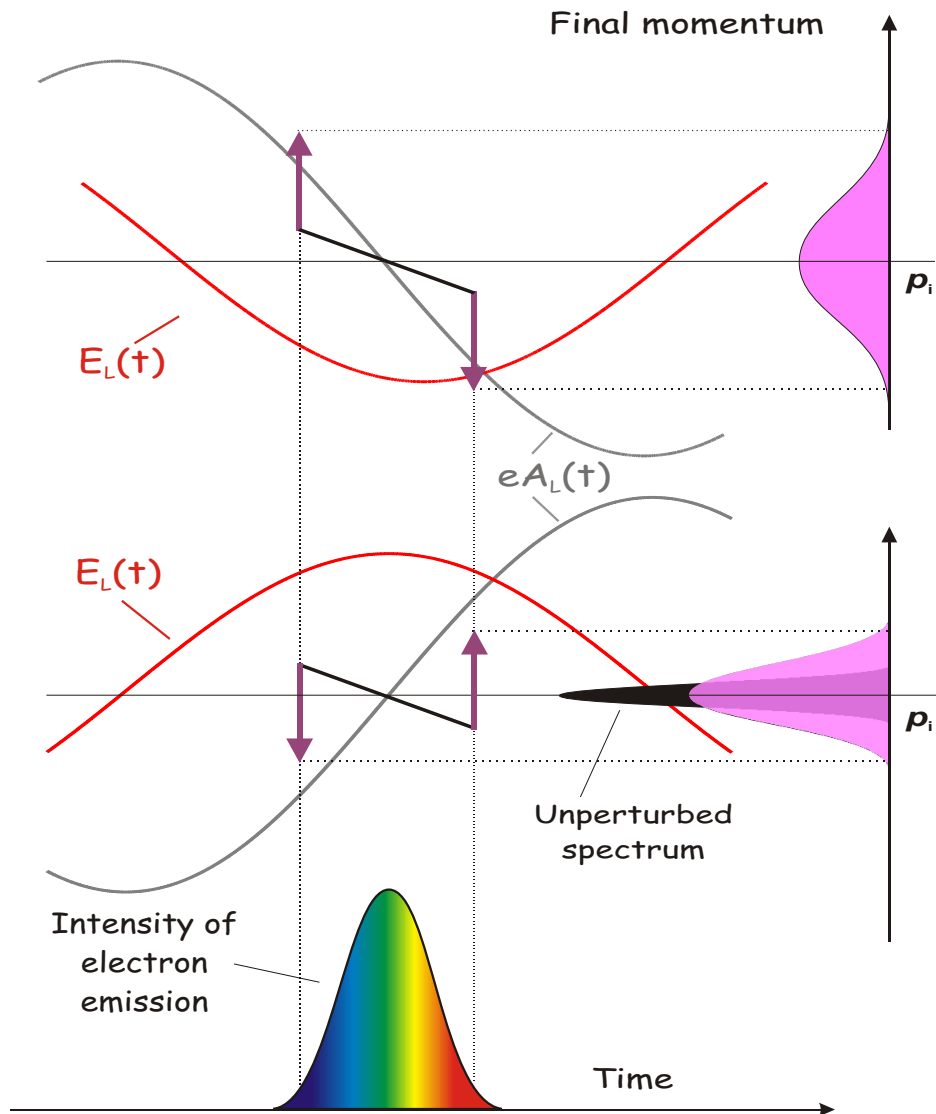


Figure 2.3: The principle of the atomic streak camera for the case of a linearly chirped momentum distribution of the electron bunch. Non identical final momentum distributions when the bunch is probed at consecutive zero transitions of the vector potential, allow the detection of the linear chirp and its retrieval (see text).

The momentum change is related with the vector potential of the field, as:

$$\Delta p(\vec{r}, t) = e \int_{t_b}^{\infty} E_l(r, t) dt = e A_l(\vec{r}, t_b) \quad (2.6)$$

where  $E_l(r, t)$  is the electric field,  $t_b$  the release instance, and  $\vec{r}$  the spatial coordinate. This fundamental equation along with equation 2.5, are the key for most of the techniques and results to be discussed in this thesis. Additionally, this equation dictates that no momentum exchange is expected if the electron is released before the pulse, in agreement with the fundamental principle that free particles do not absorb radiation. If instead a bunch of electrons, with a momentum (or energy) distribution given by 2.7 is employed:

$$\sigma(p) = \int_{-\infty}^{\infty} n_e(p, t) dt \quad (2.7)$$

The effect of the field to the final distribution can be written as:

$$\sigma(p) = \int_{-\infty}^{\infty} n_e(p - e A_l(t), t) dt \quad (2.8)$$

where  $n_e$  is the number of electrons and  $p$  the momentum. The initial momentum distribution can be produced by the photoionization of atoms in gas phase, and imitates the temporal characteristics of an XUV pulse.

Figure 2.2 illustrates the effect of the light electric field, to an attosecond electron bunch precisely synchronized to the field. If we observe electrons at the direction of the light polarization, the field results in a modification of the final kinetic energy of the electrons initially ripped off from the atom, by the XUV burst. In this introductory case, an electron bunch generated by a Fourier transform limited pulse, is probed at two consecutive zero transitions of the vector potential. For the analysis of the concept through the rest of the paragraph, the vector potential will be considered instead of the electric field. The reason is that the vector potential, is proportional to the momentum imparted to the particles, depending on their generation time according to the equation 2.6 and therefore supports an intuitive picture. Electrons born at different instances accumulate different amount of momentum (black arrows) from the field according to 2.6. If the electron bunch is synchronized with a zero transition of the vector potential, the corresponding final momentum distribution (pink) is broadener as compared to the field free spectrum (black). If the electron bunch is probed at a consecutive zero transition ( $\pi$ ), the action of the electric field leads to identical broadening as compared to the previous case.

If a linearly chirped XUV pulse, is employed to generate an electron bunch, the temporal distribution of electrons inside the bunch mimics the chirp of the light burst in analogy with the previous discussion. Low energy electrons for example at the leading edge, and high ones at the trailing edge would correspond to a positive chirp. In this case, because of this asymmetry, when the bunch is probed at subsequent zero transitions of the vector potential (maxima of the field), non-identical broadened final momentum electron distributions will be formed, figure 2.3. This feature is the one that provides a direct link between a relatively

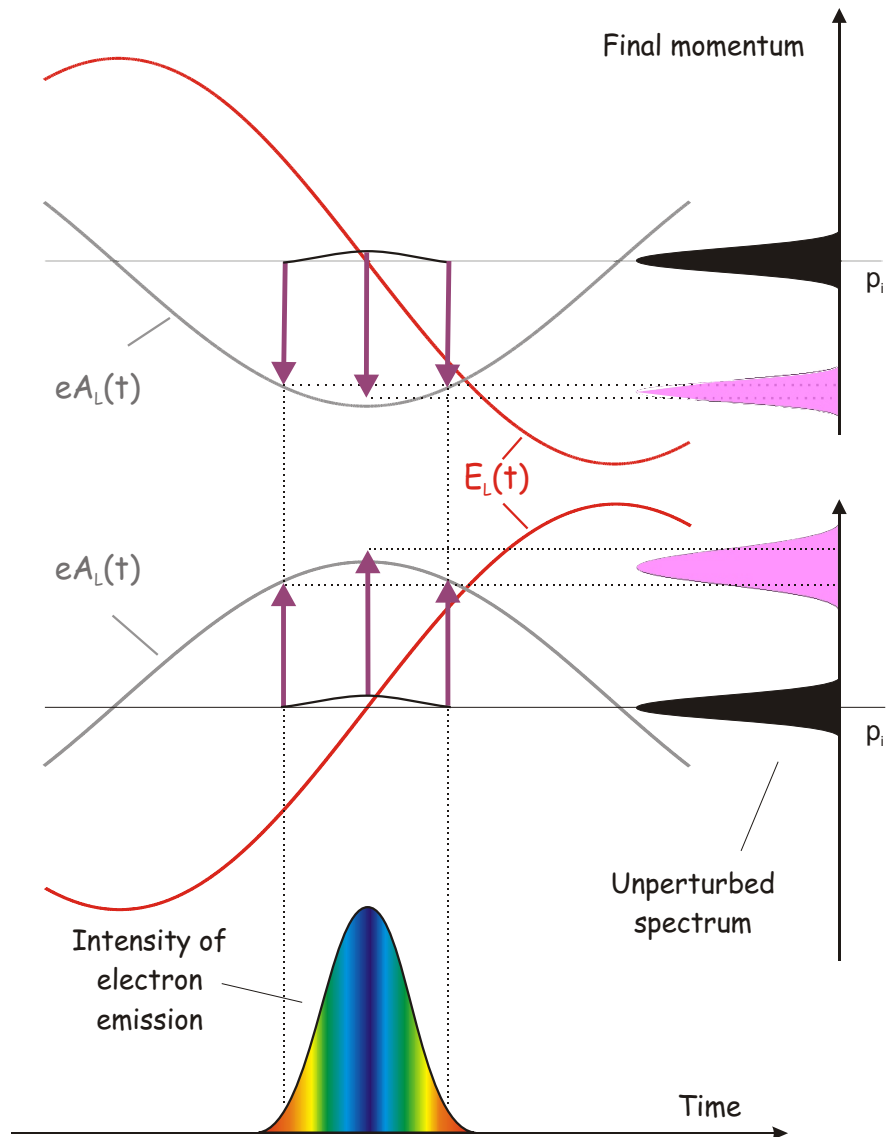


Figure 2.4: Quadratic chirp determination by means of the atomic streak camera. An electron bunch with nonlinear momentum distribution (black line) is released in the field of the laser. Black profile (field free final momentum distribution). Asymmetric broadening of the final electron distribution (probed at consecutive symmetric maxima of the vector potential (red line)) allows the detection and the determination of the nonlinear chirp.

easy measurable parameter, which is, an electron spectrum with the temporal chirp of the XUV pulse.

Temporal chirp of higher orders and namely the quadratic chirp, can be also accessed by means of this concept. The electron bunch is now probed at the maximum of the vector potential rather at its zero transition as illustrated in figure 2.4. Note that momentum is imparted almost symmetrically to the entire electron bunch, resulting in an energetic streaking of the momentum distribution away from its field free momentum (black distribution). On top of that, if nonlinear chirp is present - similarly with the previous case - the spectra will appear to have non identical broadening for consecutive maxima of the vector potential.

Under certain initial momentum distributions easier to handle theoretically (like a Gaussian distribution for example), one could conclude by means of equations 2.6, 2.8 and the field function to quasi-analytical expressions for the determination of the chirp [21], [70]. In practice however, spectral distributions employed for the synthesis of attosecond pulses might differ substantially from a Gaussian and a possible analytical formula is therefore only estimative.

Similarly as in a conventional camera, the corresponding pulse duration (in this case after the determination of the chirp) of the electron bunch can be inferred, if the laser field magnitude (the streaking ramp) is precisely defined. Equation 2.6 dictates that this information is also retrieval by the same measurement, provided that the electron bunch is released at consecutive delays inside the field over an entire laser period and therefore the magnitude of the field is sampled. If the sampling step is small enough, the derivative of the recovered  $A(t)$ , results in the electric field of light at the same time. This key feature of the technique is the basis not only for the characterization of the attosecond pulses accurately, but also the underlying principle to allow direct and complete characterization of light waveforms, demonstrated experimentally in chapter 6.

## *2.2 Streak camera on an attosecond time scale*

---

# Chapter 3

## A laser source of few-cycle phase stabilized pulses

The instrumental role of controlling the phase, or generally the waveform of light, specially when the latter is employed to steer or to track ultrafast phenomena on an attosecond time scale, has been extensively addressed in the preceding chapters. Besides the required degree of control over the waveform, light pulses shall be at the same time intense enough in order to induce and to track ultrafast nonlinear phenomena. These two basic prerequisites motivate the development of laser sources that provide few cycle intense light pulses. Developments on such a source are discussed in this chapter. In the first part, after a brief but necessary introduction to the operation of the amplifier system, a hollow fiber-chirped mirror compressor generating pulses of 4.3 fs is presented. In the second part, developments on the generation of phase controlled amplified pulses are discussed. Finally, in the third part, experiments aiming to characterize the phase noise introduced unavoidably by the amplification process, the pulse compression and phase stabilization schemes are presented.

### 3.1 The laser system

#### 3.1.1 The laser oscillator

The laser consists of a dispersive-mirror-Kerr-lens mode locked oscillator 80 MHz, 5 nJ,  $\sim 10$  fs ( Femtosource Compact Pro, Femtolasers GmbH) pumped by a CW Coherent Verdi 5 at 532 nm. The concept of the oscillator is presented in detail in [71], [72], [73].

#### 3.1.2 The laser amplifier

The above mentioned oscillator seeds an amplifier (Femtopower Compact Pro, Femtolasers GmbH) schematically illustrated in figure 3.1. The concept of the amplifier is presented in detail in [5]. However several features of the system are of particular interest here and therefore a brief description becomes necessary. The pulses delivered by the oscillator after

### 3.1 The laser system

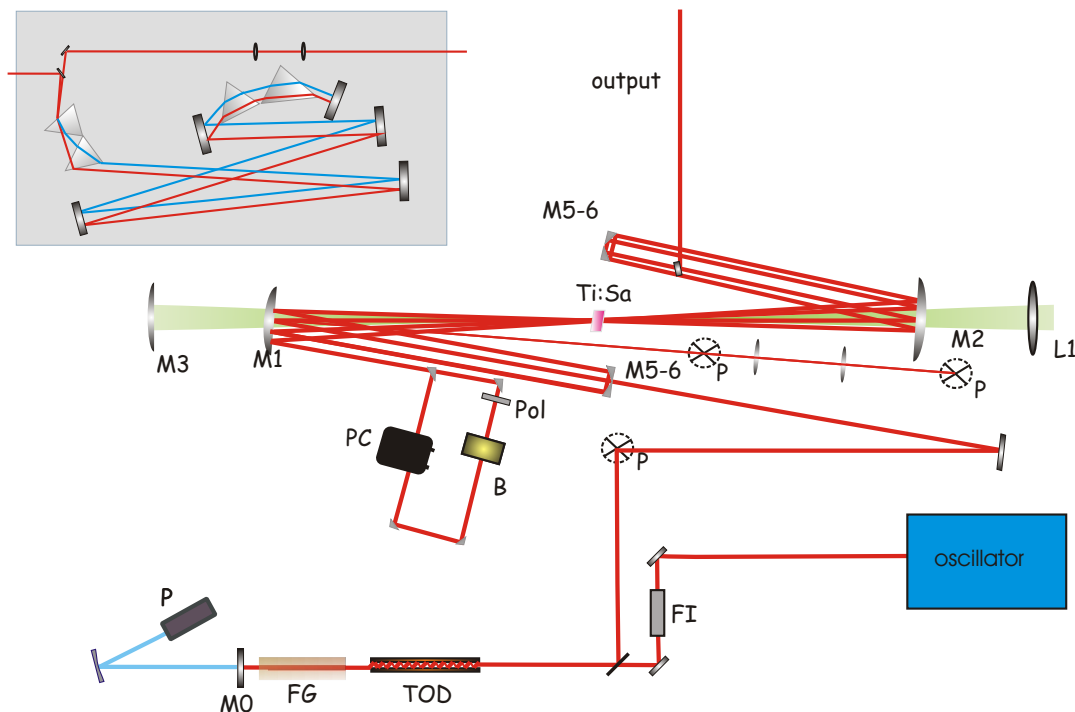


Figure 3.1: Schematic of the laser system. FI: Faraday isolator, FG: Bulk material, TOD: third order dispersion chirped mirrors, P: Periscope, M0,M1,M2: Dichroic Mirrors, L1: lens, M3: Focusing mirror of the pump beam. M5-6 retro reflectors, PC: Pockels cell, B: Berek polarizer, Pol: Polarizer, P: Photodiode. (Inset) the prism based pulse compressor. More detailed description can be found in [5].

passing through a Faraday isolator, are stretched by a double pass through a 5 cm flint glass, to several tens of picoseconds. Sixteen reflections over a pair of specially designed chirped mirrors are employed in order to correct the high order dispersion introduced [74]. The amplifier is designed to attain the shortest possible pulses at its output and therefore, these mirrors are aiming to pre-compensate for higher orders of dispersion, accumulated during stretching and along the amplification process, as well.

The pulse train is subsequently injected into the amplifier, based on a 4 mm Brewster angle cut Ti:Sapphire crystal, installed inside a vacuum sealed aluminum pot. The crystal is cooled down to  $-30^{\circ}\text{C}$  for reducing the effects of thermal lens to the beam profile. The pumping source for the amplifier crystal is a Corona, Coherent Nd:YAG, diode pumped laser system with intracavity doubling at 532 nm. The power here is almost 10 W at 1 kHz. After the first four passes the energy of the pulses is boosted up by a factor of  $10^4$ . A pockels cell synchronized with the pump laser and the oscillator via a MEDOX divider, picks a single pulse which in turn is sent to the crystal for further amplification. After a second set of four passes the beam profile is corrected by a negative lens in order to avoid

focusing and damaging of the amplifier crystal. The last pass ( $9^{th}$ ) through the amplifier is extracted, having a pulse energy of about 1.2 mJ. In order to reduce the spectral narrowing of the amplified pulses introduced by the spectrally limited amplification gain curve of the Ti:Sapphire - resulting in substantial limitation of the shorter potential pulse - a spectral filter with a Gaussian absorption curve centered at about 800 nm is inserted into the beam path, for 8 of the 9 passes through the crystal. Two prism pairs introduced in a Brewster angle into the beam path, form a dispersive compressor and reduce the pulse duration down to 25-20 fs with an energy of 850-900  $\mu$ J/pulse. The energy loss in the prism compressor is approximately  $\sim$  15%. The beam profile is Gaussian and the  $M^2$  has been measured to be less than 1.2. The pulse to pulse stability for the system has been measured to be approximately 1% RMS. This stability is an important issue for the phase stabilization, as it will be discussed later in this chapter.

### 3.1.3 Hollow fiber-chirped mirror laser light compressor for sub 4.5 fs waveform controlled pulses

The employment of Ti:Sapphire for amplification, imposes severe restrictions to the broader bandwidth that can be amplified in a modern laser amplifier, and therefore to shorter pulses that can be delivered to experiments accordingly. Laser amplifiers based on optical parametric chirped pulse amplification (OPCPA), are expected to overwhelm this bottleneck, providing with smooth amplification over a few hundred nanometers spectral range. This technology is already on the way to mature, and interesting results have demonstrated the huge potential of these concepts [75] to reach impressively high amplification over a large spectral bandwidth in a single pass. Here Ti:Sapphire technology combined with a post pulse compression technique initially suggested and put forward by [7], is employed. A theoretical approach regarding hollow fiber based wave guiding and broadening has been performed by [76], [77]. Recently the possibility for employing cascaded configurations based on a sequence of hollow fibers, has been reported for the generation of pulses shorter than 4 fs [78]. Here, the pulses initially delivered by the amplifier, have a duration of 20-25 fs and a corresponding bandwidth of 40-60 nm centered at about 805 nm. These pulses are focused gently using a thin  $f=1.5$  m AR coated lens, into the entrance of a hollow core fused silica fiber, installed inside a tube filled with  $\sim$  2 bar of Ne gas. The fiber has an entrance diameter of 260 $\mu$ m (FiberTech GmbH) and the focal spot is optimized and precisely tuned, utilizing the telescope of the amplifier compressor, in order to match the fundamental transversal mode of the hollow fiber. With this configuration an efficiency of 65% has been achieved, though typically a 45-50% is provided on a day to day basis to experiments. The fiber-chirped mirror based pulse compressor, is schematically depicted in figure 3.2. In figure 3.3, the spectrum at the output of the laser amplifier and the hollow fiber based compressor are shown. The Fourier-transform limited pulse associated with these spectra is  $<$  25 fs and about 4.3 fs respectively. These pulses specially the shorter ones can be realized provided that the dispersion introduced by the broadening processes, is effectively managed. Managing the dispersion of such a broad spectrum, is a rather

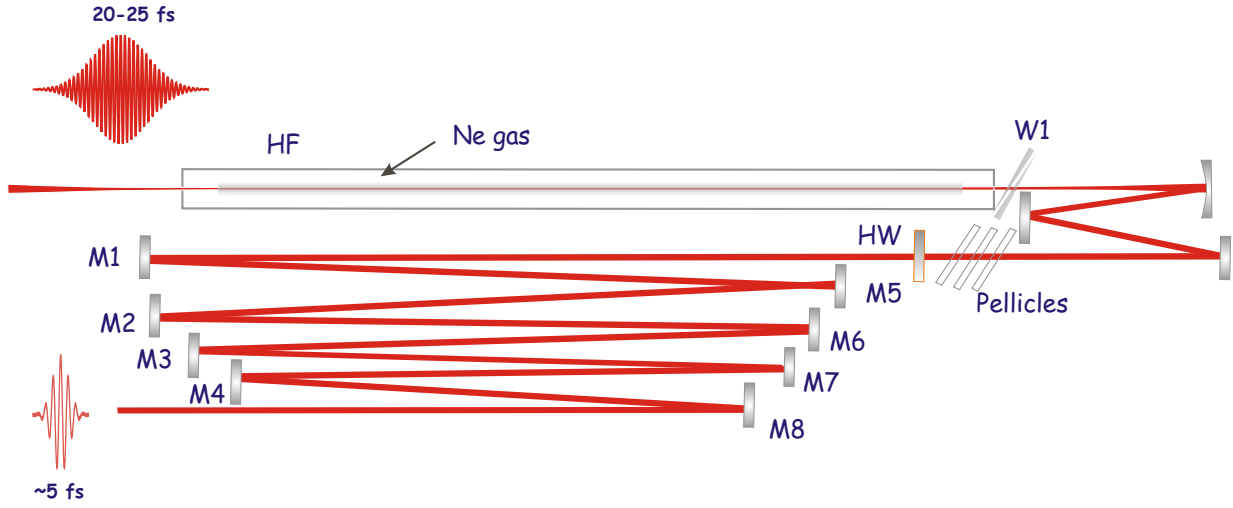


Figure 3.2: Hollow fiber-chirped mirror light compressor. HF: hollow fiber, W1: pair of wedges, HW: thin  $\lambda/2$  waveplate, M1-8: chirped mirrors with GDD  $-40 \text{ fs}^2$  per reflection. Eight reflections on chirped mirrors, in combination with positive dispersion introduced by the wedges, allow control of the dispersion of the spectrally broadened light.

demanding issue possible either employing prisms [79], or chirped mirrors. Chirped mirrors constitute a revolutionary approach to control the dispersion of light and thereby its temporal characteristics, without cumbersome alignment of a prism compressor. Though positive dispersion, can be typically accumulated by the propagation of multicolor light through a material, negative dispersion is possible only close to the physical resonances of matter [80]. This factor restricts the applicability of materials providing negative dispersion to certain spectral regimes - usually located in the UV part of the spectrum - and applications only. The operation of the chirped mirrors [74], [81] is based on the interference of light reflected by a sequence of material layers. Accurate optimization of these layers, the number and the thickness, has resulted to chirped mirrors with ever higher control of the dispersion [82]. A set of eight chirped mirrors that exploit the above mentioned principle, are employed for this setup. The group delay dispersion (GDD) introduced by chirped mirrors, is oscillatory around a certain value within the range of interest and therefore, two different types with slightly displaced GDD curves are employed complementarily and result into a smooth dispersion curve. The negative dispersion introduced by the mirrors is approximately  $-40 \text{ fs}^2$  per reflection across the range of 600-1100 nm. A pair of wedges placed at a Brewster angle at the output fiber, introduce variable positive dispersion allowing full control of the overall dispersion of the system. Small degree of ellipticity in the broadened spectrum of the order of 10% arising from non uniform stress on the windows of tube that houses the fiber, has to be eliminated. To this end a thin broadband  $\lambda/2$  waveplate (Karl Lambrecht Corporation), and a series of three  $5 \mu\text{m}$  thick pellicles (National photocolor), have been introduced into the beam path at Brewster angle. The

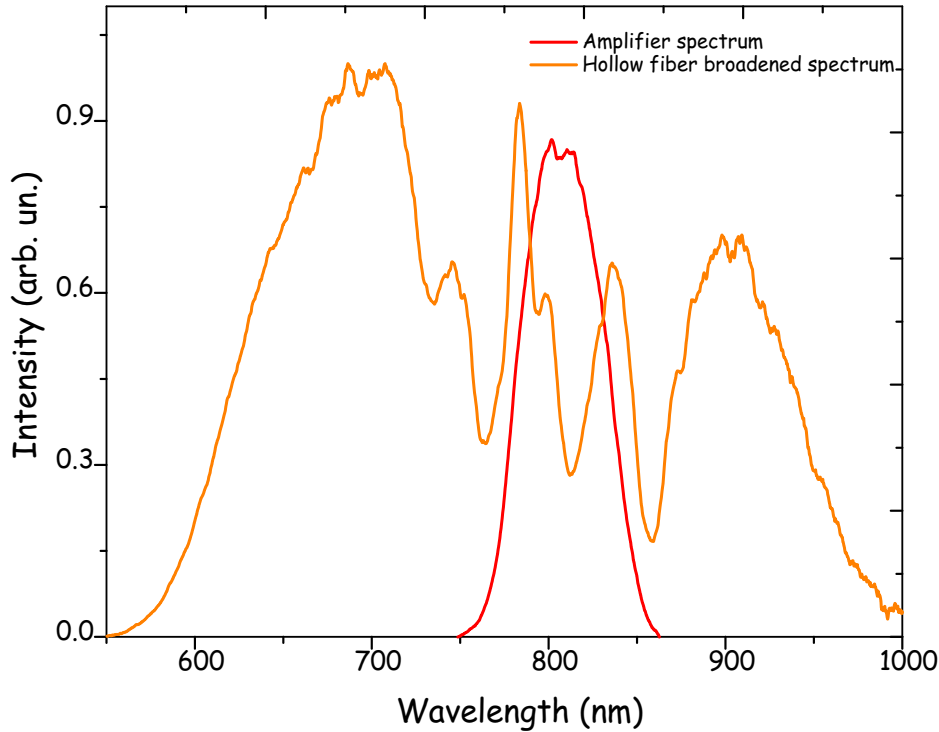


Figure 3.3: Laser spectrum at the output of the amplifier (red line) and broadened spectrum using the hollow core fiber compressor (orange line). The broadening of the 50 nm initial spectrum to almost 75-80 % of an optical octave, supports the generation of pulses of less than 2 optical oscillations in the IR, that is less than 5 femtoseconds.

former, to slightly turn the polarization in order to match the plane of the pellicles, while the latter, to eliminate the vertical component of the field which is totally reflected at Brewster angle. A tiny reflection (1%) of an 1 mm thick broadband beam splitter, is sent to an autocorrelator where the pulse is characterized online (approximately 1 trace/sec). An autocorrelation trace is depicted in figure 3.4. Though for extremely short pulses with non gaussian spectrum an autocorrelation trace can be considered only a good estimation for the pulse duration, a FWHM consisting of 2-3 cycles is indicative for the status of the pulse as well as the laser source conditions. Owing to the efficient broadening and the high degree of recompression, the discussed compressor delivers few cycle pulses as short as  $4.3 \text{ fs}^1$ , comprising the shortest optical pulse ever delivered by a single stage hollow fiber-chirped mirror compressor, at intensities enabling full exploitation of these pulses to attosecond pulse generation and metrology (discussed in next chapters), as well as, phase sensitive few cycle laser light experiments as presented in [83], [65], [66].

<sup>1</sup>measured with attosecond sampling, as to be discussed in chapter 6.

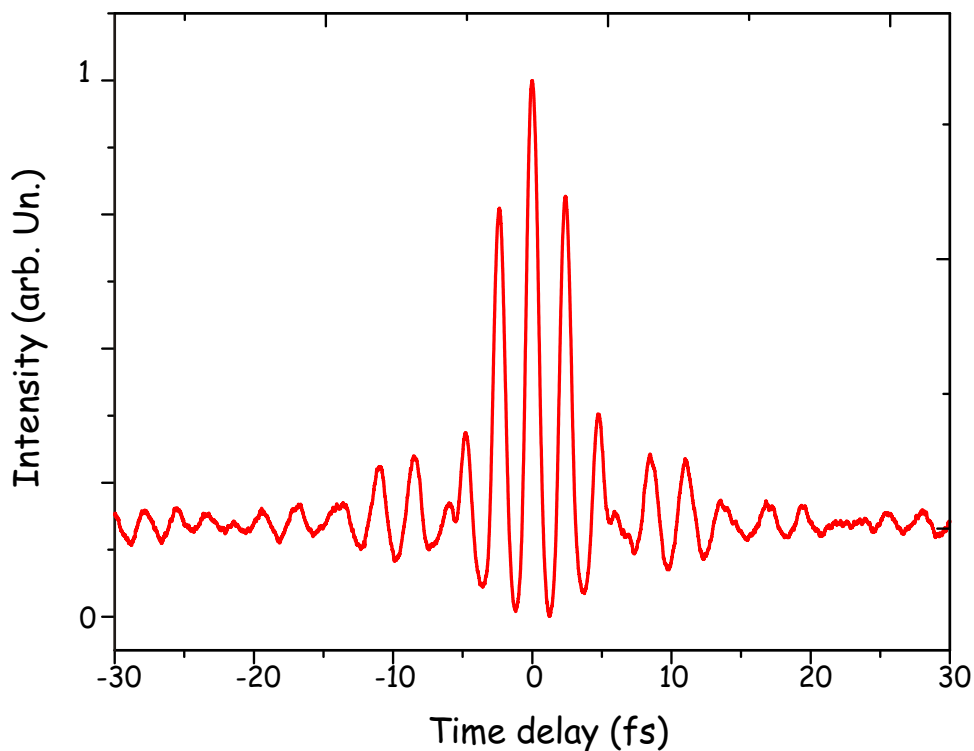


Figure 3.4: Fringe resolved autocorrelation trace of the pulses, at the output of the hollow fiber chirped-mirror compressor.

## 3.2 Carrier-envelope phase of a laser

### 3.2.1 CE phase of a mode locked pulse train

The temporal evolution of a linear polarized electric field of a pulse can be expressed as:

$$E(t) = A(t)\cos(\omega t + \phi) \quad (3.1)$$

where  $A(t)$  is the pulse envelope,  $\omega$  the frequency and  $\phi$  the phase. In general, a universal reference for defining an absolute phase for light does not exist. In the case of a short light pulse, such a definition is possible utilizing the offset between the carrier frequency of light, with respect to the peak of the pulse envelope. This definition is not arbitrary and accidental at all, as a plethora of phenomena are particularly sensitive to this offset, especially when few cycle pulses are employed. For this reason, the term carrier envelope (CE) phase  $\phi$ , is often employed to describe the waveform of a short pulse. Different phase settings of the carrier under the envelope of a pulse are schematically illustrated in figure 1.5 of chapter 1.

When a pulse propagates through a medium other than vacuum, a difference between phase velocity  $u_p$  and group velocity  $u_g$  results in a slippage of the carrier wave under the

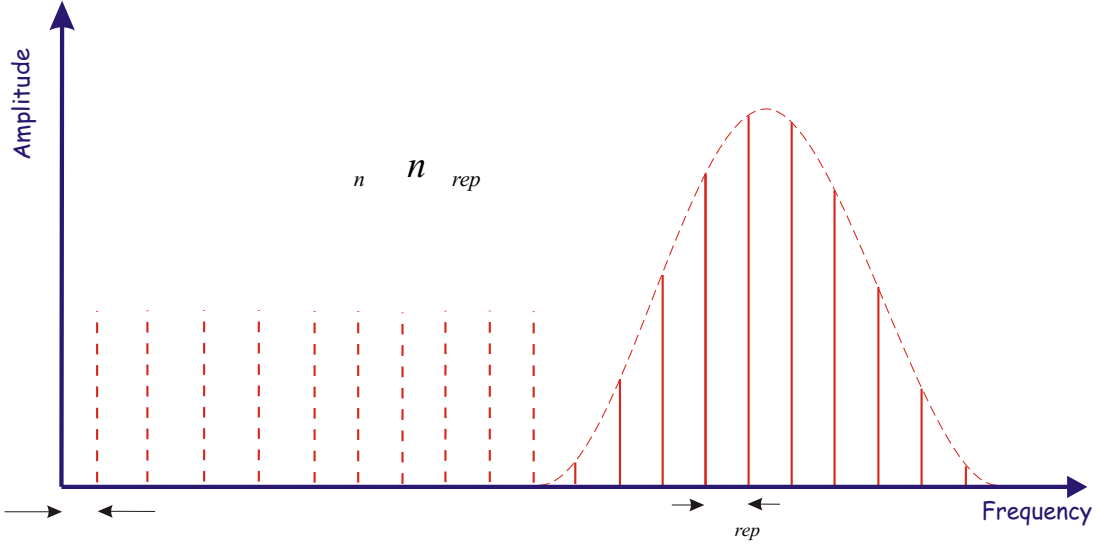


Figure 3.5: Modes of a laser cavity separated by  $\omega_{rep}$ . An offset  $\delta$  making the frequency  $\omega_n$  of each mode of the comb to differ from being an integer multiple of the repetition rate  $\omega_{rep}$ , is the spectral manifestation of the phase drift between successive pulses in a train.

envelope and therefore to a phase offset  $\Delta\phi$ . The same applies inside a laser cavity where the dispersion in this case is introduced by the active medium. A pulse is leaving a laser cavity through the output-coupler each time a full round-trip is accomplished. In this case the pulse to pulse phase drift  $\Delta\phi$  can be expressed as:

$$\Delta\phi = \left( \frac{1}{u_g} - \frac{1}{u_p} \right) l_c \omega_c \text{mod}[2\pi] \quad (3.2)$$

with  $l_c$  the cavity length and  $\omega_c$  the carrier frequency. The above argumentation is in principle sufficient for giving an intuitive picture about the phase shift. To describe these properties mathematically, frequency rather than time representation is usually invoked. In the frequency domain, the spectrum of a train of identical pulses consists of a comb of integer multiples of the repetition rate  $\omega_{rep}$ . However, the phase drifts from pulse to pulse mentioned above - responsible for a train of non-identical pulses - result in an offset of the frequency of the  $n^{\text{th}}$  mode, preventing it from being an exact integer of the repetition rate and it is given by:

$$\omega_n = n\omega_{rep} + \delta \quad (3.3)$$

where  $n$  is the mode number,  $\omega_{rep}$  is the repetition rate of the laser and  $\delta$  is the offset. A mathematical derivation can be found in [84], [85]. If  $\delta$  has any value different than zero, this results in a phase advance for consecutive pulses given as:

$$\Delta\phi = \frac{2\pi\delta}{\omega_{rep}} \quad (3.4)$$

A simple inspection of this equation, suggests that the frequency  $\delta$  is of fundamental importance for the measurement and at a next step, for the control of the CE phase of pulses generated by a laser oscillator. It is therefore critical to measure this parameter. A key idea for realizing such a measurement, is based on the so called "self-referencing" techniques. These are based on the heterodyne mixing of the fundamental and its second harmonic, provided of course that the fundamental spectrum is broad enough so that a partial spectral overlap between them is possible. Mathematically the interference of the overlapping spectral components can be written as:

$$2\omega_n - \omega_{2n} = 2n\omega_{rep} + 2\delta - (2n\omega_{rep} + \delta) = \delta \quad (3.5)$$

Access to this parameter is essential for measuring the pulse to pulse phase drift and it becomes clear that an experimental realization of the above ideas can provide the means for such a measurement. In what follows, it is discussed how these ideas can be put into practice.

#### 3.2.2 Observing phase drifts of laser oscillators

The observation of carrier-envelope phase drifts from pulse to pulse of a laser source employing the above ideas, requires that the inspected pulses spectrally span over an octave. Of course, most of the laser oscillators do not comply with this requisite and therefore, an external broadening technique is necessary. Photonic crystal fibers (PCF) [86] have allowed steps in this direction. By coupling pulses of nanojoule energy into a PCF, broadened spectra spanning over an optical octave can be efficiently generated. These broad spectra serve as the basis for the experimental realization of a "self referencing" technique, as discussed in the previous section by means of the so called f-to-2f interferometers<sup>2</sup>, which in its typical form is shown in figure 3.6.a. An interferometer of this type, is also employed for tracking and controlling the phase of the oscillator of the laser system presented in this chapter.

The beam is coupled into a piece of PCF, and is re-collimated behind it with a pair of microscope objective lenses. The blue-shifted part of the resultant white light, is separated from the red-shifted spectral wing with a dichroic mirror. A fraction of the infrared beam is then frequency doubled in the second-harmonic generation crystal (SHG), and recombined with the blue portion of the white light continuum on a polarizing beam-splitter. Two glass wedges in one of the interferometer arms, are used to adjust the timing of the two interfering wave packets. The polarizing cube enables their interference by selecting a common polarization component of the beams. Several half-wave plates are employed for choosing polarizations appropriate for the frequency doubling and the subsequent interference. A bandpass filter, consisting of a diffraction grating and a slit, selects a narrow frequency interval within the spectral overlap between the white light and its frequency-doubled part. This filtering enables observation of a beat between two quasi-monochromatic frequency

---

<sup>2</sup>Commercial product of Menlo-Systems GmbH

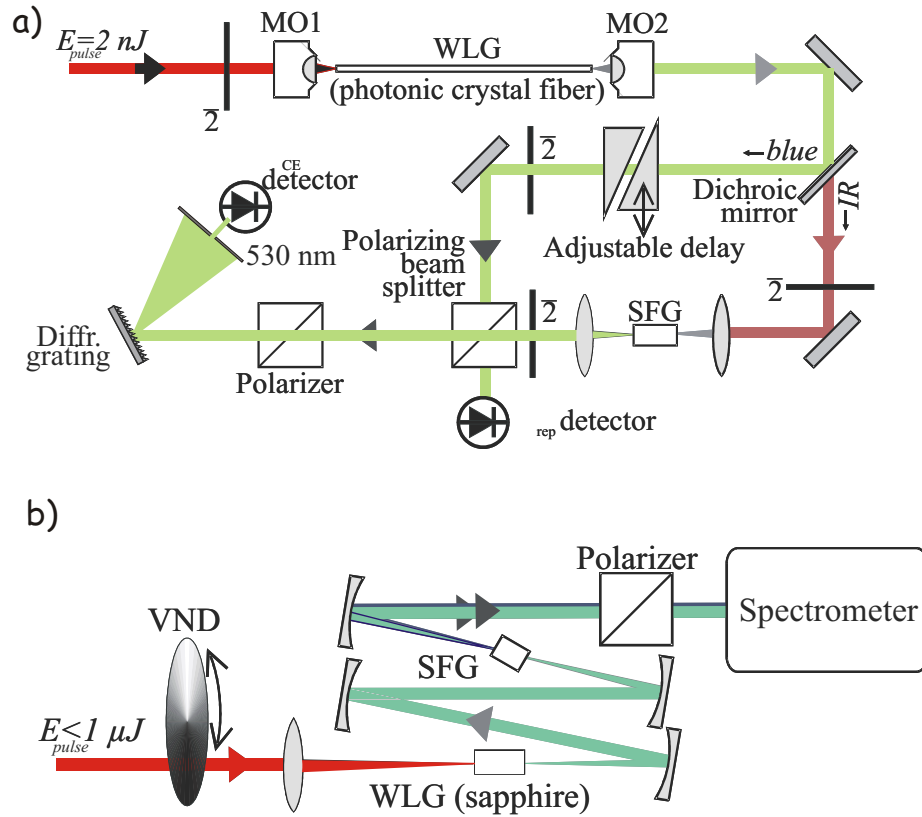


Figure 3.6: Schemes for measurement of CE phase drift. (a) Nonlinear Mach-Zender interferometer for characterization of low-energy mode-locked oscillators. (b) Setup for phase characterization of amplified pulses by nonlinear spectral interferometry. MO1,2: microscope objective lenses. VND: variable neutral density filter. SFG: sum frequency generator. WLG: white light generator.  $\lambda/2$ : half-wave plates.

components, as suggested in equation 3.5. Two avalanche photodiodes detect the repetition frequency and the offset frequency, respectively. According to equation 3.3, the information provided by the measurement  $\omega_{rep}$  and  $\delta$ , is sufficient to characterize the drift of CE phase. The use of these inputs will be addressed below in the description of the feedback loop for CE phase stabilization of an oscillator.

### 3.3 Observing phase drifts of amplified pulses

Amplification of light pulses is not possible at the repetition rates of an oscillator and therefore a reduction of the repetition rate by selecting pulses from a train before injecting them into an amplifier is something common. The phase characteristics however of a pulse used to seed an amplifier, are not necessarily preserved during the amplification process. One could divide the phase drifts introduced by the amplification process, into two main categories; the linear and the nonlinear ones.

Linear phase drifts can be attributed to the path length fluctuation of the amplified beam, especially when one considers a typical 10 m propagation, in a multipass amplifier and a prism or grating pulse compressor. Usually thermal and mechanical stability in the amplifier environment, could restrict linear drifts to vary slowly as a function of time.

The second category of phase drifts is associated with nonlinear phase accumulation of a pulse and they emerge from all those processes that link the intensity and the phase of light. Therefore, these drifts can be completely random in accordance with the intensity fluctuations. The two quantities are related through the so called B integral as:

$$B = n_2 \int I(z, t) dz \quad (3.6)$$

where  $n_2$  is the nonlinear index of refraction and  $I(z, t)$  the intensity of the propagating light at the coordinate  $z$ , the time instance  $t$ . Hence, high stability of the pumping source according to this equation, can keep nonlinear phase accumulation at low levels. Phase drifts of this kind have been recently measured to be of the order of 0.1 rad from pulse to pulse or less [87] when flash lamp based laser sources are employed for the pumping of the laser amplifier crystal.

The effects discussed so far, indicate that tracking and controlling the phase of amplified pulses along with that of an oscillator, are necessary for the generation of ultraintense field reproducible waveforms. Conceptually, f-to-2f interferometers could be employed to track the phase of amplified pulses as well. However the dramatic reduction of the repetition rate down to  $< 20$  kHz (typical for amplifiers), complicates the accurate simultaneous detection of  $\Delta$  and  $\omega_{rep}$ . Therefore some critical modifications become necessary. On the other hand, the energy abundance per pulse, allows the employment of significantly easier to implement broadening techniques, important for f-to-2f schemes. Nowadays, phase tracking after amplification has been possible [88] in single shot schemes by means of nonlinear spectral interferometry. There, following the generation of white light using gas filled hollow fiber based spectral broadening, the spectrum is subsequently frequency

doubled using a SHG crystal. The interference of the overlapping parts of the broadened and the frequency doubled spectrum in such a scheme is given by:

$$S(\omega) = I_{WL}(\omega) + I_{SHG}(\omega) + 2\sqrt{I_{WL}(\omega)I_{SHG}(\omega)} \times \cos(\phi_{SHG}(\omega) - \phi_{WL}(\omega) + \omega\tau_0 + \varphi) \quad (3.7)$$

where  $\tau_0$  is the delay between fundamental and harmonic pulse and  $\phi$  is the phase to be retrieved. If the delay is adjusted so to result in adequate number of fringes between fundamental and second harmonic, the argument of the cosine can be numerically retrieved using standard algorithms of spectral interferometry. Even though the phase recovered by the interferometer is arbitrary, the phase difference for consecutive pulses can be accessed as dictated by the argument of the cosine in equation 3.7. The employment of an external source of calibration based on the generation of XUV light by phase control few cycle laser pulses, is discussed in chapter 5. For putting the above ideas in to practice, the hollow-fiber employed in [88] is replaced by a 2 mm thick sapphire window, as shown in figure 3.6 for the apparatus presented here. The broadened spectrum is in turn refocused to a 1 mm BBO crystal. The doubled red “components” of the spectrum, can interfere with the blue part of the broad spectrum over a range of several tens of nanometers (typically around 510 nm) upon their passage through a polarizer. Owing to the dispersion of the sapphire plate and as well that of the BBO crystal, the fundamental and the second harmonics pulse, are sufficiently delayed, resulting in adequate number of spectral fringes, necessary for the accurate retrieval of the phase, by an algorithm based on Fourier transformations. The interferogram is measured by a fiber coupled spectrometer (AD2000 Ocean optics), capable for almost single shot spectra acquisition.

### 3.4 Phase stabilization of amplified pulses

Phase stabilization of oscillators, has been achieved already by [89], [90], [91] employing the self referencing techniques discussed previously. For the phase stabilization of the laser system discussed in section 3.1, both the above mentioned approaches have been employed for tracking the phase drifts of the generated by the oscillator pulses as well as during their amplification. A logical step is to take advantage of the ability to track phase drifts from pulse to pulse and to convert this information to a feedback aimed to drive a process that can affect the phase of the generated pulses. This is by definition a control loop. For the phase stabilization method presented here the so called phase locked loops, or shortly PLLs, broadly exploited in nearly all modern electronic devices are employed. The idea behind PLLs, is that a frequency  $A$  can be locked to a reference  $B$ , if a feedback proportional to their difference (error signal) is used to drive the generation of the frequency  $A$ .

For stabilizing the phase of a pulse train delivered by the oscillator, a 50 % of its energy is injected into an f-to-2f interferometer for tracking the phase offset which is as alluded, proportional to the beating frequency resulting from the heterodyne mixing of the broadened fundamental with its second harmonic. The repetition rate of the laser divided by a factor of 4 electronically is used here as a reference ( $1/4 \omega_{rep} = 20MHz$  for the current oscillator). The error signal derived from the comparison of the two frequencies, is used

### 3.4 Phase stabilization of amplified pulses

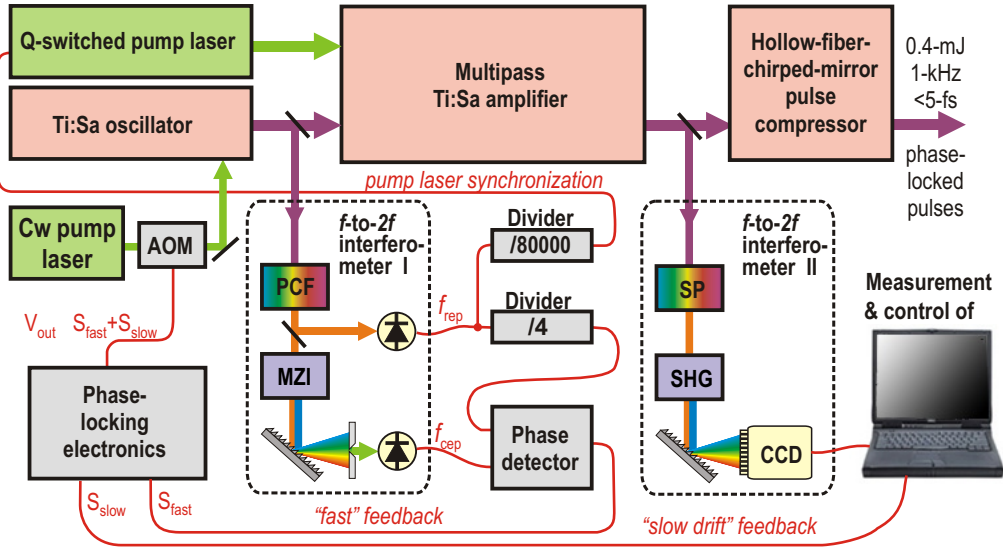


Figure 3.7: Schematic of the phase stabilized high power laser system. Details about the multipass amplifier in figure 3.1. AOM: Acousto-optical modulator, PCF: Photonic crystal fibre, MZ: MachZehnder set-up, SP: 2-mm sapphire plate, FDC: Frequency-doubling crystal. The CE phase of the pulses delivered by the (Ti:Sa) oscillator is controlled by tracking the f-to-2f signal in interferometer I and controlling the pump power through a feedback based on the AOM. Frequency dividers /4 and /80,000 are used to derive, respectively, the reference frequency for the stabilization of the phase slip behind interferometer I and the repetition rate of pulses amplified in a multipass amplifier. With this technique the CE phase recurrence of the Ti:Sa oscillator is set such that every fourth pulse (and therefore also every 80,000<sup>th</sup> pulse) exhibits the same electric-field waveform.

to modulate temporally the intensity of the pumping source of the oscillator by means of an acousto-optic modulator installed in its beam path. The Kerr lens nonlinearity to that intensity variations translates to a  $\Delta\phi$  for the generated pulses. Locking the beating signal (and thus the offset) to a frequency different than zero, means that the oscillator delivers pulses having reproducible phase under certain periodicity. In this case  $(1/4)\omega_{rep}$  suggests that the phase changes from pulse to pulse as  $\Delta\Phi = 2\pi(m + 1/4)$  with  $m$  an integer and therefore every  $4m$  pulse, has the same (CE) phase. The rest 50% of the oscillator light is injected into the amplifier, and the repetition rate is chosen so that the Pockels cell delivers a pulse for amplification exactly every integer multiple of 4. In our case 1 kHz corresponds to  $250 \times 4$  and therefore each pulse injected to the amplifier, has exactly the same carrier envelope phase. For tracking and controlling the phase at the output of the amplifier, a less than 1% of the laser output is coupled in the sapphire based f-to-2f interferometer, shown in figure 3.6 and discussed in the previous section. The phase drift retrieved by the analysis of the recorded spectrum, is used to generate a second feedback which is plugged

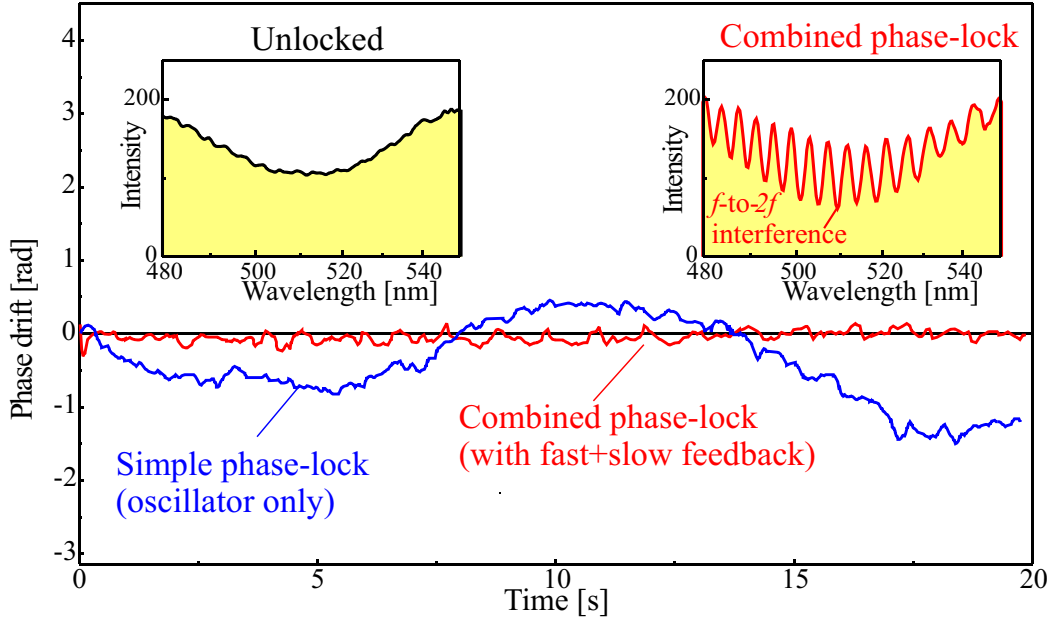


Figure 3.8: Pulse to pulse phase retrieval by means of the sapphire based spectral interferometer at the output of the amplifier. Blue line, with the phase of the oscillator pulses locked, without activation of the second control loop. A mHz oscillatory drift of the phase can be observed. When the second controlled loop is activated, a stable phase trace (red) line can be attained. The phase stability as inferred from this measurement is better than  $\pi/6$  (left inset). Interference fringes recorded by the f-to-2f interferometer, without phase stabilization over a few hundreds of laser shots. The random drift of the spectral fringes results in a smeared pattern and in a stable one (right inset), when both feedback loops are active.

to the phase electronics. A vital issue for mixing the two feedback signals for stabilization, is that the phase drift after the amplification of the pulses, is varying relatively slow as compared to the MHz drift of the phase in an oscillator. This is shown in figure 3.8. The blue line corresponds to the phase drift measured for the amplified pulses, when only the fast stabilization loop is activated. The period of these drifts is of the order of hundreds of mHz, making possible their pre-compensation, by means of the “error” signal derived by the second interferometer. The red line in the same figure corresponds to the phase drift of the amplified pulses, when both loops are activated. The stable interference pattern shown in the right inset when both loops are active, is completely washed out after a few hundreds of shots if the phase stabilization is switched off (left inset). The phase stability of the order of  $\pi/6$  as shown in figure 3.8, can be preserved today up to several hours and by means of new detection techniques developed to completely compensate for slow phase drifts of any origin [65], [92].

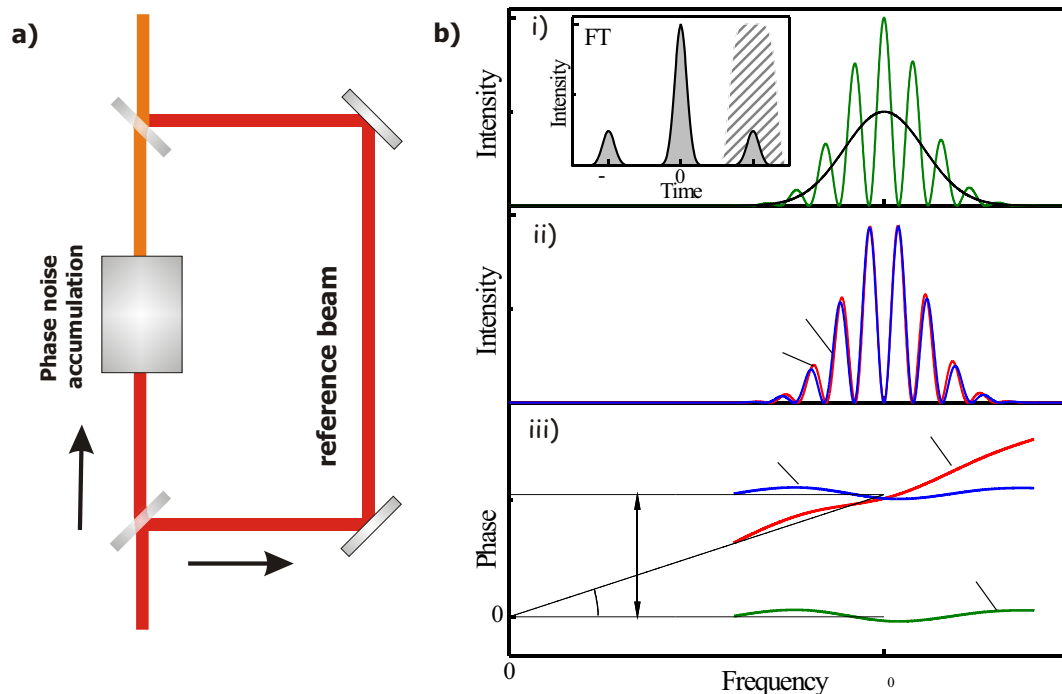


Figure 3.9: a) Linear interferometry by means of a simple Mach-Zehnder interferometer. (b) Discrimination between phase and timing jitter in the Fourier-transform spectral interferometry. (i) Intensity spectrum (solid curve) and spectral interferogram (green curve). (ii) Spectral interferograms modified by a timing shift (red curve) and a frequency-independent phase shift (blue curve). Note fringe period change in the case of timing shift. (iii) Differential spectral phases after time-delay slope subtraction. Green blue and red curves correspond to interferograms in (i) and (ii), respectively. Inset shows the power spectrum of the Fourier transform to the time domain. Dashed contour corresponds to a possible filter (usually supergaussian) required in the phase extraction to isolate the temporal peak at  $\tau_0$ .

## 3.5 Phase noise of white light continuum generation- Influence on phase stabilization schemes

### 3.5.1 Sources of phase noise

So far techniques for retrieving and controlling the phase of laser pulses, have been presented without considering the phase noise introduced by the measuring devices, the f-to-2f interferometers employed. Moreover, it has been assumed that the phase stability is preserved after the hollow fiber-chirped mirror light compressor, though essentially the CE phase is measured and stabilized right at the output of the amplifier. These issues are addressed in this section. In all three cases, white light generation is a prerequisite for the operation of the relevant device. However, the nonlinearity associated with white light

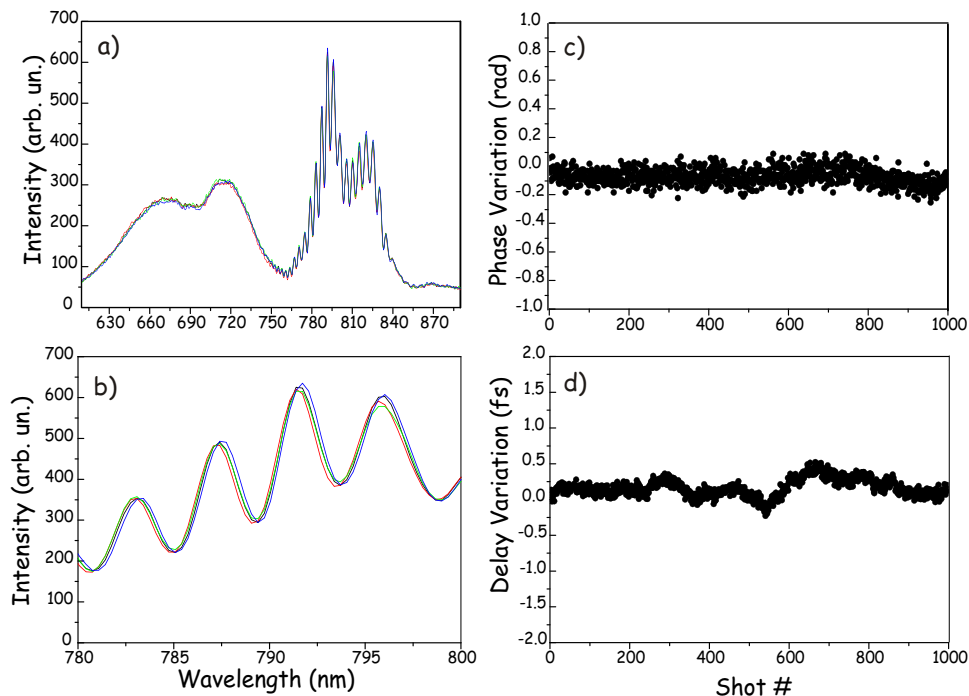


Figure 3.10: a) Three single shot interferograms between the fundamental and the broadened spectrum, at the output of a neon gas filled hollow fiber waveguide recorded every 100 ms. The interference is observed in the regime that the two beams are spectrally overlapped. The analysis of the traces is performed by means of linear spectral interferometry and results in the phase and delay retrieval traces as a function of the shot number depicted in (c) and (d). A blow up around 790 nm (b) shows the drift of the pattern associated with the phase jitter.

generation could be responsible for the so called intensity-phase coupling, where intensity fluctuations could translate to phase noise and to result in a misleading signal for the compensation loops. For the case of PCF based interferometers, the relative phenomena have been extensively studied [93]. Here the phase noise introduced in the measurement by the white light generation in sapphire (slow loop f-to-2f interferometer) as well from the broadening processes in a hollow fiber compressor, will be discussed.

### 3.5.2 Linear spectral interferometry

The technique employed here to retrieve the phase noise associated with white light generation is linear spectral interferometry [94], [95]. The idea behind this technique, is that by means of an interferometer the phase drift of a beam propagating through the one arm is retrieved, having as a reference the phase of the beam of the other arm. The object

of scrutiny in this case can be either a complete device i.e. a nonlinear interferometer, or the principal parts like the bulk sapphire (or a gas filled hollow fiber) introduced as shown schematically in figure 3.9.a, in the one of the two arms of a Mach-Zender type interferometer.

The principle of linear spectral interferometry (LSI) is illustrated in figure 3.9. Figure 3.9.b(i) shows a typical interferogram and the power spectrum of its Fourier transform (inset), used for the phase retrieval. When a time shift  $dt$  and a phase drift  $d\varphi$  between the two pulses is introduced, there is a well resolved impact to the interferogram as shown by the green and red lines respectively. The corresponding phases after subtracting the slope, which is due to the delay between the test and reference pulses, are presented in figure 3.9.b(ii). This important feature, that is, disentangling unambiguously the delay and the phase contribution to the interferogram, enables the employment of the technique also to larger scale interferometers, where the delay jitter between the two arms is unavoidable.

#### 3.5.3 White light generation in a gas filled hollow fiber

By employing a Mach-Zender interferometer in which the hollow fiber is installed along the one arm, the phase noise introduced to the broadened pulses in the gas medium is studied. A fraction of the laser beam is coupled into the neon filled fiber (as in section 3.1.3) by an  $f=1.5$  m thin lens and the broadened continuum is brought to interference with the fundamental reference beam. Interference is taking place over a spectral range of 60 nm. Quasi-single shot acquisition of spectra enables rapid recording of data to observe shot-to-shot phase fluctuations. Typical quasi single shot interferograms are shown in figure 3.10.a and 3.10.b in expansion. The three different colors correspond to spectra recorded every 100 ms. We have studied the phase noise introduced at laser energies between 600-800  $\mu$ J and various pressures setting for the Ne gas inside the capillary. The intensity noise emerging from the white light generation inside the capillary is approximately 1.6 % rms for the IR components and 4% for the blue parts of the spectrum (600-650 nm). Studying the phase noise introduced as a function of the intensity of the light coupled to the fiber, resulted to a 3.4 mrad/ $\mu$ J slope for injected energies around  $\sim 700$   $\mu$ J. The retrieved phase drift and delay jitter, are shown in figure 3.10.c,d, in a series of 1000 laser shots. The limited spectral overlap, does not allow direct conclusion for the entire spectrum. However, the stability of the measured pulse duration at the output of the chirped mirror compressor allows the assumption that spectral components preserve similar phase relation from pulse to pulse. Evidence for such a claim, can be directly inferred from single shot duration measurements for few-cycle pulses generated under comparable experimental conditions [96] employing gas filled hollow fiber waveguides. The remarkable stability of the pulse duration from shot to shot - result of reproducible phase relationship for spectra components over the entire pulse spectrum - allows the conclusion that spectral interferometry techniques applied only to a certain part of the spectrum, allow more general conclusions for the phase noise, introduced by nonlinear processes like white light generation.

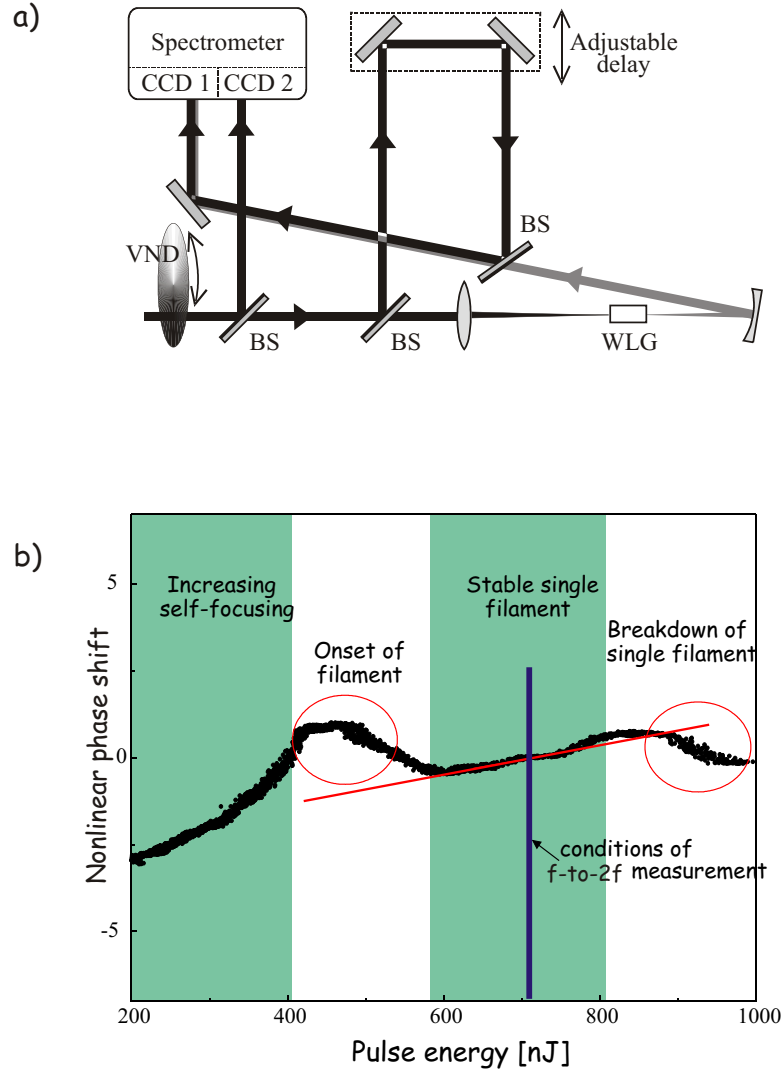


Figure 3.11: a) Single-shot spectral interferometer for measurement of CE phase jitter arising from white light generation (WLG). VND: variable neutral density filter. BS: dielectric beamsplitter. b) Intensity-phase coupling of the white light generation in bulk sapphire. Solid dots depict phase changes extracted from single-shot interferograms. Straight line shows a linear fit marking the slope of phase intensity-dependent variation in the vicinity of the pulse energy, used for f-to-2f characterization.

### 3.5.4 White light generation in a sapphire plate

For studying the phase jittering introduced by the white light generation in bulk sapphire, a simple interferometer as shown in figure 3.11 has been employed. The intensity of the incoming laser beam can be tuned by a variable density filter, while a tiny portion of the same beam is injected to the one of the two channels of a dual-spectrometer. The residual beam is injected to the interferometer and the output is diverted to the second channel of the spectrometer. The first channel records energy fluctuations and plays the role of a fast energy-meter for the injected beam, perfectly synchronized with the spectral acquisition at the output of the interferometer. The acquisition is as fast as 1 spectrum per 3 ms, allowing an almost pulse to pulse phase jitter retrieval at 1 kHz. The computer software allows online recording of a series of pulses as a function of time. The analysis of the data, has revealed a phase jitter of the order of  $\sim 100$  mrad at an energy of  $0.7 \mu\text{J}$ . The focal spot of the focused beam in the sapphire plate was approximately  $30 \mu\text{m}$ .

In order to study the phase noise introduced by bulk sapphire based white light generation, at different energy regimes, we record spectra at different input energy settings and retrieve the phase noise similarly as in the case of the hollow fiber as shown in figure 3.11(b). The discrimination of four main regimes has been possible and it is indicated by the vertical sections. The first regime is characterized by an abrupt phase change, due to the gradual formation of the filament in the sapphire. This abrupt drift can be probably attributed to the intensity dependence of the diffraction index of sapphire, resulting in a corresponding change in the group velocity of the pulses. The formation of the filament is indicated in interval (2), while the phase rebound after the onset can be attributed to the increase of the filament length. A stable interval over a  $\pm 8\%$  of the pulse energy, marks the third regime. Increasing the energy even further, results in a collapse of a single filament to multiple filaments (4). The set point for the operation of the f-to-2f interferometer employed in the slow loop, is set at the middle of the third interval. The phase drift slope has been retrieved from the data to about  $12 \text{ mrad/nJ}$ , corresponding to an  $\sim 84 \text{ mrad}$  for an  $1\%$  intensity fluctuation of the injected beam to the interferometer.

The presented phase measurement covers only the spectral overlap region between the white light and the input pulse, which is, approximately a  $60\text{-nm}$  bandwidth. Therefore, the results of this correspond to the best-case scenario since phase excursions in the blue spectral region cannot be visualized. Additionally, the SHG of the red-shifted part of the continuum also causes an intensity-dependent phase shift and, consequently, is likely to worsen the precision of the f-to-2f CE phase drift characterization further. The considerations about the phase properties of WLG, presented in this section, are important to identify the limitations of CE phase control schemes discussed below and to evaluate the applicability of WLG as a tool for retrieving and controlling the phase of femtosecond pulses.

Currently tracking the phase of amplified pulses employing asymmetry of above threshold ionization has turned out to be one of the most promising ways [65], [92].

# Chapter 4

## Attosecond pump-probe apparatus

The realization of the schemes proposed so far aiming the characterization and exploitation of attosecond pulses, calls for an experimental setup that incorporates: a) efficient generation of XUV light, employing the few cycle phase controlled laser pulses. b) an experimental scheme for the direct spectral characterization of the emitted XUV light with a descent resolution. c) selective spectral isolation and focusing of XUV light along with laser light with precise synchronization, for the realization of the streak camera concept and d) electron spectroscopy tools. The above shall be also endowed with diagnostic tools for signal stability, beam alignment e.t.c. These key technological prerequisites are discussed in this chapter. The experimental setup is schematically illustrated in figure 4.1. Practically it can be divided into two main parts denoted in figure 4.1 as the generation and the detection area. The former is devoted to the focusing and generation of XUV light, while the latter houses the focusing optics for the XUV and laser light, XUV grating spectrometer, electron spectrometer and diagnostics.

### 4.1 XUV light Generation

With the few cycle phase controlled laser light pulses presented in the previous chapter being the source, XUV light can be generated. To this end, pulses of approximately 5 fs in duration and 300  $\mu J$  of energy, are focused as shown in figure 4.1, into a gas target, using a 50 cm spherical Ag coated mirror. In order to keep aberrations low, a beam folding configuration that steers the beam to the spherical mirror at almost normal incidence (M2) is employed. The focal spot is approximately 100  $\mu m$  in diameter almost circular. The attained intensity in the focal volume has been estimated to be around  $7 \times 10^{14} W/cm^2$ .

For the production of XUV light by means of short laser pulses, several schemes have been introduced so far aiming efficient conversion as discussed in section 1.2. On the other hand, keeping the background pressure at low levels in the generation area is important, for avoiding reabsorption of the generated XUV light. Most commonly pulsed gas nozzles are employed to release atoms in the focus of the laser [34], [97]. This kind of sources however fail to supply gas reliably, under kHz repetition rates. Here a quasi-static cell configuration,

## 4.1 XUV light Generation

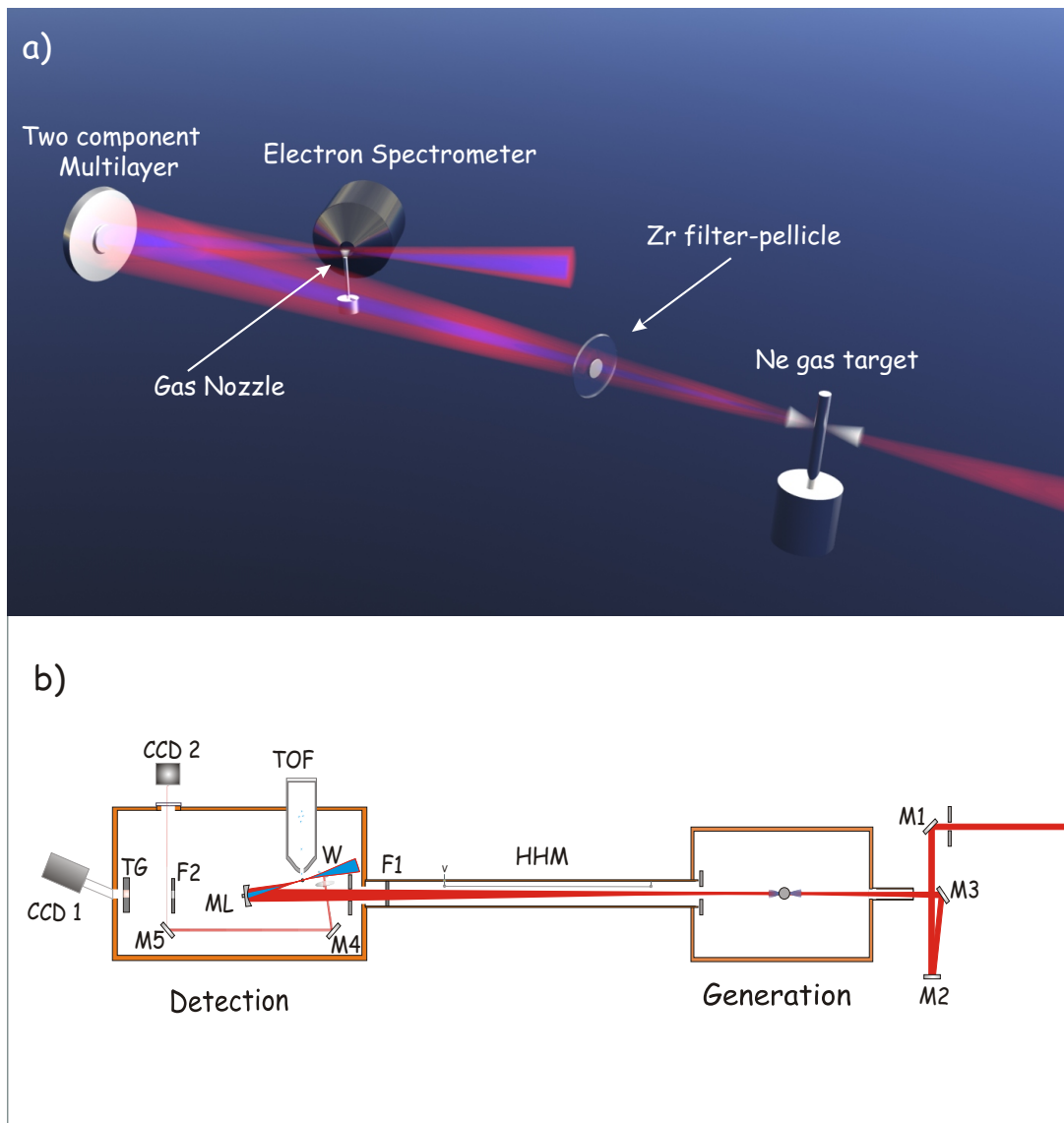


Figure 4.1: a) 3D representation of the experimental setup. b) A schematic of the experimental setup as discussed in the text. M1, M3: Flat silver mirrors, M2: Focusing 50 cm, F1: Pellicle-Zirconium Module, ML: Multilayer mirror, W: Wedge, M4, M5: Steering mirrors for the imaging system, F2: Second Zr filter 150 nm, TG: Transmission grating, TOF: time of flight detector, CCD 1: X-ray camera, CCD 2: Optical camera for alignment purposes, HHM: XUV detector based on ionization of residual gas.

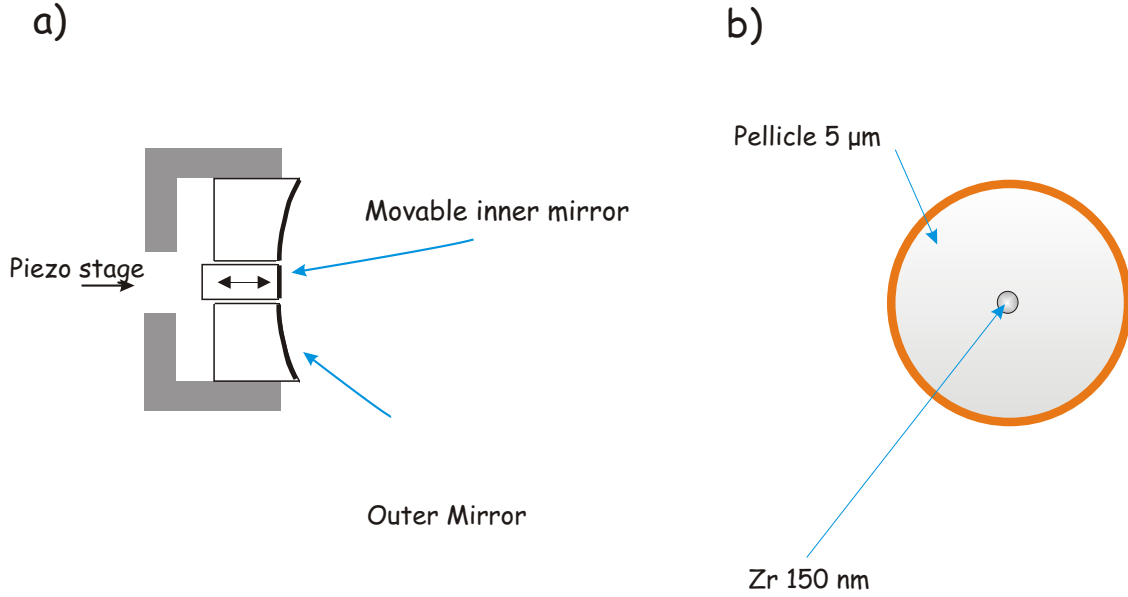


Figure 4.2: a) Schematic of the two component Mo/Si mirror. The outer annular part has a diameter of 1 cm while the one of the inner miniature-mirror is  $\sim 3$  mm. b) A module based on an 150 nm thin Zr filter - 3 mm in diameter - mounted at the center of a  $5 \mu\text{m}$  thin nitrocellulose pellicle, separates spatially XUV and the laser light.

results in a highly confined generation volume inside the laser focus. The cell is based on a thin nickel tube ( $50 \mu\text{m}$  wall thickness) filled with Neon gas. Ne has been chosen among other rare gasses because it supports efficient generation of XUV at the range of 80-100 eV, [98]. The interaction region is confined practically within the area between the two outlets drilled on the walls of the tube by the focused laser beam as shown in 4.1. The Ni tube can be squeezed down to 1-2 mm so that the propagation length requirements for efficient phase matching can be met. In order to maintain a constant pressure inside the interaction region, a flow controller in combination with a pressure gauge has been used. The optimal pressure range for efficient generation at 80-100 eV has been 160-200 mbar of Ne gas. The low gas load in the generation chamber is maintained, employing a roots pump with high pumping efficiency in the range of  $10^{-2} - 10^{-1}$  mbar. In order to further optimize generation the target is positioned a few millimeters after the focus [46], [47], [99]. Practically, the XUV photon yield is experimentally optimized by adjusting the position of the gas target along the longitudinal direction, by means of a translational stage installed inside the vacuum chamber. The  $100 \mu\text{m}$  pinhole, acts also as a geometrical aperture for the reproducible alignment of the beamline. The divergence of the generated XUV light, has been estimated to be  $< 1$  mrad by measuring the XUV beam size at about 1.5 m downstream, and considering a typical size of 10-15  $\mu\text{m}$  for the generation volume [97].

## 4.2 XUV detector based on ionization of residual gas

After its generation, XUV light propagates along with the laser light for some 1.5 m, before reaching the experimental chamber as shown in figure 4.1. Such a design supports three particular aims.

- The low divergence associated with the XUV beam ( $\sim 1$  mrad) calls for a long propagation, before a descent beam size enabling tight refocusing, is possible. The importance of this task, will be discussed later in the text.
- It enables the realization of a simple XUV detector, which can provide a reliable indication of the stability of the XUV generation. The concept of this detector is not different than that of a Geiger-Muller. XUV photons with energy much higher than the ionization potential  $I_p$  of the residual gas inside the tube, can generate electron- ion pairs by photo-ionization. A negative voltage applied to a conductive wire mounted along the tube, maintains a constant electric field that repels the electrons towards the tube surface, where a sensitive detector capable to measure nA currents is plugged. It is important to note that there is no need for a gas supply into the detector area as the residual gas from the generation process is exploited. Though the calibration of such a device is challenging, because of the gas pressure dependence of the signal, it can be used to track the efficiency of the XUV source, the laser pulse energy and pointing stability, all critical for sensitive attosecond experiments.
- Differential pumping stages installed along the connection tube, results in an almost 5 orders of magnitude ( $10^{-2}$ - $10^{-7}$ ) difference in background pressure, between the two chambers enabling the utilization of MSP (micro-sphere plate) electron detectors in the detection chamber, without risk of damage.

## 4.3 Spatial Separation XUV-laser light

The radically different divergence [100], [101] of XUV and laser light, due to the high nonlinearity of generation of the latter, is a key aspect for their spatial separation and subsequent recombination in this experimental setup. In most of the experiments presented here, a 150 nm thick Zr filter properly mounted at the center of a thin pellicle ( $5 \mu m$ ), allows this separation as shown in figure 4.2.b. This module is installed in the beam path about 1 m downstream. The Zr foil transmits almost 80 % of the XUV light over 85 eV and filters out lower energies and laser light, which is transmitted through the  $5 \mu m$  pellicle around the filter forming an annular beam. For the transmission of Zr, see Appendix A.

## 4.4 XUV light detection

For the XUV spectral measurements, a simple spectrometer based on a transmission grating and an X-Ray back illuminated CCD camera from Roper Scientific, are employed. The quantum efficiency in the range of interest 80-100 eV, is of the order of 50 %. The pixel size is  $20 \mu m \times 20 \mu m$ . In order to keep the noise level low, the chip is cooled down to  $-40 C$

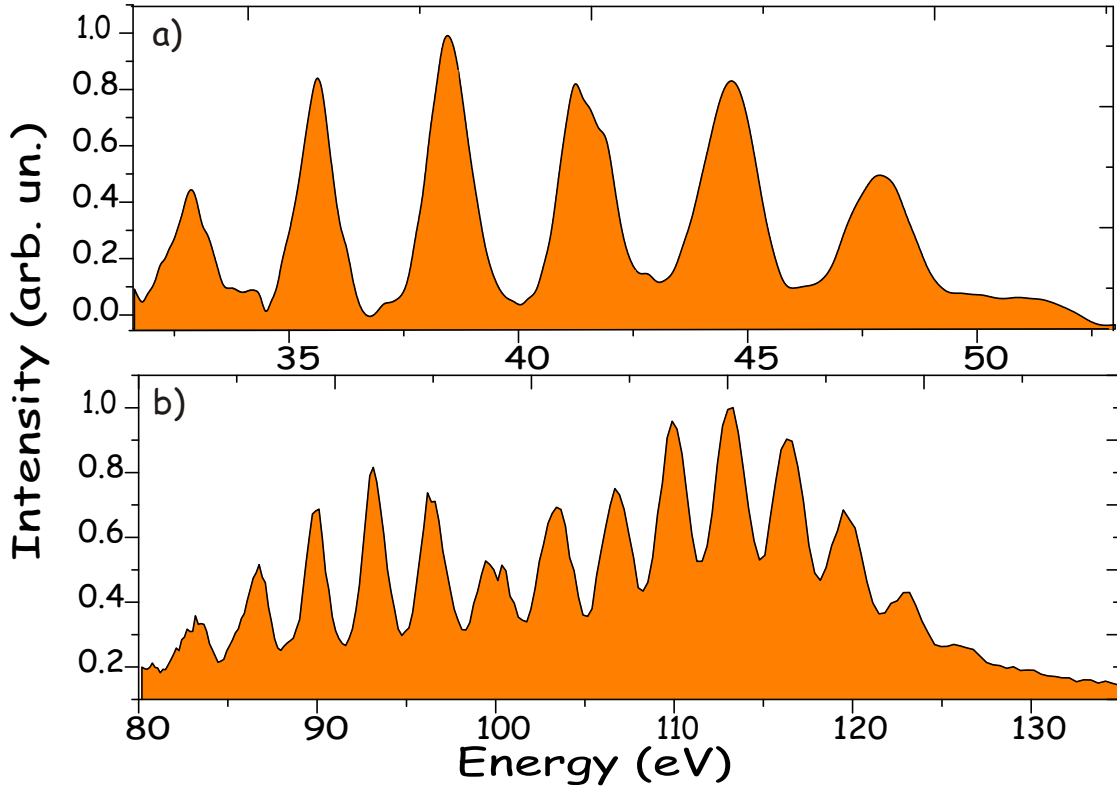


Figure 4.3: XUV spectra recorded at different regimes and generation conditions. a) 30-55 eV laser pulse 15 fs pulse, filter: Al 150 nm b) 80-130 eV, laser pulse 5.4 fs, filter: Zr 150 nm

by an integrated peltier cooler. The silicon-gold based transmission grating, has a density of 10000 *lines/mm* and provides high dispersion in the spectral range of interest 80-130 eV with satisfactory efficiency. The support grid of the grating has a period of 1  $\mu m$ . The CCD camera chip is positioned 0.4 m after the grating. The calculated resolution is of the order of 0.1 eV at the range of 90 eV, and suffices for spectral measurements of high harmonics, as two subsequent harmonics are separated energetically by  $\sim 3$  eV. Figure 4.3 shows typical XUV spectra, recorded in the range of 30-55 eV and 80-130 eV respectively by means of this spectrometer. Data in panel (a) have been recorded in Argon (30 mbar) transmitted through a 150 nm Aluminum filter by means of 15 fs laser pulses. The second panel (b) depicts XUV spectra generated in 200 mbar Ne by a 5.4 fs laser pulse. Filtering of lower orders was performed by a Zr filter. The exposure time was 10 sec and 0.5 sec respectively.

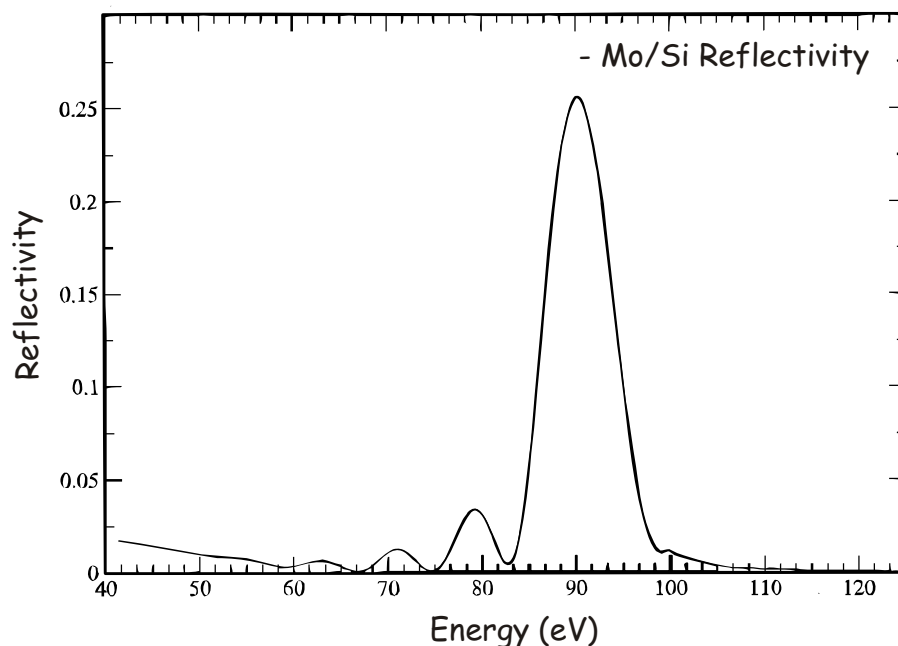


Figure 4.4: Calculated reflectivity curve for the Mo/Si based multilayer mirror employed in the experiments. An approximately  $\sim 30\%$  reflectivity over a band of 9 eV located at 93 eV constitutes multilayers an ideal tool for selective, free of dispersion, employment of XUV light to experiments.

## 4.5 The Mo/Si multilayer mirror

Employment of XUV to experiments, requires spectral filtering and focusing, without compromising either its intensity - given the low efficiency of conversion - or its temporal characteristics. Whilst grazing incidence focusing optics can offer substantially high reflectivity, spectral filtering requires more advanced technology.

Multilayer mirrors comprise such advanced tools, where reflectivity and phase of the spectral components are treated by controlling the number, the material and the thickness of a sequence of layers coated on a substrate. The realization of such mirrors requires a delicate technology of e-beam evaporation techniques [102]. The mirror used here is a concave  $f=12$  cm Mo/Si, provided by the group of Prof. Heinzmann in Bielefeld, Germany. The sequence of layers of Mo and Si have been calculated and optimized so that reflectivity and dispersion are optimal for the energies of interest (approximately at 90-100 eV). The reflectivity curve, is shown in figure 4.4. In order to allow delay between the laser and the XUV pulses, the inner part of the mirror is cut and can be translated with respect to the outer one as shown in figure 4.2.a. The outer annular part of the mirror is used to focus the laser beam, and because of that a silver coating is in principle also appropriate. The profile of the focus of the inner section (a) and the outer section (b) of the mirror, are shown in figure 4.6 (a) and (b) accordingly, for the laser beam. These patterns, represent

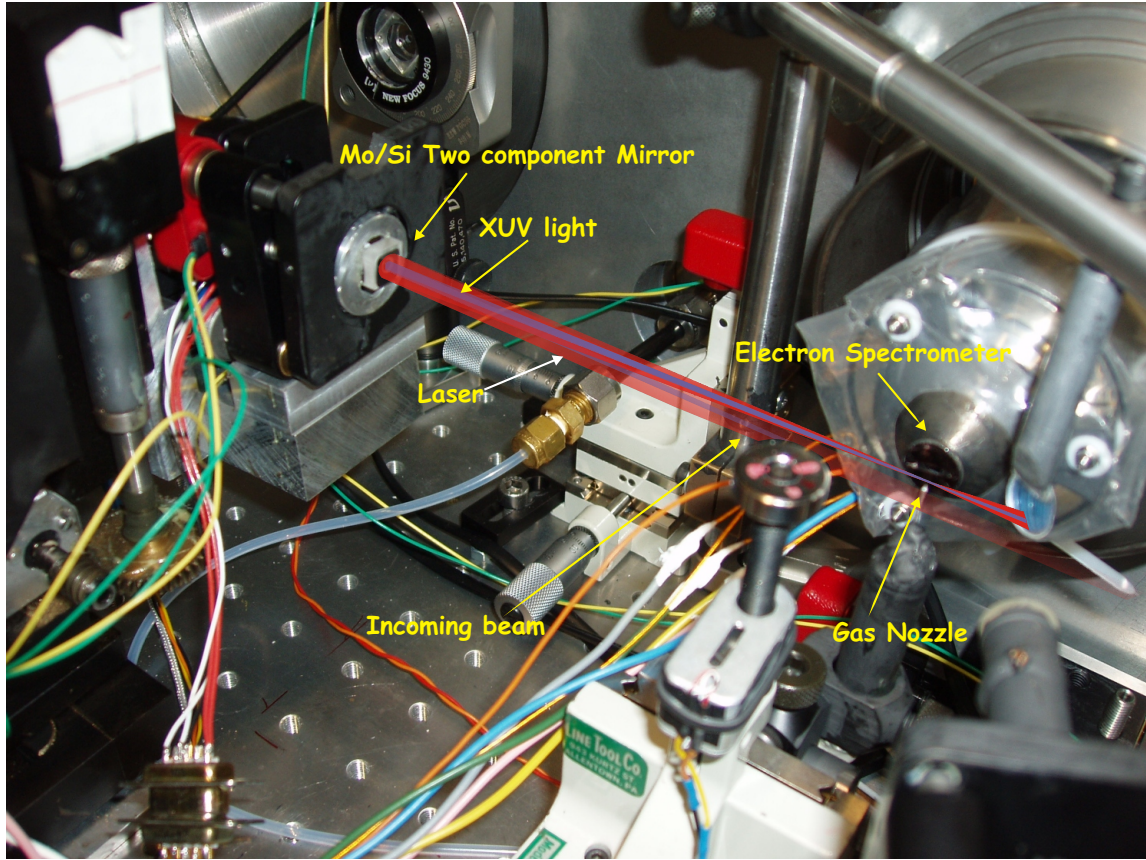


Figure 4.5: Photograph of the detection chamber. The two component Mo/Si mirror employed for the focusing of the XUV and the annular laser beam right at the gas outlet (Nozzle), placed in front of the electron spectrometer entrance. The residual laser beam is used to image the laser focus on a CCD camera chip, allowing beam positioning and diagnostics.

the brute improvements on the beam profile as compared to the previous generation of optics used for attosecond experiments, allowing higher intensities in the focus, while at the same time preserving high quality of the beam profile. The profile of the focus of the beam reflected by the outer mirror is as expected the Fourier transform of an annular beam, that is a two dimensional squared-sinc distribution. Because the amount of laser energy released in the focus is varied by an aperture installed before the mirror, control of the focal spot size is also possible in this fashion by adjusting the  $f\#$  of the annular beam. The spherical aberrations however introduced by a focusing mirror are getting more pronounced by employing high aperture [103]. Given the low divergence of the XUV beam, the XUV focus is safely locked inside the focus of the laser light which is of the order of  $20\text{-}30\mu\text{m}$ . The accurate translation of the inner mirror with respect to the outer is attained by a Piezo-system Jena, closed loop piezoelectric crystal based translation stage, that provides

a resolution of 100 as/step.

## 4.6 Alignment procedures

A critical issue for the experiments to be discussed is the accurate alignment of the optical and the XUV beam, so that the XUV light focus is well positioned inside that of the laser light, their wavefronts are parallel, and their temporal delay is properly adjusted. Additionally, the gas orifice shall be inserted precisely below the laser focus, providing high density of atoms in a well confined volume. For all three requisites, a couple of techniques have been developed during the last few years that these concepts are employed in attosecond experiments. The direct optical interference between laser light reflected by the inner and outer mirror, is the very first step to adjust their delay, while the uniformity of this interference along the profiles, suggests that the phase fronts of the two beams are parallel. Optical interference pattern between inner and outer mirror is shown in figure 4.6.c. Figure 4.6.d shows the image of the gas orifice, while inserted inside the beam focus. A sharp image, guarantees the appropriate positioning of the nozzle right below the laser focus.

Apart from the optical interference that can roughly determine the degree of temporal overlap between light reflected by the inner and the outer mirror (and therefore between XUV from the inner and laser from the outer<sup>1</sup>), a complementary method for the determination of the zero delay, has been employed. By allowing laser light to be reflected by both mirrors, ATI electrons are generated by the strong field ionization of atoms effusing from the nozzle. If the most energetic of those electrons are recorded by an electron spectrometer<sup>2</sup> as a function of the relative delay, a high order autocorrelation of the laser light right at the detection chamber is possible. A typical ATI autocorrelation trace is shown in figure 4.7. Given the high nonlinearity (typically higher than 3-4), the zero delay between inner and outer mirror is determined with accuracy better than 1 cycle of the field, that is, 2.5 fs. The determination of this relative delay is important for the experiments discussed in the following chapters, specially when the full exploitation of the strength of the electric field of the pulse close to the pulse peak is essential.

## 4.7 A sample of atoms-the gas orifice

The interaction volume is formed by a stream of gas atoms emerging from a metal coated glass orifice, with an inner diameter of 20  $\mu m$ . The aim of using such an atom source is to confine the flow of particles, only within a well defined volume inside the beam waist. This restriction is of major importance, if averaging of measured effects along the laser focus,

---

<sup>1</sup>When the Pellicle-Zr filter module is introduced in the beam path, the delay between inner and outer mirror shall be corrected for the thickness of the pellicle. This is essential for the temporal synchronization of laser and XUV.

<sup>2</sup>See subsection 4.8.

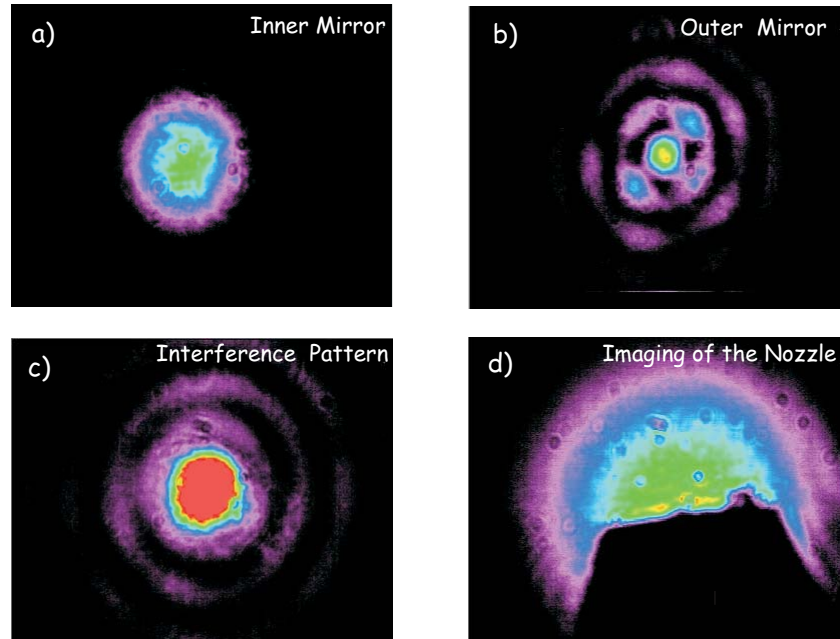


Figure 4.6: The focus of a) the inner, b) outer, and their interference if the delay is adjusted to result in a bright optical fringe c). d) The shadow of the nozzle inserted into the beam. Adjusting for a sharp image supports accurate positioning. Estimation of the focus size is also possible by the given size of the nozzle tip, here  $50 \mu\text{m}$ .

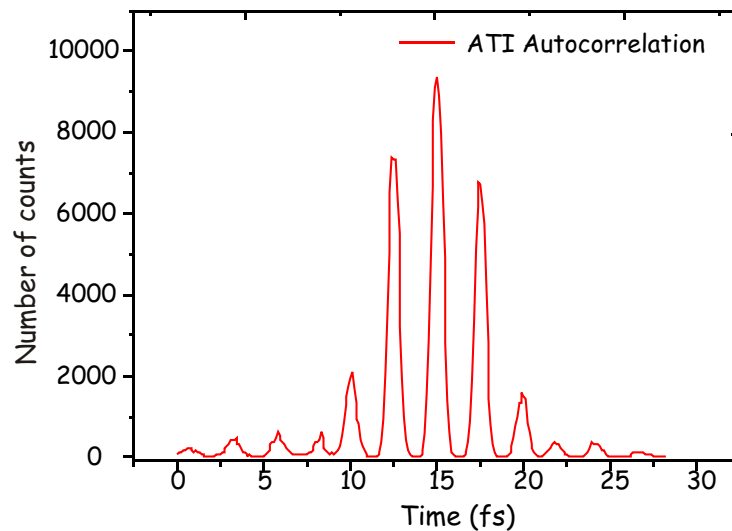


Figure 4.7: Above threshold ionization based autocorrelation trace, between optical beams focused by the inner and outer section of the two component mirror into a Ne gas jet. Such a trace allows precise determination of the optical zero delay between the two mirrors.

are to be avoided. A driving pressure of about 2 atm is necessary for achieving sufficient particle density at the nozzle outlet.

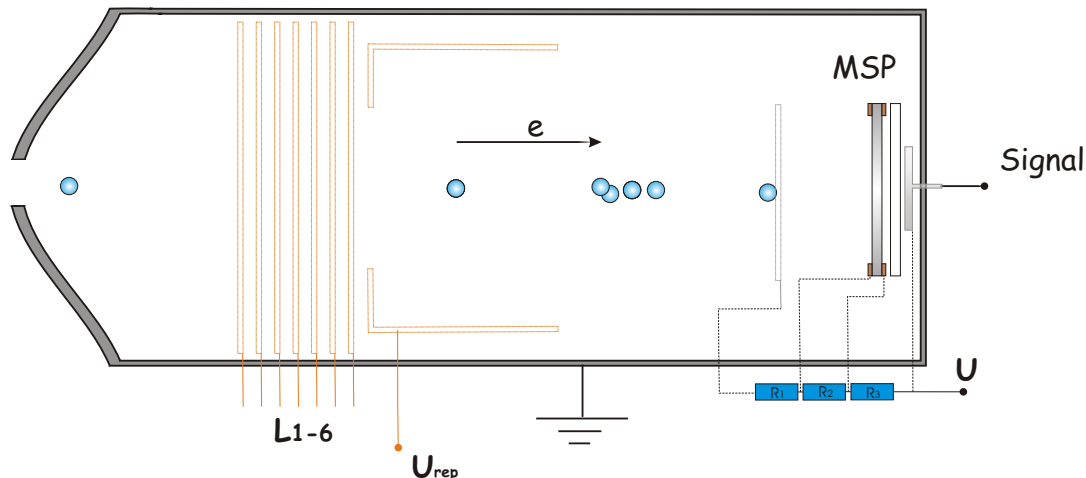


Figure 4.8: Schematic of the time of flight spectrometer (TOF). A 3800 V applied voltage is divided by a  $R_1=3.3 \text{ M}\Omega$ ,  $R_2=22 \text{ }\Omega$ ,  $R_3= 3.3 \text{ M}\Omega$ . A negative voltage applied as  $U_{rep}$  can increase the virtual path of the electrons, allowing higher energy resolution of the detector. L1-6: electrostatic lenses.

## 4.8 Electron spectrometer

A time-of-flight spectrometer (TOF) is the principal tool for investigations in the electron spectra domain and has been extensively employed in the X-ray, XUV spectroscopy, ion spectrometry, mass spectrometry and nuclear physics. It draws on the essential principle that fragments of different mass or kinetic energy, in the case of an electron spectrometer, have a different flight time to a detector, placed at a certain distance away from their generation point. The implementation of the concept, calls for a time-resolved detection of the arriving fragments (electrons), with descent resolution. If the minimal time interval that electronics can resolve is  $\Delta t$  and the length of the drift tube is  $L$  the energy resolution  $\Delta E$  is given by:

$$\Delta E = \frac{2\sqrt{2}\Delta t}{m_e L} E^{3/2} \quad (4.1)$$

where  $m$  is the electron mass and  $E$  the energy of the electrons.

A time of flight electrons spectrometer initially designed by M. Drescher has been used for a series of attosecond experiments so far and it is also employed in the experiments presented in this thesis. A schematic of the TOF spectrometer is shown in figure 4.8. It

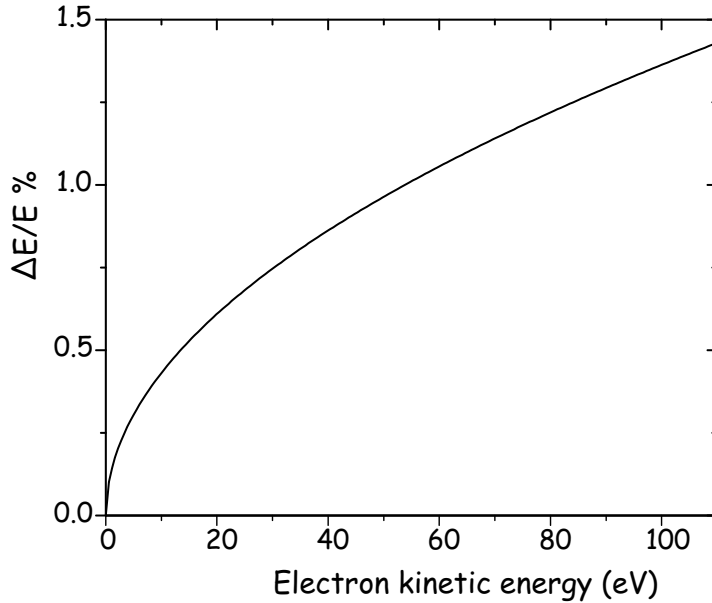


Figure 4.9: The resolution of the time of flight electron spectrometer (TOF). Total length  $L=40$  cm  $dt=0.45$  ns for single electron acquisition per laser shot. For the energy range 50 eV - 100 eV the resolution is about 1 % or better.

consists of a 40 cm long magnetic shielded drift tube, equipped by a 5 cm microsphere plate detector. A series of electrostatic lenses (see schematic) L1-6 installed along the tube, allows increasing the acceptance angle of the electron collection. For a more technical perspective on electrostatic focusing see also [104]. This feature of the TOF detector is not utilized in any of the experiments presented here, however for experiments where low electron count rates are typical, its use might be advantageous. In order to get the highest possible spectral resolution, the signal from the MSP detector is amplified and digitized using an Analog to Digital converter, before analyzed by a (1024 channel) multi-channel analyzer. The temporal resolution of this analyzer (FAST COM) is about 0.45 ns. In figure 4.9 the resolution of the TOF as a function of the energy is shown, with  $L=40$  cm and  $dt=0.46$  ns. The resulting  $\simeq 1\%$  resolution for the range 50-100 eV can be considered satisfactory for the experiments carried out (see also chapter 5). For multi-electron acquisition per laser shot, several limitations are imposed by the rise time of the Microsphere plate detector, which typically exceeds 1-2 ns and restricts the resolution severely. However the single electron detection per laser shot is an effective way to preserve high resolution, provided that the total number of electrons is not much higher than one per laser shot, otherwise this would translate to an inefficient signal acquisition. Figure 4.10 depicts the electron spectrum resulting from the ionization of Ne atoms by the 9 eV band of XUV photons located at  $\approx 93$  eV as defined by the reflectivity curve of the Mo/Si multilayer mirror shown in figure 4.4.

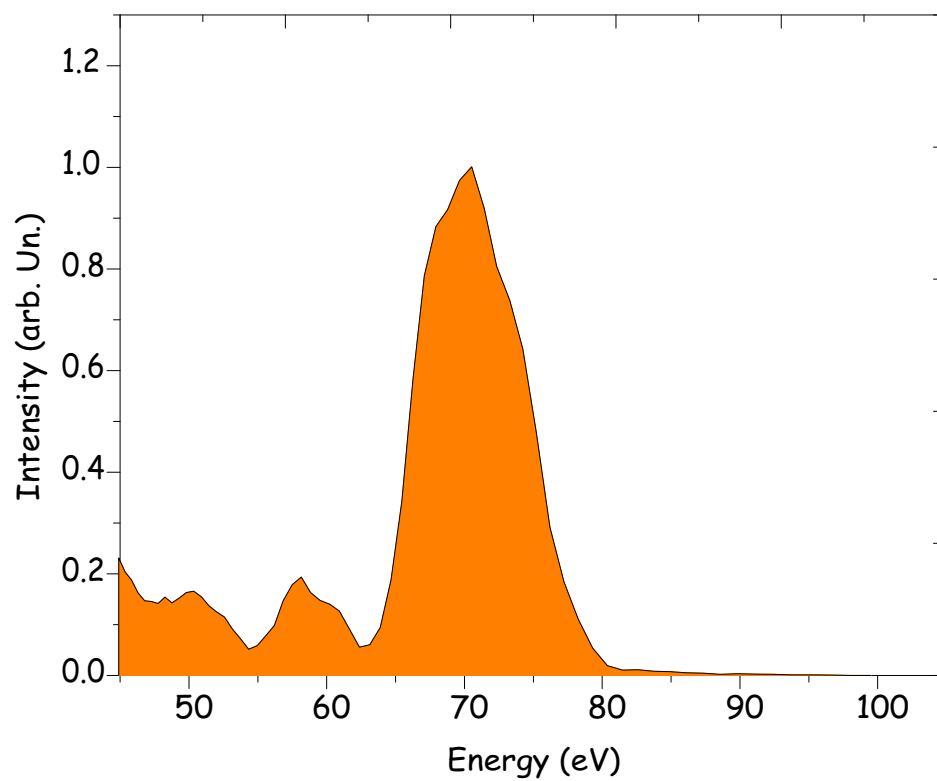


Figure 4.10: Electron spectrum measured with the TOF electron spectrometer. It corresponds to photoelectrons generated when XUV light reflected from the Multilayer mirror reaches the Ne nozzle, installed right in front of the spectrometer entrance.

# Chapter 5

## Metrology of attosecond pulses

In this chapter observation, measurement and control of XUV attosecond pulses are experimentally demonstrated. In the first section, localization of XUV light generation within a fraction of the light field oscillation is observed by means of direct spectral observation of the emanating XUV spectra. The second section presents the experimental realization of the atomic streak camera and its employment for the temporal characterization of attosecond pulses. Improvements that have been possible on the resolution and dynamic range expanding the capabilities of the measuring techniques are discussed.

### 5.1 Spectral manifestation of attosecond pulses

The potential to synthesize attosecond pulses, employing the continuum XUV radiation close to the cut-off emerging from the most prominent half cycle close to the peak of a cosine like few-cycle laser pulse, has been pointed out in the first chapter as well as the main physical aspects which allow a linkage between time and spectral domain. In order to observe spectral signatures of the generated bursts, except the descent resolution of an XUV spectrometer, short laser pulses allowing a highly pronounced threshold for a single half cycle and phase control of the waveform, or alternatively, single shot spectral acquisition, are important. Here phase controlled 5.4 fs pulses at  $\lambda_0=760$  nm are focused into a neon gas target. The gas pressure is approximately 160 mbar and the estimated intensity at the focus is  $7 \times 10^{14} \text{ W/cm}^2$ . The emanating XUV light is observed using an XUV spectrometer discussed in section 4.4. To make sure that propagation effects have negligible contribution the length of the interaction region  $L_{int}$  is confined by the thickness of the tube to be  $L_{int} < L_{coh}/2$  [43]. A series of XUV spectra at different phase settings of the laser pulse, are subsequently recorded and are depicted in figure 5.1. The integration time was 0.5 sec. Last panel depicts spectra recorded in the absence of phase stabilization.

#### Discussion

According to the discussion in section 1.4, attributing a specific CE phase for the light pulse to the spectral pattern of each panel is possible. If the generation is restricted only

within a single cycle around the peak of the pulse, the spectrum is expected to form a continuum around the cut-off as shown in panel (d). In the case of a "sine like" pulse, the generation of extreme ultraviolet light in the cut-off regime can be possible for two successive cycles. Two successive bursts of XUV light result in an interference pattern if observed in the spectral domain. This is shown in panel (c),(f) while in the rest of the panels a gradual conversion of the broad continuum to a spectrum with the highest modulation is clearly notable. There the two generated bursts contribute with different weights resulting in intermediate patterns, e.g. between full continuum and fringes of high visibility. For XUV photons generated over more cycles and therefore several re-collisions of the electron with the core, due to lower energy threshold of generation, the interference results in the "high harmonic like" spectrum as shown in lower energies in (a),(b),(c). Last panel shows the average over several pulses without pulse to pulse phase stabilization. The previously observed effects are now smeared out owing to the random phases, resulting in different temporal and therefore spectral patterns from pulse to pulse.

An energetic displacement for discrete "harmonic like" peaks of the spectral pattern for different phase settings, can be attributed to a complex interference between successive XUV bursts generated by neighboring half cycles. The effect has been studied in detail also elsewhere [105]. Recently, similar behavior has been observed also without phase stabilization [106] employing single shot acquisition of XUV spectra, emanating from atoms irradiated by few cycle pulses with randomly varying phase.

To further support the intuitive picture presented so far, calculations employing the numerical integration of the Schrödinger equation are presented in figure 5.3. The results of these simulations along with previous studies [107] fully support the intuitive picture presented for the underlying mechanism of the few cycle light driven XUV generation.

The observation of the signature of the attosecond pulses in the spectral domain constitutes also the basis of experiments discussed later in this thesis, because it provides a simple and reliable way to ensure the existence of a double or an isolated XUV burst. This technique was the first not only to directly observe attosecond signatures, but also a method to allow phase calibration of the few-cycle laser pulse source based on the association of each of the XUV spectra to a certain pulse phase. Inversion symmetry associated with XUV light generation into a gas medium results in a  $\pm\pi$  ambiguity for the determination of the pulse phase. That means that a "cosine like" pulse can not be discriminated from an "anti cosine pulse". This ambiguity has been lifted in subsequent experiments [65] employing above threshold ionization (ATI) of atoms. Electrons generated by above threshold ionization of atoms with phase controlled pulses are emitted asymmetrically along the polarization direction depending on the absolute phase of the pulse.

Nevertheless, even with the  $\pm\pi$  ambiguity of phase determination based on the analysis of the XUV spectra, a detection system capable to record spectra in a single shot fashion, could provide a reliable single shot phase detection and at the same time a reliable feedback to be employed for the compensation of slow phase drifts of the few cycle pulse. The obvious advantage here is that this method retrieves the phase of the pulse at the generation volume, in contrast to other methods that require separate experimental devices and the retrieved phase shall always be linked with that of the pulse at the corresponding experimental area.

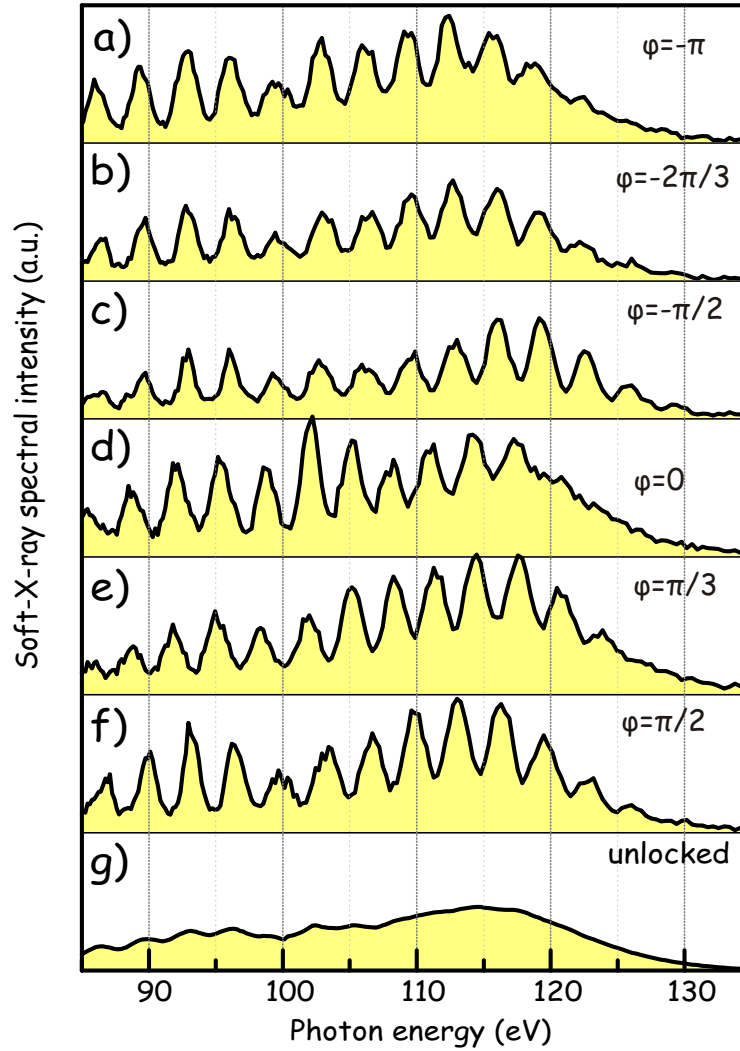


Figure 5.1: Measured spectral intensity for XUV emerging from few cycle phase controlled laser pulses, interacting with a Ne atomic target. (a) to (f) spectra measured under different phase settings. Continuum spectrum around the cut-off in (a) and (d) can be attributed to a cosine like pulse and manifest in the spectral domain that generation is restricted within a half cycle of the field. The discrete peaks appearing at (b) and (f) correspond to spectral interference between XUV pulses generated at two consecutive recombinations of the electron with the core, resulting in interference in the spectral domain. (g) Spectrum measured without phase stabilization.

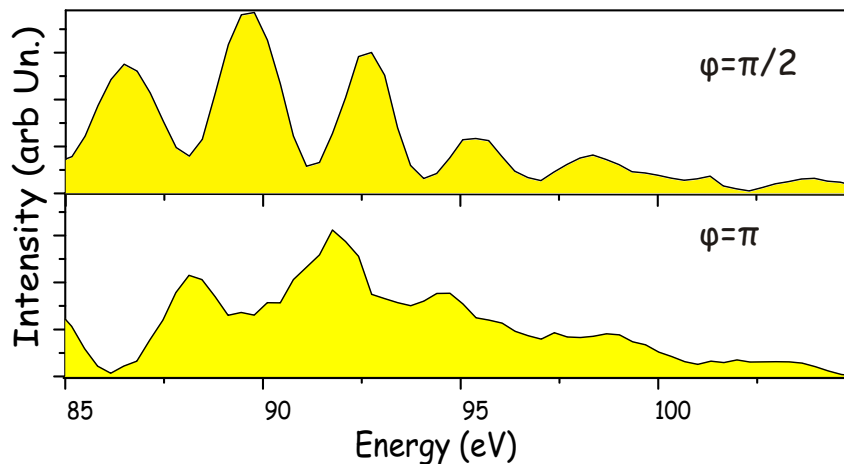


Figure 5.2: XUV spectra intensity in the range of 90-100 eV where the reflectivity band of the multilayer Mo/Si optics is located. Cases for  $\varphi = \pi/2$  and  $\varphi = \pi$  for the phase of the few-cycle driving pulse are shown.

The above measurements confirm the potential to synthesize attosecond pulses by exploiting the continuum spectrum close to the cut-off. The practical synthesis of these pulses, requires spectral isolation of XUV light from this regime which can be done by means of multilayer optics. In figure 5.2 spectra recorded at the regime of 90-100 eV are presented, where same behavior is observed for a cosine and a sine pulse shape, respectively. Owing to the spectral reflectivity of the Mo/Si multilayer mirror to be employed later in this chapter for the generation of isolated bursts within this regime (centered at 93 eV), observation of same behavior is essential.

## 5.2 Spectral selection, synthesis, and measurement of isolated attosecond pulses: The attosecond streak camera concept put into practice.

The ability to control the generation of XUV light by means of the phase of the driving pulse along with the compelling evidence of this control on the observed spectra, motivated the next step, which is, the spectral isolation of the XUV continuum generated by the most prominent half cycle of the pulse to synthesize an isolated attosecond burst. Additionally, but equivalently important to employ the scheme of the atomic streak camera to characterize this attosecond burst.

For the experiments, phase stabilized 5 fs laser pulses introduced in chapter 3 and the experimental setup in chapter 4 are employed. Briefly the scheme: The XUV radiation

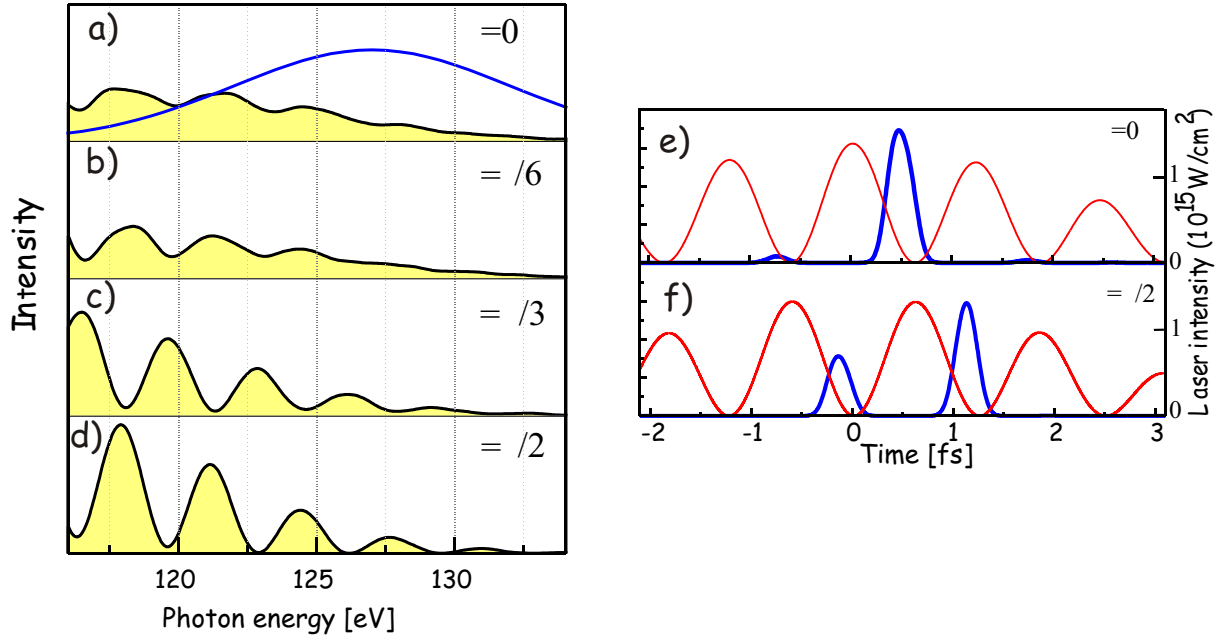


Figure 5.3: Numerical simulations of few-cycle-driven coherent XUV emission from atoms. (a)(d) Cutoff-range spectra for different CE phase settings of the driving laser pulse. (e)(f) Blue curves depict the temporal intensity profile of the cutoff harmonic radiation filtered through a Gaussian bandpass filter with a full-width at half maximum of 7 eV [Blue line in (a)], whereas the red curves plot the squared field. These results support the intuitive analysis discussed in the text. The field carrying  $\phi = 0$  is predicted to produce a single soft-X-ray burst [filtered in the cutoff, (e)]. Deviation of  $\phi$  from zero gradually suppresses the magnitude of the main burst and gives rise to a satellite spike. If the phase of the driving field is chosen to  $\phi = \pi/2$  two prominent spikes appearing in the time domain (f) correspond to a highly modulated spectrum around the cut-off. (d)

produced by the laser light focused into a Ne gas target, along with the residual laser light, are subsequently focused using a two component Mo/Si mirror into a second Ne atomic target. The selective spectral reflectivity of the Mo/Si mirror isolates a band of 9 eV around 93 eV (figure 4.4). The XUV pulse ionizes the Ne atoms, and electrons are produced with a kinetic energy of  $93 - 21.5 = 71.5$  eV. A typical electron spectrum produced by the XUV is shown in figure 4.10. The majority of the electrons counts form a highly pronounced peak in the regime of high reflectance for the Mo/Si multilayer-mirror. Shake off process of the XUV ionization of Ne, gives rise to a background spanning from the highest energy photon of the XUV burst down to a few tens of electronvolts [108], [109]. These processes though of great interest because they can probably allow insight to intra-atomic dynamics, will not be considered in this study, since they are not entangled with the studied effects. In order to ensure the isolation of photons generated only by a pair of pronounced cycles of the laser pulse, the XUV spectrum is initially recorded using the spectral technique discussed

in the previous section and the cut off is adjusted to match the reflectivity of the Mo/Si mirror. At a next step the ionization of Ne atoms by XUV photons focused by the inner Mo/Si mirror into the gas target is dressed by laser light using the outer part of the double mirror module which at the same time allows the introduction of delay between XUV and laser light. The very first experimental version of this concept was demonstrated in [110], by focusing XUV and laser light to a Neon gas target employing the same reflector, without the ability to introduce delay between them. Here, the concept is extended by the introduction of a delay between laser and XUV light. This delay can be varied by a minimal step of 100 as, using a piezo-translator. We study two main schemes, employing a) pulses with random phase b) pulses with controlled phase.

### 5.2.1 Scheme I (Pulses with random phase)

At a first step we study the case where the generation of XUV light is not controlled, but still the laser pulses employed are as short as  $\sim 5$  fs. With pulses consisting of only two oscillations even with completely random phase settings, generation of XUV takes place only within the two most prominent cycles inside the pulse; according to the theory. If the generation is not controlled, then the expected temporal structure of the XUV light, differs dramatically from pulse to pulse. For a "sine like" waveform, two prominent re-collisions of the electron generated XUV bursts separated by half a period of the light field ( $\sim 1.3$  fs) while a single re-collision for a cosine and its counterpart (anti-cosine) waveform-as explained schematically in figure 1.6- generate a single burst. Intermediate phase settings between a cosine and an anti-cosine would lead always to two XUV bursts with non-equal amplitude. Owing to the ability to accurately introduce delay between XUV light and laser light that dresses the ionization, when the double burst - the statistical result of all phase settings - is probed by the field at a different phase, it translates into a different amount of momentum imparted to electrons generated by each of the two XUV bursts. Actually the delay of 1.3 fs, that is, half a period of the fundamental, translates into opposite momentum shift for the two pulses by the field at any delay.

This results in an energetic separation of electrons from the two bursts, if probed at the right phase of the field. Figure 5.4 shows in false color representation a series of spectra, recorded as a function of the delay between the XUV light and the laser pulse with step of 100 as, and over a range of almost 12 fs, across the entire laser pulse field. The out of phase oscillation of electrons generated by each of the two XUV bursts, is apparent. When both of them cross a zero transition of the vector potential, they collapse to a single spectral peak, like the one of figure 4.10 while synchronized to the maxima of the vector potential, are energetically streaked apart by several tens of electronvolts.

### Discussion

These experiments, though no control to the waveform has been employed so far, allow two important conclusions.

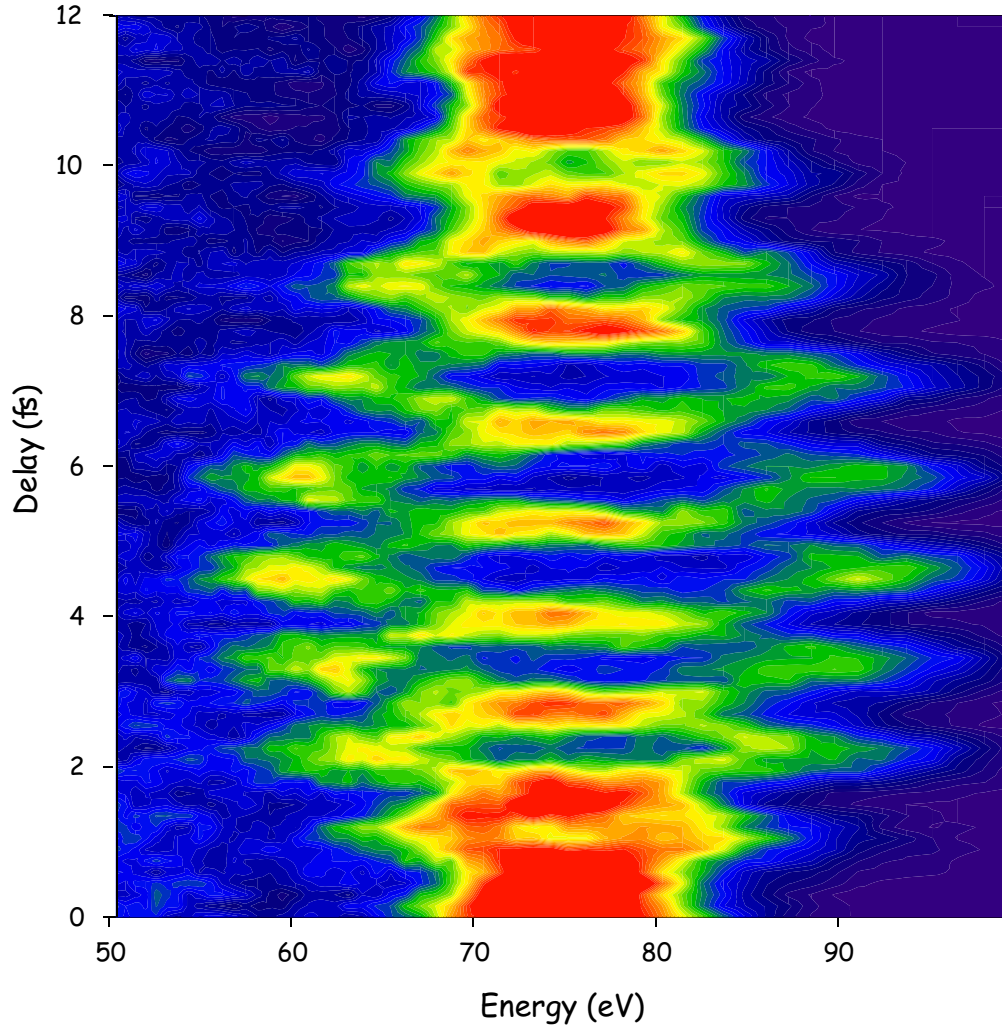


Figure 5.4: A series of photoelectron spectra plotted as a function of the delay between XUV and laser pulse in the absence of phase stabilization. The upshifted and downshifted peak in this case, is a result of multiple contributions from pulses with random phase settings. However, if a few cycle driving pulse is employed, the generation of XUV is restricted to only a pair of the most prominent energetically cycles and thus it can be considered as the result of an ensemble of cosinusoidal, anti-cosinusoidal and sinusoidal pulses. The ability to energetically break up the initial spectrum into two energetically upshifted and downshifted spectral peaks, demonstrates similarly with the spectral measurements presented in the previous section the sub-cycle temporal localization of XUV light, not only during the generation process but also after spectral filtering and focusing of the XUV radiation.

The signature of sub-cycle localization of the generation of XUV light observed by spectral techniques in the previous section, is present also when electrons are probed by the electric field of light. The generated electrons by the XUV burst are well localized within a fraction of the cycle and that allows streaking and energetic displacement, rather than broadening that would indicate release of electrons among several cycles. Actually, the smearing effect appearing at the high harmonic XUV spectra, when random phase pulses (last panel figure 5.1) arise, is not apparent here, because pulses with different phases add up electron counts on the same energy peaks.

The second important feature is that the generation is not only localized within a fraction of a cycle, but additionally, that this occurs for a maximum of two laser driven recombinations, if the XUV cut-off is properly adjusted. If this was not the case, delaying a train of XUV bursts (and therefore electron bunches) with respect to the laser field, would have resulted in a smearing of the pattern, due to the non-uniform streaking strength of non-neighboring cycles of a short laser pulse.

### 5.2.2 Scheme II (Phase controlled laser pulses)

The generation of a single XUV burst requires phase stabilization of the pulse locked to a cosine waveform. Additionally, the concept of the atomic streak camera, calls for a stable waveform for probing an electron bunch.

Before employing phase stabilized pulses for carrying out a similar scan, the delay is adjusted so, that the up-shifted and the downshifted spectral peaks of the previous case, are maximally separated. With the laser pulses phase stabilized, the phase is accurately adjusted using a pair of thin fused silica wedges introduced into the laser beam path (figure 3.2), so that a single pronounced upshifted or downshifted peak in the photoelectron energy spectrum survives at the expense of its counterpart. A series of spectra are recorded as a function of the delay between XUV and laser light, using a step of 150 as and integration over 80000 shots of the laser per spectrum. The results are plotted in false color in figure 5.5. The scan extends over a range of 7 fs in delay time. The existence of only a single spectral peak, displaced by several tens of eV in the energy domain driven by the laser pulse, verifies the generation of a single electron burst and therefore an isolated XUV pulse in the time domain. According to the description of the concept as presented in chapter 2, a scan over a single oscillation of the laser field ensures the probing of the electron bunch, through all necessary instances in order to access its exact temporal structure. The analysis of the data is performed using a theoretical model where parameters like laser field strength, chirp, as well as a potential jitter between attosecond and laser pulse; result of possible interferometric instabilities (jittering), have been taken into consideration. The development of this model and its practical implementation by a numerical code has been done by Dr. Vlad Yakovlev and Dr. Armin Scrinzi. A review of the mathematical techniques employed for the reconstruction of the temporal characteristics of the attosecond pulse has been published recently [111]. Contributions from shake off process by the XUV ionization, result in a continuum background as can be seen also in figure 4.10. This background is mostly subtracted due to its negligible contribution to the studied effects.

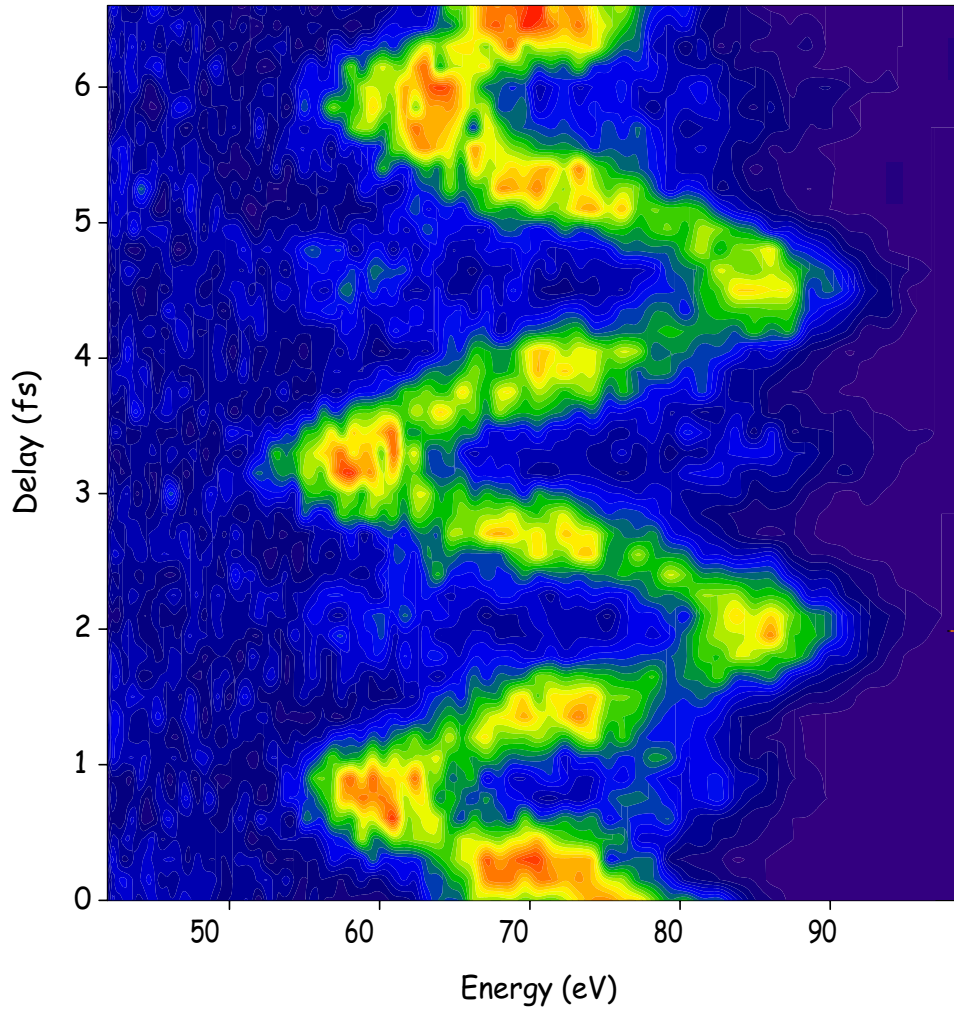


Figure 5.5: A series of photoelectron spectra, recorded as a function of the delay between XUV and laser light, generated and probed by phase stabilized few-cycle laser pulses. The phase has been adjusted to support a single pronounced photoelectron peak. Probing the energy distribution of the electrons at different instances of the field, has allowed the full reconstruction of the temporal profile of the attosecond pulse, employing the concept of the atomic streak camera. The pulse duration has been inferred to be 250 as, by means of numerical analysis of the spectra, closely related with the Fourier transform limited pulse, expected for the current Mo/Si spectral bandwidth.

Selected "streaked" photoelectron spectra corresponding to zero transitions of the vector potential, highly sensitive to the chirp of the electron bunch as discussed in chapter 2, are depicted in figure 5.6. The best fit to this data results in a pulse duration of 250 as for the XUV pulse, corresponding to the Fourier transform limited duration associated to the Mo/Si mirror reflectivity employed to select the  $\sim 9$  eV band of the continuum spectrum. Finally it is important to mention that the code employed for the data analysis, takes into consideration not only spectra corresponding to particular field transitions (e.g. field maxima of minima), but every measured spectrum. This concept reduces dramatically the error for the reconstruction of the attosecond pulse characteristics, inferred in this case by several tens to hundreds of electron spectra.

### 5.3 Discussion on the results

The first experimental results and experimental realization of an attosecond streak camera have been recorded in late 2003, utilizing a  $\sim 9$  eV concave 3.5 cm focal length, two component multilayers and have been published in Nature [112]. The maximum streaking field that could be attained while preserving high optical quality of the laser beam in the focus, was rather limited by that module due to technical imperfections. The maximum field achieved utilizing this module was capable to energetically streak photoelectron peak by approximately  $\sim 25$  eV in a static configuration, that is, when light and XUV attosecond pulse are reflected by the same Mo/Si mirror. In a time delay geometry between XUV and optical light and by keeping the optical quality of the beam high, the maximum attainable field strength could energetically streak the electron distribution by  $\sim 5$  eV. However the full potential of the technique can be exploited only if high energetic streaking is available also in the delay time, that is, the attosecond pulse can be precisely synchronized to different instances under the oscillation of the laser light field as the concept of the camera dictates. The resolution of the attosecond streak camera in the time domain, is strongly depended on this streaking field according to the equation [111]:

$$\delta t = \frac{T_0}{2\pi} \sqrt{\frac{\hbar\omega_l}{\Delta W_{max}}} \quad (5.1)$$

where  $\delta t$  is the minimal time interval between two events to be resolved,  $T_0$  is the period,  $\omega_l$  the frequency of the laser oscillation respectively, and  $\Delta W_{max}$  is the maximal energetic streaking of the photoelectron distribution.

The electric field in this improved version as shown in figure 5.5 is capable of a  $\sim 15$  eV energetic displacement, corresponding to a resolution better than 200 as. The radical improvement responsible for this advance is basically due to the implementation of higher quality multilayer substrates, ensuring a uniform wavefront for the laser light dressing the ionization of the XUV attosecond pulse. The above mentioned improvements, have several implications for the utilization of the technique in order to carry out attosecond experiments. In a recent publication [8] the employment of the technique in order to perform atomic studies in Lanthanides in time-resolved fashion, is proposed. Using the

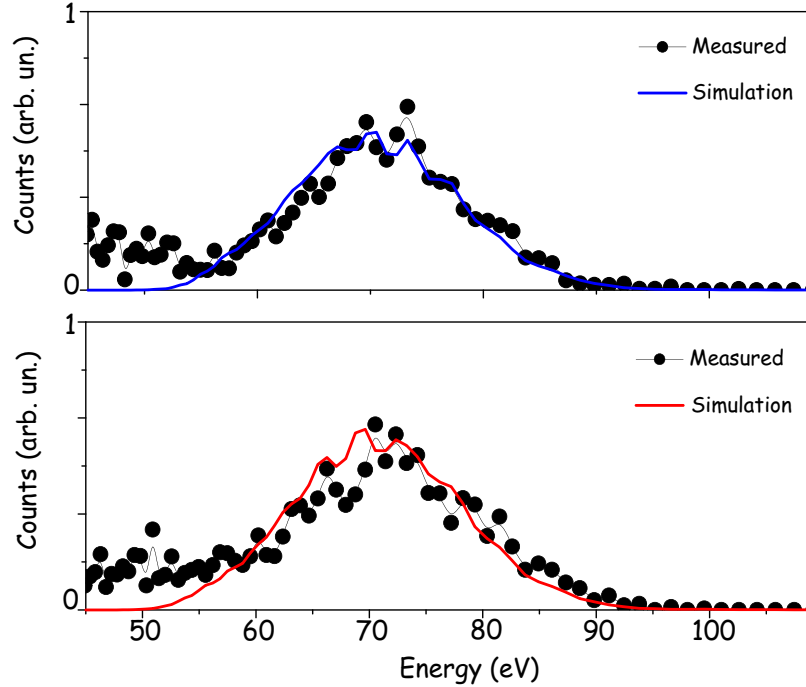


Figure 5.6: Selected spectra corresponding to synchronized photoemission by the XUV attosecond pulse to adjacent zero transitions of the vector potential of the probing light field. Measured data are plotted with dots while blue and red line correspond to best fitting. The retrieved pulse duration of the attosecond pulse is 250 as in accordance with the fourier transformed limited duration supported by the Mo/Si reflectivity.

scheme discussed here, dynamic observation of Fano-type resonances has been proposed. The resolution offered by this scheme will allow reliable access to the studied phenomena.

The second key implication, is that, now, the dynamic range of streaking is such that the technique can be used also for the characterization of the light field responsible for the streaking. The relation between the field strength and the streaking of the electron peak in the energy domain, has been extensively addressed so far. Though the oscillation of the steering light is definitely trackable already in figure 5.5, a complete characterization would require scanning over a delay at least two to three times larger than the expected pulse length (of the order of 5 fs), so that the complete build up and subsequent disappear, becomes visible. If so, information of the absolute phase, the chirp and the pulse duration can be accurately inferred from the same measurement.

The above quantities can be simultaneously accessed only if a scan with high dynamic range capable to resolve the field oscillation also far from the pulse peak is possible, unveiling its envelope. The dynamic range provided with these advancements, opens the way for such a measurement. A complete characterization has been possible and it is presented

separately in the next chapter, where additionally the potential of using such a technique for the characterization of extremely broad and arbitrarily shaped light waveforms, is addressed.

The aforementioned equation implies also that higher temporal resolution can be attained by increasing the streaking field. However this is not valid infinitesimally due to the fact that the laser field might get strong enough to induce non negligible effects, by interacting with the atoms conceptually ionized only by the XUV field. Generation of electrons with high kinetic energies resulting from the above threshold ionization of atoms by the laser field, might become important. A possible entanglement of a background that ATI electrons form at high kinetic energies with the streaked photoelectron peaks is undesirable. These limits will be discussed in detail in the last chapter, along with points related with the dynamic range of the field characterization technique.

High dynamic range for attosecond measurements, implies also additional control on the efficient isolation of an attosecond pulse, because the contribution of a possible satellite burst -result either of an erroneous absolute phase setting or duration of the laser pulse - is easily resolved provided that the spectra can be energetically separated by approximately  $\Delta E_{mirror}$ , that is the spectral bandwidth of the attosecond pulse. In the case of the present measurements, this implies a  $\Delta W \geq 5$  eV. The currently available resolution allows the characterization of pulses with  $\Delta t_p < 100$  as. If shorter pulses (and therefore broader corresponding spectra) are to be characterized this dynamic range has to be improved accordingly.

# Chapter 6

## Complete characterization of light waves

Techniques developed over the last decades, have allowed accurate characterization of femtosecond pulses, down to sub-ten femtosecond durations. Except the autocorrelation technique [113] mostly accurate for regular spectral shapes, techniques like FROG (frequency resolved optical gating) [114], and SPIDER (spectral interferometry for direct electric field reconstruction) [115] and variations as GRENNUILLE [116] and TADPOLE [117], have been broadly proliferated. FROG and SPIDER undoubtedly are dominant. FROG is based on the interaction of light with a nonlinear medium in order to gate the unknown field of its replica and to extract phase and amplitude information at the same time for reconstructing the field. SPIDER on the other hand is employing the generation of two delayed replicas of a pulse as well as a temporally broadened (chirped) one by a bulk material, which are subsequently mixed in a nonlinear medium. By delaying the two pulses with respect to the broadened replica, the spectra phase can be retrieved.

Despite the success of these techniques [118], [96] there are profound limitations if they are to be employed for the characterization of ultra broad waveforms or multi-octave waveforms based on discrete sidebands. To manipulate pulses in a characterization scheme like the aforementioned, germane handling of these sensitive light entities including splitting, reflection, focusing by appropriate optics for the entire spectrum, is essential. On top of that, materials in which nonlinear processes that can be driven by the entire spectrum, are also necessary. A final state of an atomic or molecular system reachable by two photons of a part of the spectrum can be at the same time accessible by one photon of its second harmonic, for spectra spanning more than an octave or multioctave spectra that consist of distinct modes. For such broadband waveforms spanning from the IR to the UV, the absence of reliable nonlinear media for the entire range imposes insurmountable frontiers to the measurement of a multicolor pulse. The above hindrances call for a technique that requires neither a nonlinear medium nor beam-splitting for the characterization of multicolor ultra-broad waveforms.

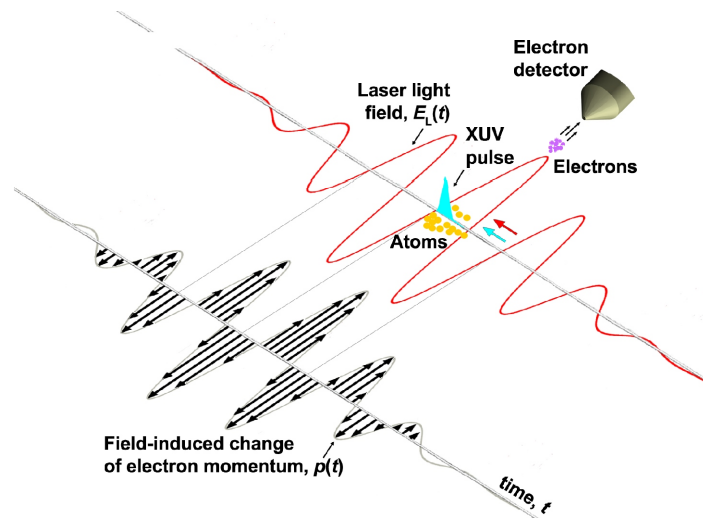


Figure 6.1: Schematic of the principle of attosecond light sampling. A few cycle pulse together with an XUV attosecond burst, are focused into an atomic gas target. The XUV burst knocks free electrons by photoionization. The momentum imparted to the electrons from the field of light  $E(t)$  scales as the instantaneous value of the vector potential of the field  $A(t)$  at the instant of their release (black arrows). An electron spectrometer measures the momentum change along the direction of the electric field  $E(\vec{r}, t)$ .

## 6.1 Attosecond oscilloscope-sampling of light waves

Here is presented how an attosecond pulse can play the role of an ultrafast sampler, in order to access directly the electric field of a light waveform, of arbitrary shape and spectrum. The technique can be considered as a high dynamic range application of the ideas and experiments presented so far, by means of the attosecond streak camera. Here the second perspective of this dual potential, namely to characterize the attosecond pulse and the light field simultaneously is presented. The most elementary way to examine the strength of a field is to introduce a probe charge and measure the force which is exerted to it according to the elementary formula  $\vec{F} = \vec{E}q$ , where  $\vec{E}$  is the electric field vector and  $q$  the probe charge. In the case of a static field, this method has its trivial application. However when an ultrafast field is to be probed, the experimental realization of such a scheme is possible only under certain conditions.

### Instantaneous release of charge

When this method is employed to track rapidly changing electric fields, implies the ability to generate electric charge by a technique that is much faster than the variation of the field to be probed. How well confined the release has to be, is practically defined by the maximum frequency that the charge bunch is expected to sample. Mathematically this is expressed

by the Nyquist theorem in sampling theory. According to that theorem the discrete time sequence of a continuous function, contains enough information to reproduce the function, if the sampling rate ( $1/T_s$ ) is at least the double of the highest frequency contained in the original signal. This elementary theorem, is fully valid if sampling of a light waveform is considered too. A period of 2-2.5 fs would in this case call for a sampling of the field faster than 1 fs. XUV attosecond pulses with a duration of 250 as characterized in the previous chapter used to ionize atoms, can provide the necessary temporal confinement of charge under the laser light period. The concept is schematically illustrated in figure 6.1.

Of course, even if electrons are released instantaneously and with high temporal confinement, they do not leave the area of their interaction with the field instantaneously. Actually upon their release and depending on their initial velocity, they experience the entire temporal field variation, until the end of the waveform. In accordance with equation 2.6, the momentum shift induced to the electron bunch, equals the vector potential. By re-writing this equation:

$$\Delta p(\vec{r}, t) = e \int_{t_b}^{\infty} E_l(r, t) dt = e A_l(\vec{r}, t) \quad (6.1)$$

from which the electric field can be expressed as:

$$E_L(\vec{r}, t) = \frac{\Delta p(\vec{r}, t - \delta t/2) - \Delta p(\vec{r}, t + \delta t/2)}{e \delta t} \quad (6.2)$$

indicating that the sampling of the pulse at two successive points temporally separated by  $\delta t$  by measuring the momentum imparted to the electrons, can define the electric field. The accuracy here is dictated by  $\delta t$ . From a mathematical point of view this is the definition of the first derivative of a function and here the way that the vector potential could allow derivation of the electric field of light. Mathematically this derivation of the electric field from the vector potential is accurate if the sampling rate is  $\delta t_s < 2\pi/\omega_{max}$ , where  $\omega_{max}$  is the highest frequency component of the reconstructed field.

## Reproducible optical waveform

Unless the waveform shape and temporal variation of the field strength is accessed within a single shot, like a conventional oscilloscope or a streak camera, the repetitive delivery of the waveform in order to sample the strength of the field at a different instance each time, is a vital issue for retrieving its temporal shape. This has been possible with the phase stabilization concept presented in chapter 2, and recently in combination with developments that draw on ATI phase detection allowing long term phase stability, necessary for experiments where decent statistics require long integration times [83].

## Precise synchronization

Synchronization in pump probe experiments is a critical issue, not only for accessing the attosecond time scale. Especially when the pump and the probe pulse are provided by different sources, accurate determination of their timing is essential before any experimental

application. In a synchrotron for example, where ultra bright XUV sources are available, the timing between a laser pulse and XUV probe, has been the key issue before a combination of those fields becomes a tool for temporal studies. Recent progress on the field has made possible synchronization down to 100 fs [119]. In the case of laser based time resolved experiments where the pump and the probe pulse are optical clones of the same initial beam, the synchronization is practically limited only by interferometric stability of the apparatus, that delivers the pulses to experiments. A light and an attosecond pulse can be precisely synchronized with attosecond resolution, if a part of the light is used to generate the attosecond pulse. The origin of the excellent synchronization is the mechanism of XUV light generation, as explained by the semi-classical model in chapter 1, where the XUV photons are emitted during a precisely driven process by the laser light [39]. Then, the re-collision of the electron, is temporally affected by the uncertainty principle, which introduces an inherent limit for the shorter pulses to be generated by exploiting this mechanism. In the case of long laser pulses, the synchronization of individual harmonics has been studied [62] and excellent timing between the cut-off harmonics has been demonstrated, even if they are produced by at least a couple of neighboring oscillation of the electric field of the pulse, due to long pulse durations in this particular study.

## 6.2 Experimental

The experimental setup employed for putting the above ideas in to practice, has been discussed in detail in chapter 4, while the laser light source and the phase stabilization concept in chapter 3. For the sake of completeness a quick description follows. A short laser pulse  $< 5$  fs (fine tuned to the shortest pulse duration as indicated by the autocorrelation trace) is focused into a Neon atomic target, and short XUV pulses are generated. Utilizing a multilayer mirror with a 9 eV spectral bandwidth, the XUV light is focused into a second Ne gas jet, along with the residual laser light to be characterized. A series of electron spectra are recorded as a function of the delay between the short XUV and the laser pulse by means of an electron spectrometer. The experimental results are shown in figure 6.2, where 120 electron spectra are put together in a false color representation. Each spectrum is the result of electrons accumulated over 100000 shots of the laser. The attosecond pulse has been characterized as in chapter 5 and has duration of 250 as. However the current data allow retrieval of this information as well by analyzing the spectra corresponding to the streaking of a couple of central cycles of the pulse. The sampling step, defined by the delay introduced between laser light and attosecond release burst, in the present case is 200 as. The scan extends over a range of 22 fs, in order to record the most important features of the light waveform as the pulse is expected to last 5 fs or less, according to its autocorrelation trace. The instantaneous value of the electric field of the pulse as a function of time, is presented in figure 6.3, as retrieved from the data in figure 6.2 by employing the simulation code developed for the streak camera measurements. It is important to mention, however, that a simple calculation of the center of gravity of each individual electron spectrum, would be sufficient to retrieve the vector potential in a first step and

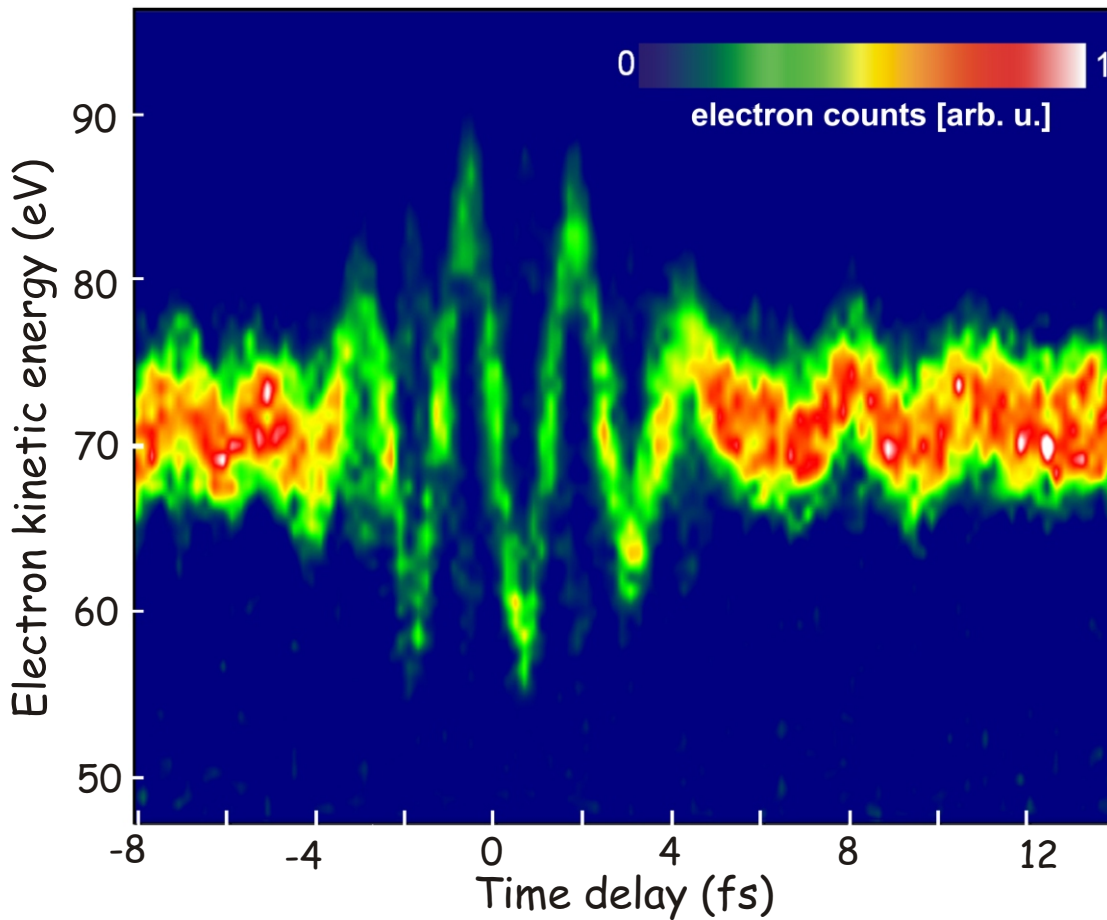


Figure 6.2: A series of 120 spectra of photoelectrons detached by a 250 as, 93 eV pulse precisely synchronized with a few cycle light waveform, in false color representation. The energy shift of the electron spectra versus the timing with the XUV pulse that launches the generated electrons, represents directly the vector potential  $A(t)$ . Sampling over a range of 22 fs, allows tracking the complete evolution of a few cycle laser light pulse. The corresponding reconstructed electric field is presented in figure 6.3.

by its differentiation, the electric field curve presented in figure 6.3.

The calibrated spectrum of the laser pulse, is depicted in figure 6.4. The wavelength axes calibration has been done by a Mercury lamp based calibration source, and the intensity has been calibrated using a white light source. The Fourier-transform limited pulse field associated with the spectrum is drawn (grey line), along with the measured pulse field (red line) for comparison. The pulse length inferred by the spectrum, is in perfect agreement with the measured trace (4.3 fs). Furthermore, the pulse is essentially chirpless.

## 6.3 Analysis and discussion

In this first proof of principle experiment, we characterize a few cycle pulse which is simultaneously the one that spawns the XUV attosecond burst, at an earlier stage of the experimental setup. There are a few advantages emerging from this particular first proof of principle direct field characterization. First, the waveform to be characterized can be accessed to a certain extent by conventional techniques, and therefore there is an approximate knowledge of the pulse duration and the shape of pulse in advance. This is important for an experiment aiming to demonstrate the proof of a concept. Second, the measurement allows direct diagnostics to the generation process that generates the attosecond pulse. The importance of a "cosine-like" few cycle laser pulse for the synthesis of an isolated attosecond burst has been repeatedly addressed up to this point. However, experimentally, the evidence up to now for this essential fact has been only circumstantial. The direct access to the field evolution of the entire pulse and thus access to the absolute phase makes unambiguously this measurement to be the first experimental demonstration, of this essential fact.

It shall be pointed out that this information can be retrieved only by sampling over the entire laser pulse and apparently not by measurements over a pair of cycles, as discussed in the previous chapter. Although the instantaneous phase is accessible, the few cycle pulse phase (CE) and thus the way that the energy is distributed to the most prominent cycles, is not. The above claims preserve their validity, even though the electric field of light is sampled at the focus of the second focusing mirror and not at the one that XUV generation takes place, that is, the primary gas target. In principle under these circumstances, one shall not underestimate the Gouy phase shift, that could lead to erroneous conclusions about the phase of the laser pulse. However, given the long confocal parameter of the focus of the beam for the XUV generation in the order of a few cm - resulting from the 50 cm focal length and the  $\sim 1$ cm aperture - and the very accurate placement of the second target nozzle at the focus of the second mirror - using the imaging techniques introduced in chapter 4 - the error is expected to be negligible. The phase shift of exactly  $\pi$ , from the first to the second focus, is of course expected, and switches a cosine pulse to its symmetric, anti-cosine. This technique actually, can be considered as the most accurate for the determination of the phase of light at each instance of the waveform, because no further theoretical treatment is necessary to extract the instantaneous phase of the field.

Of particular importance for the demonstrated technique is the extent to which the

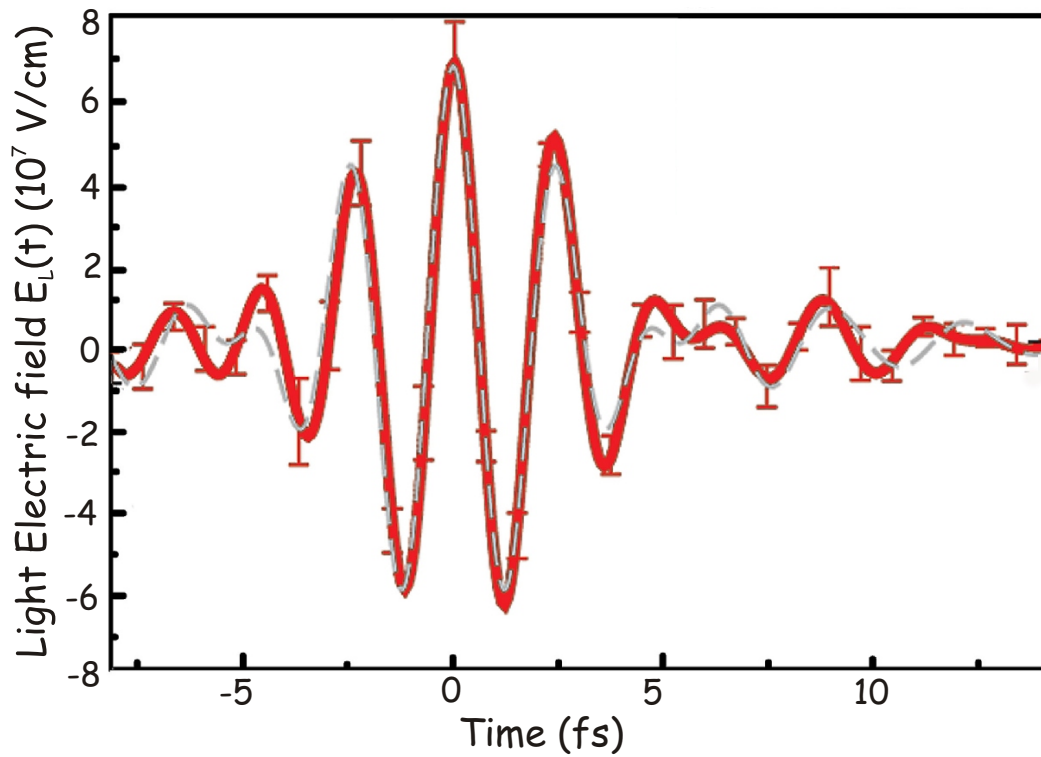


Figure 6.3: The reconstructed electric field of a few cycle laser pulse, for the spectra presented in figure 6.2. The pulse duration is 4.3 fs in agreement with the fourier transform limited duration calculated from its spectrum, figure 6.4. Grey line corresponds to the calculated value of the field from the spectrum of figure 6.4, with the phase  $\varphi_0$  and the field amplitude  $E_0$  chosen so to afford optimal matching to the measured field evolution.

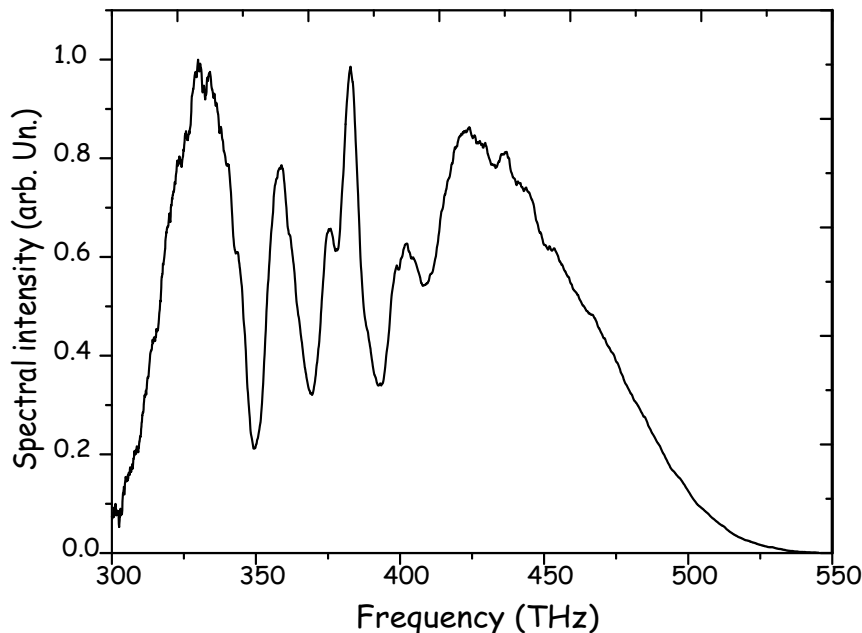


Figure 6.4: The spectrum of the few cycle laser light pulse as measured by a wavelength and intensity calibrated spectrometer. It spectrally extends over the range 650-1050 nm.

attosecond pulse characteristics, pulse duration, chirp, affect the accuracy of the measurement of light. In other words, to what extent are light waveform, and attosecond pulse characterization entangled? According to the discussion of the atomic streak camera concept in chapter 2, any possible degree of chirp, linear or not, results in symmetric broadened spectrum (with respect to a center defined by the field free electron distribution), when the latter is probed by a light field. This translates to the fact that a zero transition of the vector potential, will be similarly identified by a chirped and a non chirped attosecond pulse, as the chirp does not result in displacement of the center of gravity of the photoelectron peak in the spectrum, but rather in its broadening. Similarly for the local field maxima of the vector potential, where a linear attosecond pulse chirp does not have any effect, quadratic chirp results in symmetric distortions as shown in figure 2.4 chapter 2. An essential condition to be fulfilled is of course, that the attosecond pulse is sufficiently short, to allow sub-cycle sampling of the optical period.

## 6.4 Universal character of the technique. Application to broadband light waveform characterization

A key requisite for a method devoted to the characterization of few cycle laser pulses is the ability to characterize spectral broadband fields as stated already in the introduction. Additionally, it becomes apparent from figure 6.2, that a high dynamic range for the

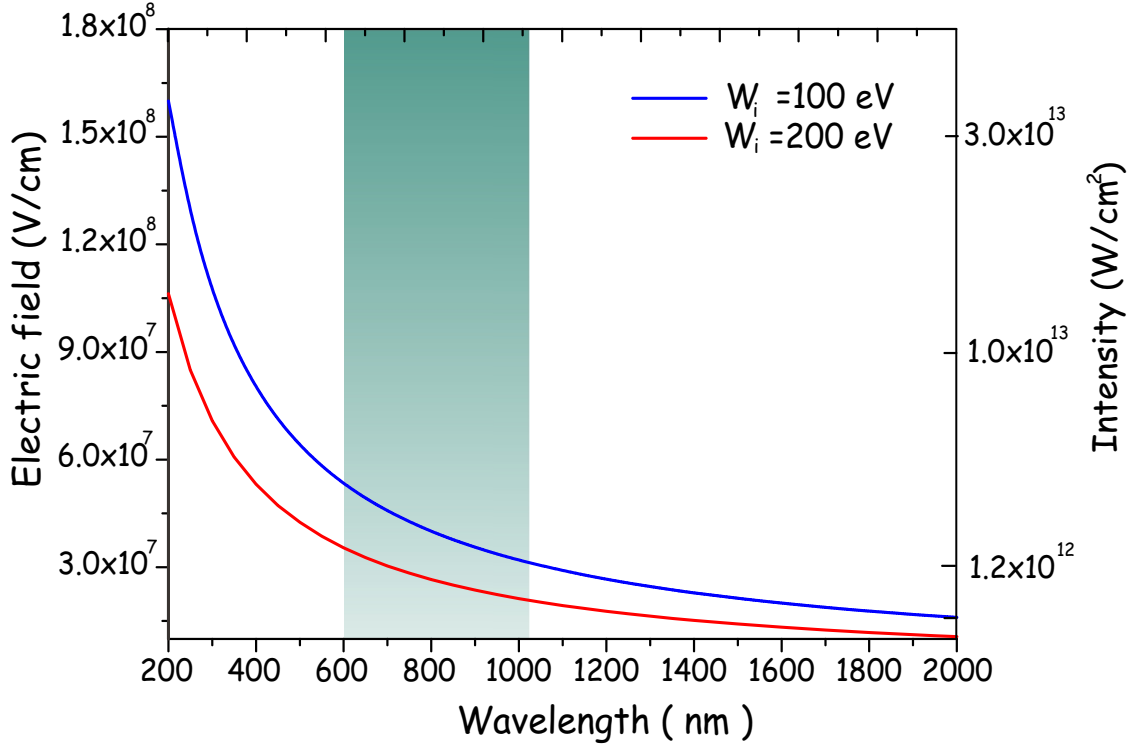


Figure 6.5: Light electric field strength necessary to attain high dynamic range for direct light characterization, over a spectral band spanning over 3 octaves e.g. from the UV to the IR. The required corresponding intensity is safely below the regime, where above threshold ionization (ATI) electrons could interfere with the streaked photoelectron peak. Blue line for photoionization energies of about 100 eV and red line for 200 eV. The criterion for the field strength, has been assumed a field capable to streak a photoelectron peak by at least its spectral width, that is here,  $\sim 9$  eV for a duration of a 250 as pulse sampler.

energetic streaking of the photoelectron distribution is a prerequisite for light metrology in terms of this technique, as it allows access to the complete evolution of the waveform. The magnitude of this energetic streaking however, depends on the frequency of light to be characterized according to equation 2.5. The electric field strength and the corresponding intensity required for an energetic streaking  $\Delta E \sim 9$  eV, for an attosecond pulse spectrally located at 100 eV and 200 eV respectively, are shown in figure 6.5 as a function of the wavelength. To derive these curves equation 2.5 is evaluated for a bandwidth covering the range of 200 to 2000 nm, or 3 octaves. Clearly, the particular spectral components can sufficiently streak the photoelectron peak while keeping the required intensity at reasonable low levels. Relatively high intensity in the focus could result in ATI spectra directly generated by the laser light field. In this regime a possible entanglement with the oscillating photoelectron peak might become possible. However, it is possible to restrict the cutoff

of ATI electrons at low energies<sup>1</sup> by keeping the intensity  $< 10^{14} \text{ W/cm}^2$ . Increasing the XUV photon energy, is an additional way to keep the required intensities of the laser light for a high dynamic range low, as shown by the second curve. A rule of thumb resulting from the above discussion about the streaking field requirement are  $E_0 < 10^8 \text{ V/m}$  for IR and  $E_0 \sim 10^8 \text{ V/m}$  for the UV.

Spatial field uniformity inside the laser focus where the attosecond burst of electrons is released, is a second but equally important issue to be considered. For these experiments, the XUV beam is confined within  $3 \mu\text{m}$ , while the laser is focused to  $30 \mu\text{m}$  according to the confocal parameter. Therefore, an order of magnitude difference ensures substantial degree of spatial field uniformity, within the generation volume. The kinetic energy of the generated electrons  $\sim 100 \text{ eV}$ , translates to a speed of  $1 \mu\text{m}/100 \text{ fs}$ . That means that the electrons are restricted within a constant field area during their interaction with the field, for a light pulse lasting less than  $5 \text{ fs}$ . Even for electron kinetic energies in the range of  $1 \text{ keV}$ , this speed is not increased by a factor greater than  $\sim 4$ , suggesting that the contribution of the non flat field distribution inside the focus can be safely neglected.

The sampling rate - as mentioned in section 6.1 - necessary to resolve a frequency in a waveform, shall be the double of the higher frequency employed in the signal. With the 250 as sampler, this condition is satisfied for the current measurement. It holds promise however for sampling spectral ranges as broad as the one illustrated in figure 6.5, without requiring temporally shorter attosecond probes.

The complete characterization of a light waveform as presented here, and the information inferred from that measurement about the waveform, can be definitely considered as the first application of attosecond pulses. That is because the retrieved information on the waveform by recording the instantaneous value of the electric field and the physics of XUV light generation, by sampling the instantaneous field value that drove the interaction over the entire temporal evolution of the pulse, cannot be measured by other means. In conclusion, the technique demonstrated here experimentally fulfils the third key objective mentioned in the introduction that is, a method for light characterization to circumvent the hindrances confronted by modern ultrafast light field metrology.

---

<sup>1</sup>The intensity dependence of the cut-off of ATI generated by  $\sim 5 \text{ fs}$  pulses, has been studied employing the same pulses and similar experimental conditions. The cut-off is limited bellow  $50 \text{ eV}$  even for intensities of  $10^{14} \text{ W/cm}^2$ . The experimental results appear in [120]

# Chapter 7

## Conclusions and future prospects

In conclusion, routes to observe natural processes in atoms and molecules with attosecond resolution, have been put into practice along with this work. The control of the phase of a few cycle intense pulses of light, allowed steering the generation process of XUV light with sub-cycle resolution. This control has been verified with spectral observations where the signatures of temporally well localized generation has been observed. By employing the technology of multilayer mirrors, the XUV continuum associated with a single recombination of an electron was isolated and temporally characterized. An isolated burst of 250 as at  $\sim 93$  eV was the result of the analysis of the experimental data. A great deal of improvements to the experimental setup, has allowed the increase of the resolution of this scheme and opened the way of its employment to experiments demanding high resolution and dynamic range.

The first experiment to utilize this dynamic range has been performed, and was the direct (and therefore complete) characterization of a light waveform where the attosecond probe is employed as a sampler with sub-cycle resolution. Direct because the instantaneous value of the field is accessed, and complete because all the relevant information of the light pulse is extracted including the phase, the chirp, the shape and its duration.

The hindrances that multicolor synthesis of optical mono-cycles or even sub-cycles confronts today, are mostly associated with the measurement rather than with the generation of the required broad spectra and spectral modes from different regimes of the electromagnetic spectrum. On the other hand synthesis cannot be considered accomplished unless a reliable measuring technique has been employed. The advantage of attosecond sampling using the techniques proposed here, arises from the fact that, broadband light beam splitting and nonlinear media, are not prerequisites for attosecond sampling and therefore the technique circumvents exactly these bottlenecks emerging from the "by definition" broadband nature of possible mono-cycles and sub-cycles.

We envisage synthesizing and measuring waveforms as schematically demonstrated in figure 7.1, where a part of the laser light is used to synthesize an attosecond pulse as discussed here, while the rest of it, is employed to generate multioctave frequency bands or spectral continua by means of nonlinear processes. These processes may include nonlinear frequency mixing in solids, super-continuum generation in gasses e.t.c. If properly manip-

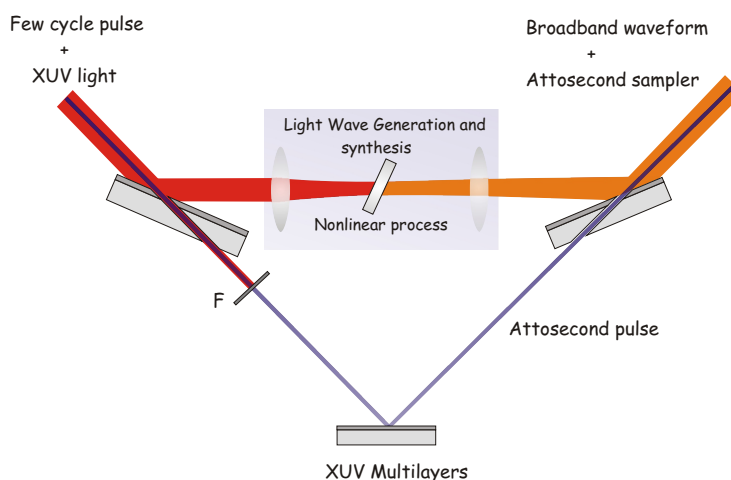


Figure 7.1: Synthesis and measurement of ultrashort light waveforms. The complete characterization of such a synthesized field is possible, by employing the attosecond oscilloscope technique and taking the advantage of the inherent sub-cycle synchronization of the attosecond pulse with the synthesized field. Beam separation and recombination by mirrors with a hole transmitting the XUV pulse and reflecting an annular part of the fundamental, is a key for the realization of such a concept. A filter F restricts propagation of laser light only in the one arm and absorbs lower XUV photon energies. A grazing incidence multilayer allows synthesis of the XUV attosecond pulse.

ulated, the spectral modes have the potential to synthesize short pulses. The generated multicolor light could be in turn probed by the attosecond pulse upon their recombination and focusing to a gas target. In this case, the inherent synchronization of XUV generation to the laser field, is an essential advantage for attaining a high sampling resolution.

Access to the instantaneous value of the electric field of light with sub-cycle precision opens the door not only to the synthesis of a single cycle pulse with a desired phase, but additionally, to reproducible, arbitrarily shaped waveforms, beyond the sinusoidal oscillation of a light field. The exact "sub-cycle" shape of the field will be determined by the relative amplitude and phase of the spectral modes employed in the synthesis.

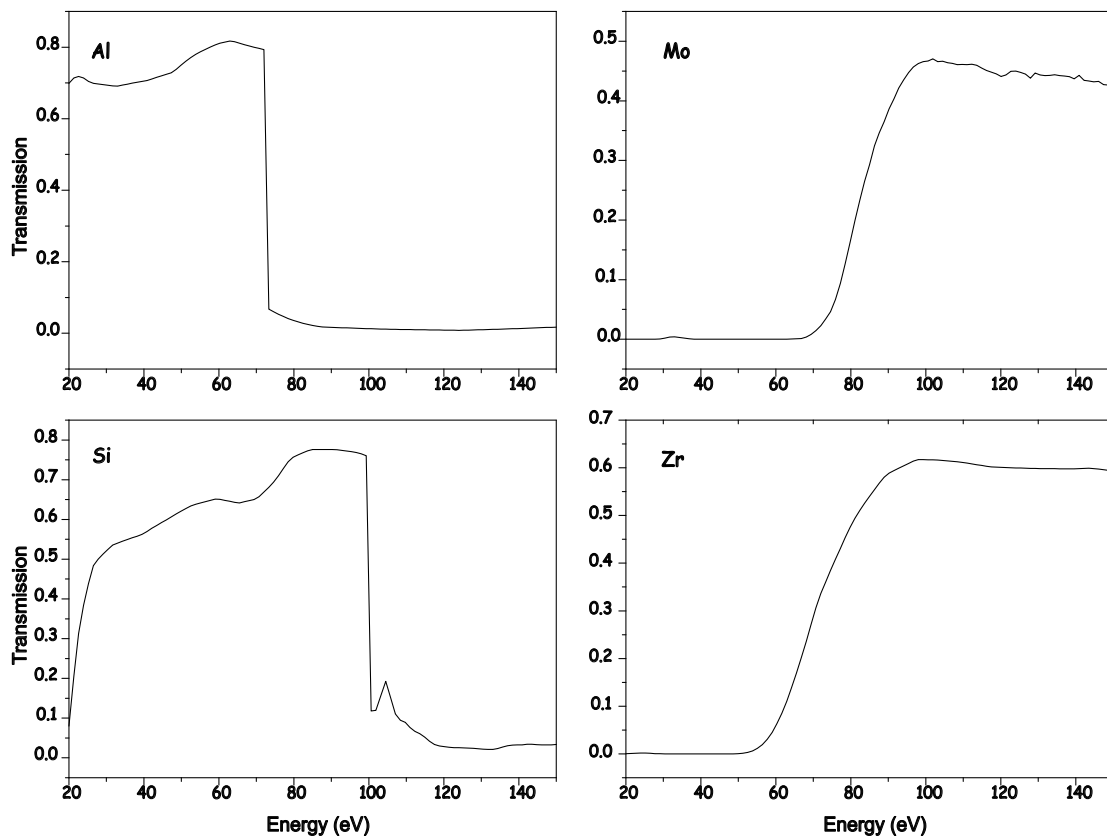
The importance of synthesized controlled light monocycles characterized with the technique presented here, emerges from two main facts; their ultrashort duration and their simple shape. Both these reasons might have high impact on Xray attosecond generation. A monocycle in this case could release all its energy with a single field swing generating XUV-Xray super-continua for the synthesis of ultraintense attosecond bursts. In that case the generated spectrum can be fully exploited in contrast to the approximately 10 % cut-off continuum today. If employed to control the motion of ionized matter with sufficiently high intensities, they might allow controlled nuclear collisions [121]. XUV - Xray attosecond pulses along with precisely shaped light waveforms employed to steer the motion of electrons in atoms and molecules hold the promise for control and applications on an attosecond time scale.

# Appendix A

## XUV transmission of thin filters

Transmission of filters in the range of 20-150 eV. Thickness 150 nm.

Source: [Center for Xray optics, Lawrence Berkeley laboratory](#).





# Bibliography

- [1] M. Eigen, *Immeasurable Fast Reactions. Nobel lectures (Chemistry)*. Elsevier, 1972.
- [2] A. Zewail, “Femtochemistry: Atomic-scale dynamics of the chemical bond,” *J. Phys. Chem. A*, vol. 104, no. 24, pp. 5660 – 5694, 2000.
- [3] A. Weiner, “Femtosecond pulse shaping using spatial light modulators,” *Rev. Sci. Instrum.*, vol. 71, no. 5, pp. 1929 – 1960, 2000.
- [4] T. Brixner, N. Damrauer, and G. Gerber, “Femtosecond quantum control,” *Adv. At., Mol., Opt. Phys.*, vol. 46, pp. 1 – 54, 2001.
- [5] S. Sartania, Z. Cheng, M. Lenzner, G. Tempea, C. Spielmann, F. Krausz, and K. Ferencz, “Generation of 0.1-tw 5-fs optical pulses at a 1-khz repetition rate,” *Opt. Lett.*, vol. 22, no. 20, pp. 1562 – 1564, 1997.
- [6] S. Backus, C. Durfee, M. Murnane, and H. Kapteyn, “High power ultrafast lasers,” *Rev. Sci. Instrum.*, vol. 69, no. 3, pp. 1207 – 1223, 1998.
- [7] M. Nisoli, S. Stagira, S. Desilvestri, O. Svelto, S. Sartania, Z. Cheng, M. Lenzner, C. Spielmann, and F. Krausz, “A novel high energy pulse compression system: Generation of multigigawatt sub-5-fs pulses,” *Appl. Phys. B*, vol. 65, no. 2, pp. 189 – 196, 1997.
- [8] M. Wickenhauser, J. Burgdorfer, F. Krausz, and M. Drescher, “Time resolved fano resonances,” *Phys. Rev. Lett.*, vol. 94, no. 2, 2005.
- [9] J. Breidbach and L. Cederbaum, “Universal attosecond response to the removal of an electron,” *Phys. Rev. Lett.*, vol. 94, no. 3, 2005.
- [10] B. Piraux, J. Bauer, S. Laulan, and H. Bachau, “Probing electron-electron correlation with attosecond pulses,” *Eur. Phys. J. D*, vol. 26, no. 1, pp. 7 – 13, 2003.
- [11] C. Chatzidimitriou-Dreismann, M. Vos, C. Kleiner, and T. Abdul-Redah, “Comparison of electron and neutron compton scattering from entangled protons in a solid polymer,” *Phys. Rev. Lett.*, vol. 91, no. 5, 2003.

- [12] C. Chatzidimitriou-Dreismann and T. Abdul-Redah, “Attosecond entanglement of protons in molecular hydrogen: neutron Compton scattering results,” *physica b-condensed matter*, vol. 350, no. 1-3, pp. 239 – 242, 2004.
- [13] M. Drescher, M. Hentschel, R. Kienberger, G. Tempea, C. Spielmann, G. Reider, P. Corkum, and F. Krausz, “X-ray pulses approaching the attosecond frontier,” *Science*, vol. 291, no. 5510, pp. 1923 – 1927, 2001.
- [14] P. Paul, E. Toma, P. Breger, G. Mullot, F. Audebert, P. Balcou, H. Muller, and P. Agostini, “Observation of a train of attosecond pulses from high harmonic generation,” *Science*, vol. 292, no. 5522, pp. 1689 – 1692, 2001.
- [15] M. Hentschel, R. Kienberger, C. Spielmann, G. Reider, N. Milosevic, T. Brabec, P. Corkum, U. Heinzmann, M. Drescher, and F. Krausz, “Attosecond metrology,” *Nature*, vol. 414, no. 6863, pp. 509 – 513, 2001.
- [16] M. Drescher, M. Hentschel, R. Kienberger, M. Uiberacker, V. Yakovlev, A. Scrinzi, T. Westerwalbesloh, U. Kleineberg, U. Heinzmann, and F. Krausz, “Time-resolved atomic inner-shell spectroscopy,” *Nature*, vol. 419, no. 6909, pp. 803 – 807, 2002.
- [17] H. Niikura, F. Legare, R. Hasbani, M. Ivanov, D. Villeneuve, and P. Corkum, “Probing molecular dynamics with attosecond resolution using correlated wave packet pairs,” *Nature*, vol. 421, no. 6925, pp. 826 – 829, 2003.
- [18] A. Sokolov, D. Walker, D. Yavuz, G. Yin, and S. Harris, “Raman generation by phased and antiphased molecular states,” *Phys. Rev. Lett.*, vol. 85, no. 3, pp. 562 – 565, 2000.
- [19] K. Shimoda, “Theory and application of optical subharmonic oscillator,” *Jpn. J. Appl. Phys.*, vol. 34, no. 7, pp. 3566 – 3569, 1995.
- [20] O. Albert and G. Mourou, “Single optical cycle laser pulse in the visible and near-infrared spectral range,” *Appl. Phys. B*, vol. 69, no. 3, pp. 207 – 209, 1999.
- [21] J. Itatani, F. Quere, G. Yudin, M. Ivanov, F. Krausz, and P. Corkum, “Attosecond streak camera,” *Phys. Rev. Lett.*, vol. 88, no. 17, 2002.
- [22] M. Kitzler, N. Milosevic, A. Scrinzi, F. Krausz, and T. Brabec, “Quantum theory of attosecond xuv pulse measurement by laser dressed photoionization,” *Phys. Rev. Lett.*, vol. 88, no. 17, 2002.
- [23] H. Niikura, F. Legare, R. Hasbani, A. Bandrauk, M. Ivanov, D. Villeneuve, and P. Corkum, “Sub-laser-cycle electron pulses for probing molecular dynamics,” *Nature*, vol. 417, no. 6892, pp. 917 – 922, 2002.

- [24] G. Mourou, Z. Chang, A. Maksimchuk, J. Nees, S. Bulanov, V. Bychenkov, T. Esirkepov, N. Naumova, F. Pegoraro, and H. Ruhl, "On the design of experiments for the study of relativistic nonlinear optics in the limit of single-cycle pulse duration and single-wavelength spot size," *Plasma Phys. Rep.*, vol. 28, no. 1, pp. 12 – 27, 2002.
- [25] L. Keldysh, "Ionization in field of a strong electromagnetic wave," *Sov. Phys. JETP-USSR*, vol. 20, no. 5, pp. 1307 –, 1965.
- [26] Bransden and Joachain, *Physics of atoms and molecules*, 2nd ed. Prentice Hall, 2002.
- [27] M. Ammosov, N. Delone, and V. Krainov, "Tunnel ionization of complex atoms and atomic ions in a varying electromagnetic-field," *Sov. Phys. JETP-USSR*, vol. 91, no. 6, pp. 2008 – 2013, 1986.
- [28] A. Scrinzi, M. Geissler, and T. Brabec, "Ionization above the coulomb barrier," *Phys. Rev. Lett.*, vol. 83, no. 4, pp. 706 – 709, 1999.
- [29] G. Yudin and M. Ivanov, "Nonadiabatic tunnel ionization: Looking inside a laser cycle," *Phys. Rev. A: At., Mol., Opt. Phys.*, vol. 6401, no. 1, pp. art. no. – 013409, 2001.
- [30] D. Spence, P. Kean, and W. Sibbett, "60-fsec pulse generation from a self-mode-locked ti-sapphire laser," *Opt. Lett.*, vol. 16, no. 1, pp. 42 – 44, 1991.
- [31] P. Moulton, "Spectroscopic and laser characteristics of ti-al<sub>2</sub>o<sub>3</sub>," *J. Opt. Soc. Am. B*, vol. 3, no. 1, pp. 125 – 133, 1986.
- [32] D. Strickland and G. Mourou, "Compression of amplified chirped optical pulses," *Opt. Commun.*, vol. 56, no. 3, pp. 219 – 221, 1985.
- [33] A. Lhuillier and P. Balcou, "High-order harmonic-generation in rare-gases with a 1-ps 1053-nm laser," *Phys. Rev. Lett.*, vol. 70, no. 6, pp. 774 – 777, 1993.
- [34] J. Macklin, J. Kmetec, and C. Gordon, "High-order harmonic-generation using intense femtosecond pulses," *Phys. Rev. Lett.*, vol. 70, no. 6, pp. 766 – 769, 1993.
- [35] C. Spielmann, N. Burnett, S. Sartania, R. Koppitsch, M. Schnurer, C. Kan, M. Lenzner, P. Wobrauschek, and F. Krausz, "Generation of coherent x-rays in the water window using 5-femtosecond laser pulses," *Science*, vol. 278, no. 5338, pp. 661 – 664, 1997.
- [36] Z. Chang, A. Rundquist, H. Wang, M. Murnane, and H. Kapteyn, "Generation of coherent soft x rays at 2.7 nm using high harmonics," *Phys. Rev. Lett.*, vol. 79, no. 16, pp. 2967 – 2970, 1997.

- [37] A. Mcpherson, G. Gibson, H. Jara, U. Johann, T. Luk, I. McIntyre, K. Boyer, and C. Rhodes, “Studies of multiphoton production of vacuum ultraviolet-radiation in the rare-gases,” *J. Opt. Soc. Am. B*, vol. 4, no. 4, pp. 595 – 601, 1987.
- [38] P. Agostini and L. Dimauro, “The physics of attosecond light pulses,” *Rep. Prog. Phys.*, vol. 67, no. 6, pp. 813 – 855, 2004.
- [39] P. Corkum, “Plasma perspective on strong-field multiphoton ionization,” *Phys. Rev. Lett.*, vol. 71, no. 13, pp. 1994 – 1997, 1993.
- [40] L. D. Landau and E. M. Lifshitz, *The classical theory of fields*, 4th ed. Pergamon Pr., 1998.
- [41] A. Gordon and F. Kärtner, “Scaling of kev hhg photon yield with drive wavelength,” *Opt. Exp.*, vol. 13, no. 8, pp. 2941 – 2947, 2005.
- [42] M. Protopapas, C. Keitel, and P. Knight, “Atomic physics with super-high intensity lasers,” *Rep. Prog. Phys.*, vol. 60, no. 4, pp. 389 –, 1997.
- [43] T. Brabec and F. Krausz, “Intense few-cycle laser fields: Frontiers of nonlinear optics,” *Rev. Mod. Phys.*, vol. 72, no. 2, pp. 545 – 591, 2000.
- [44] E. Goulielmakis, “A dispersionless, transmission grating based michelson interferometer, for the characterization of harmonics,” Master’s Thesis, Physics Department, University of Crete, 2002.
- [45] M. Lewenstein, P. Balcou, M. Ivanov, A. Lhuillier, and P. Corkum, “Theory of high-harmonic generation by low-frequency laser fields,” *Phys. Rev. A*, vol. 49, no. 3, pp. 2117 – 2132, 1994.
- [46] P. Salieres, A. Lhuillier, and M. Lewenstein, “Coherence control of high-order harmonics,” *Phys. Rev. Lett.*, vol. 74, no. 19, pp. 3776 – 3779, 1995.
- [47] E. Constant, D. Garzella, P. Breger, E. Mevel, C. Dorrer, C. Le blanc, F. Salin, and P. Agostini, “Optimizing high harmonic generation in absorbing gases: Model and experiment,” *Phys. Rev. Lett.*, vol. 82, no. 8, pp. 1668 – 1671, 1999.
- [48] N. Burnett, C. Kan, and P. Corkum, “Ellipticity and polarization effects in harmonic-generation in ionizing neon,” *Phys. Rev. A*, vol. 51, no. 5, pp. R3418 – R3421, 1995.
- [49] Y. Liang, M. Ammosov, and S. Chin, “High-order harmonic-generation in argon by elliptically polarized picosecond dye-laser pulses,” *J. Phys. B: At., Mol. Opt. Phys.*, vol. 27, no. 6, pp. 1269 – 1276, 1994.
- [50] F. Weihe, S. Dutta, G. Korn, D. Du, P. Bucksbaum, and P. Shkolnikov, “Polarization of high-intensity high-harmonic generation,” *Phys. Rev. A*, vol. 51, no. 5, pp. R3433 – R3436, 1995.

- [51] O. Tcherbakoff, E. Mevel, D. Descamps, J. Plumridge, and E. Constant, "Time-gated high-order harmonic generation," *Phys. Rev. A*, vol. 68, no. 4, 2003.
- [52] E. Goulielmakis, G. Tempea, E. Mevel, and E. Constant, "Polarization gating, priv. communication," 2003.
- [53] E. Gibson, A. Paul, N. Wagner, R. Tobey, D. Gaudiosi, S. Backus, I. Christov, A. Aquila, E. Gullikson, D. Attwood, M. Murnane, and H. Kapteyn, "Coherent soft x-ray generation in the water window with quasi-phase matching," *Science*, vol. 302, no. 5642, pp. 95 – 98, 2003.
- [54] J. Hergott, M. Kovacev, H. Merdji, C. Hubert, Y. Mairesse, E. Jean, P. Breger, P. Agostini, P. Salieres, and B. Carre, "Generation of absorption-limited high-order harmonics: Microjoule reached at 53 nm," *JOURNAL DE PHYSIQUE IV*, vol. 108, pp. 97 – 100, 2003.
- [55] E. Seres, J. Seres, F. Krausz, and C. Spielmann, "Generation of coherent soft-x-ray radiation extending far beyond the titanium l edge," *Phys. Rev. Lett.*, vol. 92, no. 16, 2004.
- [56] J. Seres, E. Seres, A. Verhoef, G. Tempea, C. Strellill, P. Wobrauschek, V. Yakovlev, A. Scrinzi, C. Spielmann, and E. Krausz, "Source of coherent kiloelectronvolt x-rays," *Nature*, vol. 433, no. 7026, pp. 596 – 596, 2005.
- [57] Y. Tamaki, J. Itatani, Y. Nagata, M. Obara, and K. Midorikawa, "Highly efficient, phase-matched high-harmonic generation by a self-guided laser beam," *Phys. Rev. Lett.*, vol. 82, no. 7, pp. 1422 – 1425, 1999.
- [58] T. Hänsch, "A proposed sub-femtosecond pulse synthesizer using separate phase-locked laser-oscillators," *Opt. Commun.*, vol. 80, no. 1, pp. 71 – 75, 1990.
- [59] G. Farkas and C. Toth, "Proposal for attosecond light-pulse generation using laser-induced multiple-harmonic conversion processes in rare-gases," *Phys. Lett. A*, vol. 168, no. 5-6, pp. 447 – 450, 1992.
- [60] S. Harris, J. Macklin, and T. Hänsch, "Atomic-scale temporal structure inherent to high-order harmonic-generation," *Opt. Commun.*, vol. 100, no. 5-6, pp. 487 – 490, 1993.
- [61] S. Harris and A. Sokolov, "Subfemtosecond pulse generation by molecular modulation," *Phys. Rev. Lett.*, vol. 81, no. 14, pp. 2894 – 2897, 1998.
- [62] Y. Mairesse, A. de bohan, L. Frasiniski, H. Merdji, L. Dinu, P. Monchicourt, P. Breger, M. Kovacev, R. Taieb, B. Carre, H. Muller, P. Agostini, and P. Salieres, "Attosecond synchronization of high-harmonic soft x-rays," *Science*, vol. 302, no. 5650, pp. 1540 – 1543, 2003.

- [63] P. Tzallas, D. Charalambidis, N. Papadogiannis, K. Witte, and G. Tsakiris, “Direct observation of attosecond light bunching,” *Nature*, vol. 426, no. 6964, pp. 267 – 271, 2003.
- [64] P. Corkum, N. Burnett, and M. Ivanov, “Subfemtosecond pulses,” *Opt. Lett.*, vol. 19, no. 22, pp. 1870 – 1872, 1994.
- [65] G. Paulus, F. Lindner, H. Walther, A. Baltuska, E. Goulielmakis, M. Lezius, and F. Krausz, “Measurement of the phase of few-cycle laser pulses,” *Phys. Rev. Lett.*, vol. 91, no. 25, 2003.
- [66] F. Lindner, G. Paulus, H. Walther, A. Baltuska, E. Goulielmakis, M. Lezius, and F. Krausz, “Gouy phase shift for few-cycle laser pulses,” *Phys. Rev. Lett.*, vol. 92, no. 11, 2004.
- [67] F. Lindner, S. M. G, H. Walther, A. Baltuska, E. Goulielmakis, F. Krausz, D. B. Milosevic, Bauer, W. Becker, and G. Paulus, “Attosecond double-slit experiment,” *Phys. Rev. Lett. (to appear)*, vol. 95, no. 4, pp. 040 401–040 404, 2005.
- [68] D. Bradley, W. Sibbett, W. Sleat, and B. Liddy, “Picosecond electron-optical chronography,” *Appl. Phys. Lett.*, vol. 20, no. 6, pp. 219 –, 1972.
- [69] J. Gex, C. Sauteret, P. Vallat, H. Tourbez, and M. Schelev, “Direct streak measurement of frequency sweeping and self focusing in single picosecond pulse,” *Opt. Commun.*, vol. 23, no. 3, pp. 430 – 434, 1977.
- [70] J. Itatani, F. Quere, G. Yudin, and P. Corkum, “Methods for measuring attosecond x-ray pulses with a strong laser field,” *Laser Phys.*, vol. 14, no. 3, pp. 344 – 353, 2004.
- [71] A. Stingl, C. Spielmann, F. Krausz, and R. Szipocs, “Generation of 11-fs pulses from a ti-sapphire laser without the use of prisms,” *Opt. Lett.*, vol. 19, no. 3, pp. 204 – 206, 1994.
- [72] A. Stingl, M. Lenzner, C. Spielmann, F. Krausz, and R. Szipocs, “Sub-10-fs mirror-dispersion-controlled ti-sapphire laser,” *Opt. Lett.*, vol. 20, no. 6, pp. 602 – 604, 1995.
- [73] C. Spielmann, P. Curley, T. Brabec, and F. Krausz, “Ultrabroadband femtosecond lasers,” *IEEE J. Quantum Electron.*, vol. 30, no. 4, pp. 1100 – 1114, 1994.
- [74] R. Szipocs, K. Ferencz, C. Spielmann, and F. Krausz, “Chirped multilayer coatings for broad-band dispersion control in femtosecond lasers,” *Opt. Lett.*, vol. 19, no. 3, pp. 201 – 203, 1994.

- [75] N. Ishii, L. Turi, V. Yakovlev, T. Fuji, F. Krausz, A. Baltuska, R. Butkus, G. Veitas, V. Smilgevicius, R. Danielius, and A. Piskarskas, “Multimillijoule chirped parametric amplification of few-cycle pulses,” *Opt. Lett.*, vol. 30, no. 5, pp. 567 – 569, 2005.
- [76] G. Tempea and T. Brabec, “Nonlinear source for the generation of high-energy few-cycle optical pulses,” *Opt. Lett.*, vol. 23, no. 16, pp. 1286 – 1288, 1998.
- [77] —, “Theory of self-focusing in a hollow waveguide,” *Opt. Lett.*, vol. 23, no. 10, pp. 762 – 764, 1998.
- [78] B. Schenkel, J. Biegert, U. Keller, C. Vozzi, M. Nisoli, G. Sansone, S. Stagira, S. De silvestri, and O. Svelto, “Generation of 3.8-fs pulses from adaptive compression of a cascaded hollow fiber supercontinuum,” *Opt. Lett.*, vol. 28, no. 20, pp. 1987 – 1989, 2003.
- [79] R. Fork, O. Martinez, and J. Gordon, “Negative dispersion using pairs of prisms,” *Opt. Lett.*, vol. 9, no. 5, pp. 150 – 152, 1984.
- [80] E. Hecht, *Optics*, 4th ed. Addison-Wesley, 2002.
- [81] G. Tempea, V. Yakovlev, B. Bacovic, F. Krausz, and K. Ferencz, “Tilted-front-interface chirped mirrors,” *J. Opt. Soc. Am. B*, vol. 18, no. 11, pp. 1747 – 1750, 2001.
- [82] V. Yakovlev and G. Tempea, “Optimization of chirped mirrors,” *App. Opt.*, vol. 41, no. 30, pp. 6514 – 6520, 2002.
- [83] X. Liu, H. Rottke, E. Eremina, W. Sandner, E. Goulielmakis, K. Keeffe, M. Lezius, F. Krausz, F. Lindner, M. Schatzel, G. Paulus, and H. Walther, “Nonsequential double ionization at the single-optical-cycle limit,” *Phys. Rev. Lett.*, vol. 93, no. 26, 2004.
- [84] J. Reichert, R. Holzwarth, T. Udem, and T. Hänsch, “Measuring the frequency of light with mode-locked lasers,” *Opt. Commun.*, vol. 172, no. 1-6, pp. 59 – 68, 1999.
- [85] T. Udem, J. Reichert, R. Holzwarth, and T. Hänsch, “Accurate measurement of large optical frequency differences with a mode-locked laser,” *Opt. Lett.*, vol. 24, no. 13, pp. 881 – 883, 1999.
- [86] J. Ranka, R. Windeler, and A. Stentz, “Visible continuum generation in air-silica microstructure optical fibers with anomalous dispersion at 800 nm,” *Opt. Lett.*, vol. 25, no. 1, pp. 25 – 27, 2000.
- [87] C. Corsi and M. Bellini, “Robustness of phase coherence against amplification in a flashlamp-pumped multi-pass femtosecond laser,” *Appl. Phys. B*, vol. 78, no. 1, pp. 31 – 34, 2004.

- [88] M. Kakehata, H. Takada, Y. Kobayashi, K. Torizuka, Y. Fujihira, T. Homma, and H. Takahashi, "Single-shot measurement of carrier-envelope phase changes by spectral interferometry," *Opt. Lett.*, vol. 26, no. 18, pp. 1436 – 1438, 2001.
- [89] A. Apolonski, A. Poppe, G. Tempea, C. Spielmann, T. Udem, R. Holzwarth, T. Hänsch, and E. Krausz, "Controlling the phase evolution of few-cycle light pulses," *Phys. Rev. Lett.*, vol. 85, no. 4, pp. 740 – 743, 2000.
- [90] D. Jones, S. Diddams, J. Ranka, A. Stentz, R. Windeler, J. Hall, and S. Cundiff, "Carrier-envelope phase control of femtosecond mode-locked lasers and direct optical frequency synthesis," *Science*, vol. 288, no. 5466, pp. 635 – 639, 2000.
- [91] T. Fortier, D. Jones, J. Ye, S. Cundiff, and R. Windeler, "Long-term carrier-envelope phase coherence," *Opt. Lett.*, vol. 27, no. 16, pp. 1436 – 1438, 2002.
- [92] M. Schatzel, F. Lindner, G. Paulus, H. Walther, E. Goulielmakis, A. Baltuska, M. Lezius, and F. Krausz, "Long-term stabilization of the carrier-envelope phase of few-cycle laser pulses," *Appl. Phys. B*, vol. 79, no. 8, pp. 1021 – 1025, 2004.
- [93] T. Fortier, J. Ye, S. Cundiff, and R. Windeler, "Nonlinear phase noise generated in air-silica microstructure fiber and its effect on carrier-envelope phase," *Opt. Lett.*, vol. 27, no. 6, pp. 445 – 447, 2002.
- [94] C. Dorrer and F. Salin, "Characterization of spectral phase modulation by classical and polarization spectral interferometry," *J. Opt. Soc. Am. B*, vol. 15, no. 8, pp. 2331 – 2337, 1998.
- [95] C. Dorrer, "Influence of the calibration of the detector on spectral interferometry," *J. Opt. Soc. Am. B*, vol. 16, no. 7, pp. 1160 – 1168, 1999.
- [96] W. Kornelis, J. Biegert, J. Tisch, M. Nisoli, G. Sansone, C. Vozzi, S. De silvestri, and U. Keller, "Single-shot kilohertz characterization of ultrashort pulses by spectral phase interferometry for direct electric-field reconstruction," *Opt. Lett.*, vol. 28, no. 4, pp. 281 – 283, 2003.
- [97] L. Poletto, G. Tondello, and P. Villoresi, "High-order laser harmonics detection in the euv and soft x-ray spectral regions," *Rev. Sci. Instrum.*, vol. 72, no. 7, pp. 2868 – 2874, 2001.
- [98] M. Schnurer, Z. Cheng, M. Hentschel, G. Tempea, P. Kalman, T. Brabec, and F. Krausz, "Absorption-limited generation of coherent ultrashort soft-x-ray pulses," *Phys. Rev. Lett.*, vol. 83, no. 4, pp. 722 – 725, 1999.
- [99] P. Balcou, A. Dederichs, M. Gaarde, and A. L’huillier, "Quantum-path analysis and phase matching of high-order harmonic generation and high-order frequency mixing processes in strong laser fields," *J. Opt. Soc. Am. B*, vol. 32, no. 12, pp. 2973 – 2989, 1999.

- [100] P. Salieres, T. Ditmire, K. Budil, M. Perry, and A. Lhuillier, "Spatial profiles of high-order harmonics generated by a femtosecond crlisa laser," *J. Phys. B: At., Mol. Opt. Phys.*, vol. 27, no. 9, pp. L217 – L222, 1994.
- [101] P. Salieres, T. Ditmire, M. Perry, A. Lhuillier, and M. Lewenstein, "Angular distributions of high-order harmonics generated by a femtosecond laser," *J. Opt. Soc. Am. B*, vol. 29, no. 20, pp. 4771 – 4786, 1996.
- [102] L. Dreeskornfeld, G. Haindl, U. Kleineberg, U. Heinzmann, F. Shi, B. Volland, I. Rangelow, E. Majkova, S. Luby, Kostic, L. Matay, P. Hrkut, P. Hudek, and H. Lee, "Nanostructuring of mo/si multilayers by means of reactive ion etching using a three-level mask," *Thin solid films*, vol. 458, no. 1-2, pp. 227 – 232, 2004.
- [103] M. Born and E. Wolf, *Principles of optics*, 7th ed. Cambridge University Press, 1999.
- [104] V. Schmidt, *Electron Spectroscopy of atoms using synchrotron radiation*, 1st ed. Cambridge University Press, 1997.
- [105] G. Sansone, C. Vozzi, S. Stagira, M. Pascolini, L. Poletto, P. Villoresi, G. Tondello, S. De silvestri, and M. Nisoli, "Observation of carrier-envelope phase phenomena in the multi-optical-cycle regime," *Phys. Rev. Lett.*, vol. 92, no. 11, 2004.
- [106] M. Nisoli, G. Sansone, S. Stagira, S. De silvestri, C. Vozzi, M. Pascolini, L. Poletto, P. Villoresi, and G. Tondello, "Effects of carrier-envelope phase differences of few-optical-cycle light pulses in single-shot high-order-harmonic spectra," *Phys. Rev. Lett.*, vol. 91, no. 21, 2003.
- [107] G. Tempea, M. Geissler, and T. Brabec, "Phase sensitivity of high-order harmonic generation with few-cycle laser pulses," *J. Opt. Soc. Am. B*, vol. 16, no. 4, pp. 669 – 673, 1999.
- [108] P. Heimann, U. Becker, H. Kerkhoff, B. Langer, D. Szostak, R. Wehlitz, D. Lindle, T. Ferrett, and D. Shirley, "Helium and neon photoelectron satellites at threshold," *Phys. Rev. A*, vol. 34, no. 5, pp. 3782 – 3791, 1986.
- [109] P. Heimann, D. Lindle, T. Ferrett, S. Liu, L. Medhurst, M. Piancastelli, D. Shirley, U. Becker, H. Kerkhoff, B. Langer, D. Szostak, and R. Wehlitz, "Shake-off on inner-shell resonances of ar, kr and xe," *J. Opt. Soc. Am. B*, vol. 20, no. 19, pp. 5005 – 5022, 1987.
- [110] R. Kienberger, M. Hentschel, M. Uiberacker, C. Spielmann, M. Kitzler, A. Scrinzi, M. Wieland, T. Westerwalbesloh, U. Kleineberg, U. Heinzmann, M. Drescher, and F. Krausz, "Steering attosecond electron wave packets with light," *Science*, vol. 297, no. 5584, pp. 1144 – 1148, 2002.

- [111] V. Yakovlev, F. Bammer, and A. Scrinzi, "Attosecond streaking measurements," *J. Mod. Opt.*, vol. 52, no. 2-3, pp. 395 – 410, 2005.
- [112] R. Kienberger, E. Goulielmakis, M. Uiberacker, A. Baltuska, V. Yakovlev, F. Bammer, A. Scrinzi, T. Westerwalbesloh, U. Kleineberg, U. Heinzmann, M. Drescher, and F. Krausz, "Atomic transient recorder," *Nature*, vol. 427, no. 6977, pp. 817 – 821, 2004.
- [113] H. Weber, "Generation and measurement of ultrashort light pulses," *J. Appl. Phys.*, vol. 39, no. 13, pp. 6041 –, 1968.
- [114] R. Trebino, K. Delong, D. Fittinghoff, J. Sweetser, M. Krumbugel, B. Richman, and D. Kane, "Measuring ultrashort laser pulses in the time-frequency domain using frequency-resolved optical gating," *Rev. Sci. Instrum.*, vol. 68, no. 9, pp. 3277 – 3295, 1997.
- [115] C. Iaconis and I. Walmsley, "Spectral phase interferometry for direct electric-field reconstruction of ultrashort optical pulses," *Opt. Lett.*, vol. 23, no. 10, pp. 792 – 794, 1998.
- [116] P. O'shea, M. Kimmel, X. Gu, and R. Trebino, "Highly simplified device for ultrashort-pulse measurement," *Opt. Lett.*, vol. 26, no. 12, pp. 932 – 934, 2001.
- [117] D. Fittinghoff, J. Bowie, J. Sweetser, R. Jennings, M. Krumbugel, K. Delong, R. Trebino, and I. Walmsley, "Measurement of the intensity and phase of ultraweak, ultrashort laser pulses," *Opt. Lett.*, vol. 21, no. 12, pp. 884 – 886, 1996.
- [118] A. Baltuska, M. Pshenichnikov, and D. Wiersma, "Amplitude and phase characterization of 4.5-fs pulses by frequency-resolved optical gating," *Opt. Lett.*, vol. 23, no. 18, pp. 1474 – 1476, 1998.
- [119] A. Cavalieri, D. Fritz, S. Lee, P. Bucksbaum, D. Reis, J. Rudati, D. Mills, P. Fussa, G. Stephenson, C. Kao, D. Siddons, D. Lowney, A. Macphee, D. Weinstein, R. Falcone, R. Pahl, J. Als-Nielsen, C. Blome, S. Dusterer, R. Ischebeck, H. Schlarb, H. Schulte-Schrepping, T. Tschentscher, J. Schneider, O. Hignette, F. Sette, K. Sokolowski-Tinten, H. Chapman, R. Lee, T. Hansen, O. Synnergren, J. Larsson, S. Techert, J. Sheppard, J. Wark, M. Bergh, C. Caleman, G. Huldt, D. van der spoel, N. Timneanu, J. Hajdu, R. Akre, E. Bong, P. Emma, P. Krejcik, J. Arthur, S. Brennan, K. Gaffney, A. Lindenberg, K. Luening, and J. Hastings, "Clocking femtosecond x rays," *Phys. Rev. Lett.*, vol. 94, no. 11, 2005.
- [120] F. Lindner, "Atoms in intense ultrashort laser pulses and the absolute phase," Ph.D. Thesis, Ludwig-Maximilians-Universitaet Muenchen, 2004.
- [121] A. Sokolov and M. Zhi, "Nuclear collisions induced by single-cycle laser pulses: molecular approach to fusion," *J. Mod. Opt.*, vol. 51, no. 16-18, pp. 2607 – 2614, 2004.

# Acknowledgments

First of all, I would like to thank Prof. Ferenc Krausz who has given me the chance to work in his group and for providing ideal conditions for this research.

I am indebted to Reinhard Kienberger, Andrius Baltūška and Matthias Uiberacker for their support and nice collaboration during these years.

Many thanks also to Vlad Yakovlev and Armin Scrinzi for their work on the analysis and interpretation of the experimental data.

I sincerely thank Ulf Kleineberg, Thorsten Uphues, Thomas Westerwalbesloh and Prof. Ulrich Heinzmann for providing the Multilayer mirror employed in the attosecond experiments presented here.

I would like to thank people from femtolasers for hints about the laser system, particularly Mike Hentschel.

I acknowledge early developments in the experimental setup and discussions with Markus Drescher.

Collaboration of our group with that of Prof. Theodore Hänsch has played an important role to the development of the tools of this research. Particularly I acknowledge Thomas Udem, Ronald Holzwarth and Christoph Gohle.

I wish to thank all members of the group for the friendly climate in Vienna and in MPQ as well.

Many thanks to Mrs. Dietlinde Egger and Mrs. Monika Wild for support during this period in Vienna and in Garching.

Thanks also to Eric Constant, Kevin O’Keeffe, Matthias Lezius, Fabrizio Lindner, Xu Liu, Eric Mevel, Gerhard Paulus, Horst Rottke, Michael Schätzel, Gabriel Tempea for their collaboration.

# Direct Measurement of Light Waves

E. Goulielmakis,<sup>1\*</sup> M. Uiberacker,<sup>1\*</sup> R. Kienberger,<sup>1</sup> A. Baltuska,<sup>1</sup> V. Yakovlev,<sup>1</sup> A. Scrinzi,<sup>1</sup> Th. Westerwalbesloh,<sup>2</sup> U. Kleineberg,<sup>2</sup> U. Heinzmann,<sup>2</sup> M. Drescher,<sup>2</sup> F. Krausz<sup>1,3,†</sup>

The electromagnetic field of visible light performs  $\sim 10^{15}$  oscillations per second. Although many instruments are sensitive to the amplitude and frequency (or wavelength) of these oscillations, they cannot access the light field itself. We directly observed how the field built up and disappeared in a short, few-cycle pulse of visible laser light by probing the variation of the field strength with a 250-attosecond electron burst. Our apparatus allows complete characterization of few-cycle waves of visible, ultraviolet, and/or infrared light, thereby providing the possibility for controlled and reproducible synthesis of ultrabroadband light waveforms.

Although the wave nature of light has long been known, it has not been possible to measure directly the oscillating field of light. Radiation in the visible and higher frequency spectral ranges can so far only be characterized in terms of physical quantities averaged over the wave period. Nonlinear optical techniques now allow measurement of  $\epsilon_L(t)$ , the amplitude envelope, and  $\omega_L(t)$ , the carrier frequency, as a function of time  $t$ , for light pulses with durations that approach the wave cycle (1, 2). The carrier-envelope phase  $\phi$ , which determines the timing between  $\epsilon_L(t)$  and  $\omega_L(t)$ , can also be measured (3). These measurements rely on carrier-envelope decomposition, which is physically meaningful only as long as the frequency spectrum of the wave is confined to less than one octave (4). If the radiation is composed of frequencies spanning a broader range (5–17), direct access to the field is required. Attosecond pulses of extreme ultraviolet (XUV) light were predicted to suit for this purpose (18, 19). We report the direct measurement of the buildup and disappearance of the electric field of a light pulse through the use of an attosecond probe.

The electric field is defined as the force exerted on a point charge of unit value. Its conceptually most direct measurement must therefore rely on measurement of this force. In a light wave, the electric field  $E_L$ , and hence the force  $F = qE_L$  it exerts on a particle with charge  $q$ , are subject to rapid variations. Access to this force is possible only if the probe charge is instantly placed in the field, i.e., within a time interval  $\tau_{\text{probe}}$  over which

the temporal variation of the force is “frozen”, i.e.,  $\tau_{\text{probe}} \ll T_0 = (2\pi)/\omega_L$ , where  $T_0$  is the wave period. The probe charge can be launched into the field by knocking electrons free from atoms or ions instantly. In a linearly polarized wave, the change of the electrons’ momentum  $\Delta p(\vec{r}, t)$  at location  $\vec{r}$  and time  $t$  along the direction of the electric field is given by

$$\Delta p(\vec{r}, t) = e \int_{-\infty}^{\infty} E_L(\vec{r}, t') dt' = e A_L(\vec{r}, t) \quad (1)$$

where  $e$  is the electron charge and  $A_L(\vec{r}, t)$  is the vector potential of the electric field  $E_L(\vec{r}, t) = E_0 \epsilon_L(\vec{r}, t) \cos(kz - \omega_L t + \phi)$ , where  $E_0$  is the maximum field amplitude, and  $k$  is the wave vector. In our analysis, we assumed the wave to propagate along the  $z$  direction, and  $t = t_{\text{real}} - z/v_g$  was defined in a retarded frame to yield  $t = 0$  as locked to the peak of the pulse travelling at the group velocity  $v_g$ .

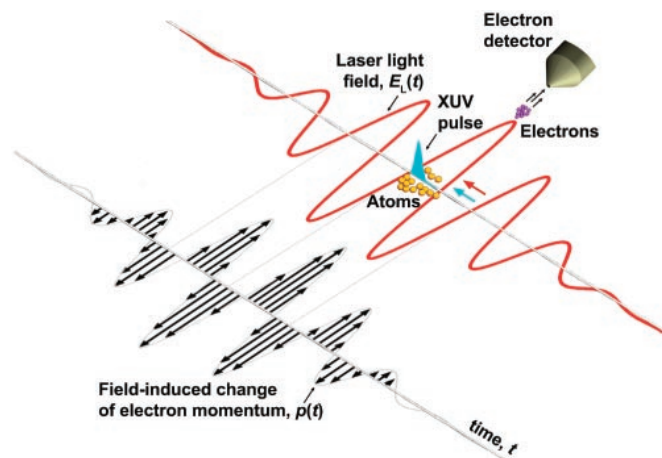
The relation  $E_L(\vec{r}, t) = -\partial A_L(\vec{r}, t)/\partial t$  implies that measuring the momentum boost  $\Delta p(\vec{r}, t)$  imparted to the freed electrons by the field at

the location  $\vec{r}$  at two instants differing in time by  $\delta t \ll T_0/4$  will yield the electric field strength and direction directly as  $E_L(\vec{r}, t) = [\Delta p(\vec{r}, t - \delta t/2) - \Delta p(\vec{r}, t + \delta t/2)]/e\delta t$ . This measurement procedure relies on a momentary release of the electrons within  $\tau_{\text{probe}} \leq T_0/4$ . For near infrared, visible, and ultraviolet light, this condition dictates that  $\tau_{\text{probe}} < 1$  fs. Varying the timing of such a subfemtosecond electron probe across the laser pulse provides complete information on the electric field of the light wave.

These considerations suggest that the electron probe needs to be localized not only in time to a tiny fraction of the wave period  $T_0$ , but also in space to a tiny fraction of the wavelength  $\lambda_L$  of the light wave to be measured. The latter requirement can be substantially relaxed if we trigger the electron release with an energetic photon pulse that copropagates with the laser wave in a collinear beam (Fig. 1). Because the timing of the probe electrons relative to the light field is invariant to space in this case, in a gently focused laser beam they can be released and are subsequently allowed to move over distances substantially larger than  $\lambda_L$ , in a volume within which the spatial variation of the field amplitude  $\epsilon_L(\vec{r}, t)$  is negligibly small for a fixed value of  $t$ .

Putting the above concept into practice requires the electron probe to be scanned through the entire laser pulse. For each newly set timing  $t$ , measurement of the momentum shift  $\Delta p(t)$  of the probing electrons requires the laser pulse to pass through the measurement apparatus again. Full characterization of the light waveform is therefore only feasible if it can be reproducibly generated for repeated measurements. Another equally important prerequisite for implementation of the above concept is the availability of an energetic instantaneous excitation (for launching the probing electrons) that is not only confined temporally to a fraction of 1 fs but is also synchronized to the light wave with similar

**Fig. 1.** Schematic of the measurement principle. A few-cycle pulse of laser light, together with a synchronized subfemtosecond XUV burst, is focused into an atomic gas target. The XUV pulse knocks electrons free by photoionization. The light electric field  $E_L(t)$  to be measured imparts a momentum change to the electrons (black arrows), which scales as the instantaneous value of the vector potential  $A_L(t)$  at the instant of release of the probing electrons. The momentum change is measured by an electron detector, which collects the electrons ejected along the direction of the linearly polarized  $E_L(\vec{r}, t)$ .



<sup>1</sup>Institut für Photonik, Technische Universität Wien, Gusshausstraße 27, A-1040 Wien, Austria. <sup>2</sup>Fakultät für Physik, Universität Bielefeld, D-33615 Bielefeld, Germany. <sup>3</sup>Max-Planck-Institut für Quantenoptik, Hans-Kopfermann-Straße 1, D-85748 Garching, Germany.

\*These authors contributed equally to this work.

†To whom correspondence should be addressed. E-mail: ferenc.krausz@tuwien.ac.at

accuracy. With the generation of waveform-controlled, intense, few-cycle light pulses (20) and their successful application to producing single 250-as XUV pulses synchronized to the driver light wave (21), these preconditions are now fulfilled. The waveform-controlled pulses—after having produced the attosecond photon probe—allow through nonlinear optical frequency conversion the synthesis of reproducible, synchronized, ultrabroadband, few-cycle waveforms (5–17). These can be repeatedly sent into the measurement apparatus with exactly the same waveform, and the subfemtosecond XUV pulse is able to produce the electrons by photoionization for probing the oscillating light field with sufficient temporal resolution.

The electrons knocked free from the atoms by the XUV pulse can be most conveniently detected if the direction of their movement is left unchanged by the light field. This applies if electrons are detected within a narrow cone aligned with the electric field vector of the linearly polarized laser wave along the  $x$  direction and are ejected with a large-enough initial momentum  $p_i$  to fulfill  $|p_i| > |\Delta p_{\max}|$ , where  $\Delta p_{\max}$  is the maximum momentum shift induced by the field. A large initial momentum also benefits the

measurement by enhancing the change of the electrons' kinetic energy  $\Delta W$ , according to  $\Delta W \approx (p_i/m)\Delta p$ , and  $m$  is the electron's mass. This expression, together with Eq. 1, implies that the energy shift scales linearly with both the electric field and the wavelength of the light field to be probed (22). The importance of a large  $\Delta W$  lies in the facts that the probing electrons are emitted with an inherent uncertainty  $\delta W_{\text{probe}} \approx \hbar/\tau_{\text{probe}}$  (where  $\hbar$  is Planck's constant  $h$  divided by  $2\pi$ ) and that the dynamic range over which the light field strength can be reliably measured scales with  $\Delta W_{\max}/\delta W_{\text{probe}}$  ( $\Delta W_{\max}$  is the maximum shift in the pulse).

Measurement of  $E_L(t)$  over a substantial dynamic range requires a  $\Delta W_{\max}$  of several tens of electron volts. For an initial kinetic energy of  $W_i \approx 100$  eV, this condition is satisfied for  $E_0 < 10^8$  V/cm for near-infrared light and requires  $E_0 \approx 3 \times 10^8$  V/cm for ultraviolet light (22). Noble gases with a low atomic number (such as helium and neon) safely resist ionization by a few-cycle field at these field strengths (23). The accuracy of definition of the location  $\vec{r}$  is dictated by the size of the volume within which  $\epsilon(\vec{r}, t)$  is approximately independent of  $\vec{r}$ . If the field is

probed in the beam focus, this condition requires the probing electrons to be confined—during their interaction with the laser field—laterally ( $xy$ ) and longitudinally ( $z$ ) to a small fraction of the diameter and to the confocal parameter of the beam, respectively.

In a proof-of-concept experiment, we directly measured the  $E_L(t)$  of the few-cycle laser pulse used for producing the attosecond photon probe (Fig. 1). Linearly polarized, waveform-controlled, <5-fs, 0.4-mJ, 750-nm ( $T_0 = 2.5$  fs) laser pulses (20), with carefully optimized values of  $\varphi$  and  $E_0$ , produce single 250-as XUV pulses at  $(\hbar\omega_{\text{XUV}})_{\text{mean}} = 93$  eV in a gas of neon atoms (21). The XUV pulse copropagates with the laser pulse in a collinear, laserlike beam to a second neon target placed in the focus of a spherical, two-component, Mo/Si multilayer mirror (21). The mirror, of 120-mm focal length, reflects XUV radiation over a band of  $\sim 9$  eV, centered at  $\sim 93$  eV. Consequently, the XUV pulse sets electrons free by photoionization with an initial kinetic energy of  $p_i^2/2m = \hbar\omega_{\text{XUV}} - W_b$ , (where  $W_b$  is the electron's binding energy) spread over an  $\sim 9$ -eV band, implying that  $\delta W_{\text{probe}} \approx 9$  eV. The electrons' energy shift  $\Delta W(t) \approx e(p_i/m)A_L(t)$  probes the laser vector potential. The volume of light-field probing is defined laterally by the  $<10$ - $\mu\text{m}$  diameter of the XUV beam at its waist and longitudinally by the  $<50$ - $\mu\text{m}$  size of the neon jet, which is well confined within the focal volume of the laser beam (diameter,  $>60$   $\mu\text{m}$ ; confocal parameter,  $>5$  mm). For  $p_i^2/2m \approx 100$  eV, the electrons traveled less than 1  $\mu\text{m}$  within 100 fs and hence remained safely confined to the region of constant laser field amplitude.

The field-induced variation of the final energy spectrum of the probe electrons versus delay between the XUV burst and the laser pulse (Fig. 2) reveal, without the need of any detailed analysis, that probing is implemented by a single burst of subfemtosecond duration that is synchronized with subfemtosecond accuracy to the measured laser field.  $E_L(t)$  can now be directly (i.e., without any iterative steps) obtained through the procedure outlined above (Fig. 3). From the measured spectrum of the few-cycle laser pulse (Fig. 3, inset), we calculated  $E_L(t)$  by a simple Fourier transformation on the assumption of absence of spectral phase variations. The result, with  $E_0$  and  $\varphi$  chosen to yield the best match to the measured values, is shown in gray. The excellent fit to the measured field evolution indicates a near-transform-limited pulse. Its duration was evaluated as 4.3 fs, in good agreement with the result of an autocorrelation measurement.

It has been predicted by theory that the few-cycle pulse pumping the XUV source has a "cosine" waveform ( $\varphi \approx 0$ ) if a single subfemtosecond pulse emerges from the ionizing atoms (24). Our results (Fig. 3) yield the exper-

**Fig. 2.** A series of kinetic energy spectra of electrons detached by a 250-as, 93-eV XUV pulse from neon atoms in the presence of an intense <5-fs, 750-nm laser field, in false-color representation. The delay of the XUV probe was varied in steps of 200 as, and each spectrum was accumulated over 100 s. The detected electrons were ejected along the laser electric field vector with a mean initial kinetic energy of  $p_i^2/2m \approx \hbar\omega_{\text{XUV}} - W_b = 93$  eV  $- 21.5$  eV = 71.5 eV. The energy shift of the electrons versus the timing of the XUV trigger pulse that launches the probing electrons directly represents  $A_L(t)$ . arb. u., arbitrary units.

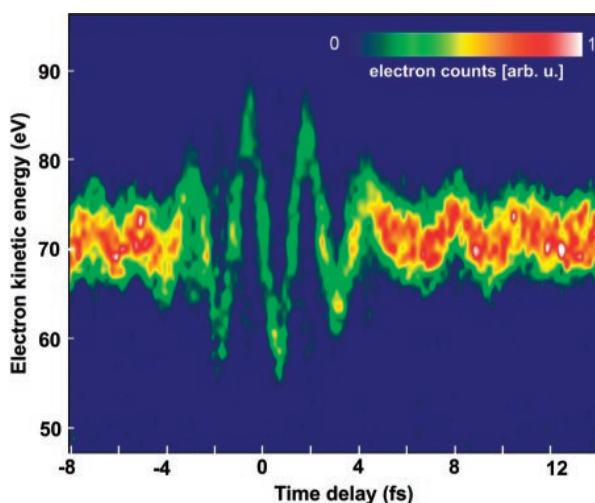
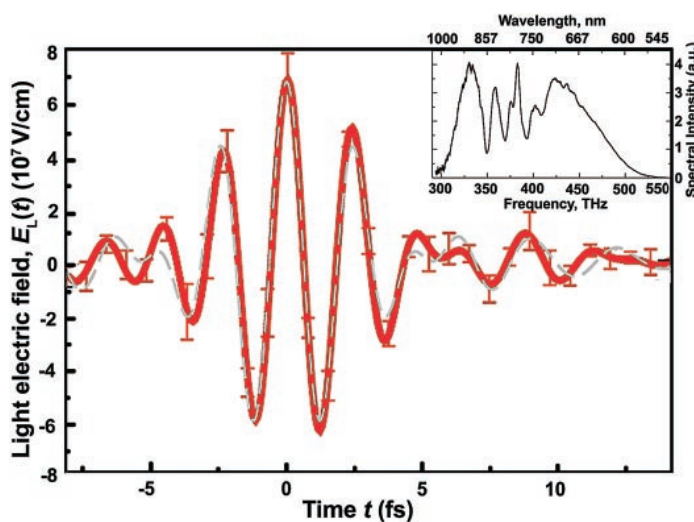


**Fig. 3.**  $E_L(t)$  reconstructed (red line) from the data depicted in Fig. 2 and calculated (gray line) from the measured pulse spectrum (inset) with the assumed absence of a frequency-dependent phase and with  $E_0$  and  $\varphi$  chosen so as to afford optimum matching to the measured field evolution. a.u., arbitrary units.



imental evidence. From this measurement, we also learn that the electric field points toward the electron detector at the pulse peak and that its strength is  $\sim 7 \times 10^7$  V/cm. With the temporal evolution, strength, and direction of  $E_L(t)$  measured, we have performed a complete characterization of a light pulse in terms of its classical electric field.

Direct probing of light-field oscillations represents what we believe to be a substantial extension of the basic repertoire of modern experimental science. The door to practical applications is opened by the creation of the key element of the demonstrated light-field detector, the synchronized attosecond electron probe, in a noninvasive manner. In fact, our intense  $<5$ -fs laser pulse appears to be capable of producing the necessary XUV trigger burst without suffering any noticeable back-action to its own temporal shape (Fig. 3). After having produced the attosecond photon probe, this powerful few-femtosecond pulse is ideally suited for the synthesis of ultrabroadband, few-cycle, optical waveforms (5–17). Being composed of radiation extending from the infrared through the visible to the ultraviolet region, the resultant few-cycle, monocycle, and conceivably even subcycle waveforms will offer a marked degree of control over the temporal variation of electric and magnetic forces on molecular and atomic time scales.

These light forces, in turn, afford the promise of controlling quantum transitions of electrons in atoms and molecules and—at relativistic intensities—their center-of-mass motion. Reproducible ultrabroadband light wave synthesis, a prerequisite for these prospects to materialize, is inconceivable without subfemtosecond measurement of the synthesized waveforms. Beyond providing the subfemtosecond electron probe for these measurements, the substantial experimental efforts associated with the construction and reliable operation of a subfemtosecond photon source will pay off in yet another way. The envisioned control of electronic motion with light forces can only be regarded as accomplished once it has been measured. Owing to their perfect synchronism with the synthesized light waveforms, the subfemtosecond photon probe will allow us to test the degree of control achieved by tracking the triggered (and hopefully steered) motion in a time-resolved fashion.

#### References and Notes

1. R. Trebino *et al.*, *Rev. Sci. Instrum.* **68**, 3277 (1997).
2. C. Iaconis, I. A. Walmsley, *Opt. Lett.* **23**, 792 (1998).
3. G. G. Paulus *et al.*, *Phys. Rev. Lett.* **91**, 253004 (2003).
4. T. Brabec, F. Krausz, *Phys. Rev. Lett.* **78**, 3282 (1997).
5. T. W. Hänsch, *Opt. Commun.* **80**, 71 (1990).
6. S. Yoshikawa, T. Imasaka, *Opt. Commun.* **96**, 94 (1993).
7. A. E. Kaplan, P. L. Shkolnikov, *Phys. Rev. Lett.* **73**, 1243 (1994).
8. K. Shimoda, *Jpn. J. Appl. Phys.* **34**, 3566 (1995).
9. S. E. Harris, A. V. Sokolov, *Phys. Rev. Lett.* **81**, 2894 (1998).
10. A. Nazarkin, G. Korn, *Phys. Rev. Lett.* **83**, 4748 (1999).
11. O. Albert, G. Mourou, *Appl. Phys. B* **69**, 207 (1999).
12. M. Wittman, A. Nazarkin, G. Korn, *Phys. Rev. Lett.* **84**, 5508 (2000).
13. Y. Kobayashi, K. Torizuka, *Opt. Lett.* **25**, 856 (2000).
14. A. V. Sokolov, D. R. Walker, D. D. Yavuz, G. Y. Yin, S. E. Harris, *Phys. Rev. Lett.* **87**, 033402 (2001).
15. K. Yamane *et al.*, *Opt. Lett.* **28**, 2258 (2003).
16. M. Y. Shverdin, D. R. Walker, D. D. Yavuz, G. Y. Yin, S. E. Harris, in *OSA Trends in Optics and Photonics Series (TOPS) Vol. 96, Conference on Lasers and Electro-Optics (CLEO)* (Optical Society of America, Washington, DC, 2004), Postdeadline paper CPDC1.
17. K. Yamane, T. Kito, R. Morita, M. Yamashita, in *OSA Trends in Optics and Photonics Series (TOPS), vol. 96, Conference on Lasers and Electro-Optics (CLEO)*, (Optical Society of America, Washington, DC, 2004), Postdeadline paper CPDC2.
18. R. Kienberger *et al.*, *Science* **297**, 1144 (2002).
19. A. D. Bandrauk, Sz. Chelkowski, N. H. Shon, *Phys. Rev. Lett.* **89**, 283903 (2002).
20. A. Baltuska *et al.*, *Nature* **421**, 611 (2003).
21. R. Kienberger *et al.*, *Nature* **427**, 817 (2004).
22. In the limit of  $|\Delta p_{\max}| \ll |p_i|$ , the change in the electrons' final kinetic energy is given by  $\Delta W_{\text{max}} \approx [8W_i U_{p,\max}]^{1/2}$ , where  $U_{p,\max} = e^2 E_0^2 / 4m_e \omega_L^2$  is the electrons' quiver energy averaged over an optical cycle at the peak of the light pulse.
23. Increase of the excitation energy  $\hbar\omega_{\text{XUV}}$  tends to reconcile the conflicting requirements of avoiding field ionization and ensuring a high dynamic range.
24. T. Brabec, F. Krausz, *Rev. Mod. Phys.* **72**, 545 (2000).
25. We are grateful to B. Ferus for creating the artwork. Sponsored by the fonds zur Förderung der Wissenschaftlichen Forschung (Austria, grant nos. Y44-PHY, P15382, and F016), the Deutsche Forschungsgemeinschaft and the Volkswagenstiftung (Germany), the European ATTO and Ultrashort XUV Pulses for Time-Resolved and Non-Linear Applications networks, and an Austrian Programme for Advanced Research and Technology fellowship to R.K. from the Austrian Academy of Sciences.

28 May 2004; accepted 20 July 2004

## Nanoribbon Waveguides for Subwavelength Photonics Integration

Matt Law,<sup>1,2\*</sup> Donald J. Sirbuly,<sup>1,2\*</sup> Justin C. Johnson,<sup>1</sup> Josh Goldberger,<sup>1</sup> Richard J. Saykally,<sup>1</sup> Peidong Yang<sup>1,2,†</sup>

Although the electrical integration of chemically synthesized nanowires has been achieved with lithography, optical integration, which promises high speeds and greater device versatility, remains unexplored. We describe the properties and functions of individual crystalline oxide nanoribbons that act as subwavelength optical waveguides and assess their applicability as nanoscale photonic elements. The length, flexibility, and strength of these structures enable their manipulation on surfaces, including the optical linking of nanoribbon waveguides and other nanowire elements to form networks and device components. We demonstrate the assembly of ribbon waveguides with nanowire light sources and detectors as a first step toward building nanowire photonic circuitry.

Photonics, the optical analog of electronics, shares the logic of miniaturization that drives research in semiconductor and information technology. The ability to manipulate pulses of light within sub-micrometer volumes is vital for highly integrated light-based devices, such as optical computers, to be realized. Recent advances in the use of photonic band gap (1, 2) and plasmonic (3, 4) phenomena to control the flow of light are impressive in this regard. One alternative route to integrated photonics is to assemble photonic circuits from a collection of nanowire elements that assume different functions, such as light creation, routing, and detection. Chemically synthesized nanowires have several features that make them good photonic building blocks, including inherent one-dimensionality, a di-

versity of optical and electrical properties, good size control, low surface roughness, and, in principle, the ability to operate above and below the diffraction limit. The toolbox of nanowire device elements already includes various types of transistors (5), light-emitting diodes (6), lasers (7, 8), and photodetectors (9). An important step toward nanowire photonics is to develop a nanowire waveguide that can link these various elements and provide the flexibility in interconnection patterns that is needed to carry out complex tasks such as logic operations (10). Our demonstration of nanowire-based photonics complements and expands upon recent work on optical beam steering in mesostructured silica cavities (11) and on subwavelength structures made lithographically (12, 13) and by the drawing of silica microfibers (14).

Nanoscale ribbon-shaped crystals of binary oxides exhibit a range of interesting properties including extreme mechanical flexibility, surface-mediated electrical conductivity (15), and lasing (16). As part of a recent study of the photoluminescence (PL) of SnO<sub>2</sub> nanoribbons, we noted that ribbons with high

<sup>1</sup>Department of Chemistry, University of California, Berkeley, CA 94720, USA. <sup>2</sup>Materials Science Division, Lawrence Berkeley National Laboratory, 1 Cyclotron Road, Berkeley, CA 94720, USA.

\*These authors contributed equally to this work.

†To whom correspondence should be addressed. E-mail: p\_yang@uclink.berkeley.edu

# Reports about this work

- Day C, *Attosecond bursts trace the electric field of optical laser pulses*, PHYSICS TODAY, 57 (10): 21-22 OCT 2004
- Overton G, *'Oscilloscope rendering' of light is achieved* LASER FOCUS WORLD 40 (11): 15 NOV 2004
- Neil Savage, *Scientists Measure Oscillations in Visible light pulses* SPIE OE MAGAZINE, NOV 2004
- Mark Peplow, *Straight to the point* NATURE, VOL 431, 34 SEP 2004.
- Eugenie Samuel Reich, *Taking snapshots of a light wave* NEW SCIENTIST VOL 186, 2494, 36 2005
- *Lichtwellen werden sichtbar* PHYS. UNSERER ZEIT, NR 36, 263, 2004

# Curriculum Vitae (June 2005)

## Eleftherios Goulielmakis

### Current Address

Max Planck Institute of Quantum Optics,  
Hans-Kopfermann-Strasse 1, Garching, Germany  
Tel: ( 49 89) 3 29 05 -732  
Fax:+49 89 3 29 05-200  
e-mail: [Eleftherios.Goulielmakis@mpq.mpg.de](mailto:Eleftherios.Goulielmakis@mpq.mpg.de)  
Web : <http://www.mpq.mpg.de/attosec>

Born: Heraklion, Crete, Greece 18/5/75  
Marital status: Single  
Nationality: Greek

### Education

**Master's Degree**, Physics Department University of Crete (2002)

**B.Sc. Physics**, Physics Department University of Crete (2000)

### Career History

- 08/04- Today Max Planck Institute of Quantum Optics, Garching, Germany (PhD Thesis)
- 09/02-08/04 Institute of Photonics, Technical University of Vienna ( PhD Thesis)
- 09/00-09/02 Institute of Electronic Structure and Laser, FORTH, Greece (Master's thesis)
- 05/99-09/00 Institute of Electronic Structure and Laser, FORTH, Greece, (Diploma Thesis)

## Teaching Experience

Teaching assistance for the undergraduate courses of the Physics Department University of Crete listed below:

- Advanced experiments in physics (ph307).

*X-ray generation and characterization, Franck-Hertz Experiment, Vacuum Techniques and Magnetic materials, Spectroscopy of Iodine molecule (2 years).*

- Introduction to computers (ph150).

*Introduction to modern software and related with physics software packages (1 year).*

## Seminars

- "Workshop on technological bottlenecks in compact high intensity short pulse lasers", April 1-4 2003, Paris France.
- The Onassis Foundation Lectures Series: The 2001 Lectures in physics and chemistry: "Ultrafast Processes, Methods and Applications" 2-6 July 2001, Foundation of research and technology, Crete, Greece.

## IT

Programming languages: C, C++, FORTRAN, Java

Scientific applications Programs: Mathematica, MS Developer Studio, Labview

Operating systems: Ms Windows, Linux, UNIX

General purpose software: Ms Office, Origin, Corel, Photoshop

## Scientific Interests

Ultraintense laser interactions with mater and harmonic generation

Attosecond pulse generation and characterization

Time resolved XUV spectroscopy

Atomic physics and phase control of atomic processes

Generation and amplification of ultrashort phase stabilized laser pulses

Synthesis of multicolor light waveforms

## Grants-fellowships

Marie-Curie early stage researcher fellowship 2004-2005

Institute of National Fellowships (I.K.Y) Postgraduate grant 2000-2001

Postgraduate grant FORTH-IESL, CRETE, GREECE 2001-2002

Postgraduate grant University of Crete 2000-2001

Undergraduate grant of FORTH-IESL, CRETE, GREECE 09/200-12/2000

## Language Knowledge

Greek (Native), English (Fluent), German (elementary)

## Publications

15 publications in refereed journals, 16 conference contributions